UNIVERSIDADE FEDERAL DE MINAS GERAIS
Instituto de Geociências
Programa de Pós-Graduação em Geologia

Salomão Silva Calegari

Estruturas Rúpteis e Expressão Topográfica na Terminação Norte da Serra da Mantiqueira, Sudeste do Brasil

Nº 55

Belo Horizonte
DATA (16/06/2021)

Salomão Silva Calegari

Estruturas Rúpteis e Expressão Topográfica na Terminação Norte da Serra da Mantiqueira, Sudeste do Brasil

Versão Final

Tese apresentada ao Programa de Pós-Graduação em Geologia do Instituto de Geociências da Universidade Federal de Minas Gerais como requisito parcial à obtenção do título de Doutor em Geologia.

Orientador: Prof. Dr. Fabrício de Andrade Caxito

Coorientadora: Profa. Dra. Mirna Aparecida Neves
Coorientador: Dr. Daniel Peifer Bezerra
Coorientador: Prof. Dr. Fábio Soares de Oliveira

Belo Horizonte
2021

C148e Calegari, Salomão Silva.
2021 Estruturas rúpteis e expressão topográfica na terminação norte da Serra da Mantiqueira, Sudeste do Brasil [manuscrito] / Salomão Silva Calegari. – 2021.
124 f., enc.: il. (principalmente color.)

Orientador: Fabrício de Andrade Caxito.
Coorientadora: Mirna Aparecida Neves.
Coorientador: Daniel Peifer Bezerra.
Coorientador: Fábio Soares de Oliveira.
Tese (doutorado) – Universidade Federal de Minas Gerais, Instituto de Geociências, 2021.
Área de concentração: Geologia Regional.
Bibliografia: f. 103-124.

1. Geologia estrutural – Teses. 2. Geomorfologia – Teses. 3. Mantiqueira, Serra da. – Teses. I. Caxito, Fabrício de Andrade. II. Neves, Mirna Aparecida. III. Bezerra, Daniel Peifer. IV. Oliveira, Fábio Soares de. V. Universidade Federal de Minas Gerais. Instituto de Geociências. VI. Título.

CDU: 551.24

Ficha catalográfica elaborada por Graciane Aparecida de Paula – CRB6 3404

UNIVERSIDADE FEDERAL DE MINAS GERAIS

PROGRAMA DE PÓS-GRADUAÇÃO EM GEOLOGIA

FOLHA DE APROVAÇÃO

Estruturas Rúpteis e Expressão Topográfica na Terminação Norte da Serra da Mantiqueira, Sudeste do Brasil

SALOMÃO SILVA CALEGARI

Tese submetida à Banca Examinadora designada pelo Colegiado do Programa de Pós-Graduação em GEOLOGIA, como requisito para obtenção do grau de Doutor em GEOLOGIA, área de concentração GEOLOGIA REGIONAL.

Aprovada em 16 de junho de 2021, pela banca constituída pelos membros:

Fabrício de A. Caxito
Prof. Fabrício de Andrade Caxito - Orientador
UFMG

Prof. Eduardo Salamuni
UFPR

Prof. Francisco Hilário Rego Bezerra

Nelson Fernandes

Prof. Nelson Ferreira Fernandes
UFRJ

Prof. Tiago Amâncio Novo
UFMG

Belo Horizonte, 16 de junho de 2021.

Aos meus pais, Humberto “*in memoriam*” e Ernesta, e a minha irmã Julieta, com todo meu amor e gratidão.

Agradecimentos

Agradeço aos orientadores desta Tese de Doutorado. Ao Fabrício A. Caxito pela confiança depositada no desenvolvimento deste estudo, pelas ótimas discussões geológicas e principalmente por mostrar como uma relação orientado/orientador pode ser sadia, incentivadora e humana. À Mirna A. Neves pela supervisão em toda minha vida acadêmica transmitindo todos os ensinamentos necessários para que eu me tornasse um bom pesquisador, transformando minha caminhada em ótimos momentos de companheirismo e amizade. Ao Daniel Peifer pela paciência durante os ensinamentos, transmitindo através de ótimos debates a paixão pela Geomorfologia e pela Ciência. Ao Fábio S. Oliveira pelo enorme apoio e confiança durante os trabalhos conduzidos na Tese.

Aos colaboradores deste trabalho pelo apoio e debates científicos, em especial a José J. L. L. Souza, Thaís R. Aiolfi, Carlos E. Ganade, Caroline C. V. Soares e Rodson A. Marques.

À Pró-Reitoria de Pós-graduação (PRPg) da UFMG e ao Programa de Pós-graduação em Geologia do Instituto de Geociências (IGC) da UFMG pela oportunidade e apoio na busca pelo conhecimento. Ao CNPq pela disponibilização da bolsa de doutorado que permitiu a realização dessa pesquisa, e à CAPES pelo apoio financeiro para os trabalhos de campo.

Aos companheiros de batalha da Pós-Graduação e aos amigos de Belo Horizonte, pelo acolhimento e amizade durante os ótimos momentos vividos na UFMG, especialmente Ygor A. T. Martins, Raíssa Santiago, Anderson M. Victoria, Samuel A. M. Silva, Márcio V. S. Dantas, Tobias M. R. Fonte Bôa, Maria Isabel P. Teodoro, Pedro B. Casagrande, Ana Carolina L. Fonseca, Renato Barros, Jhonny N. Silva, Daniel A. Miranda, Cristina S. Araújo e Carolina Deluca. Aos professores da UFMG, pelos ensinamentos e bons momentos durante a jornada do doutorado, em especial ao Tiago A. Novo, Cristina H. R. R. Augustin, Bráulio M. Fonseca, Alexandre Uhlein, Mahyra F. Tedeschi, Antônio C. Pedrosa Soares, Rosaline C. Figueiredo e Silva e Gabriel J. Uhlein.

À Sara B. Valentim por me lembrar diariamente o significado da palavra companheirismo, andando lado a lado com enorme carinho a cada passo e conquista, tanto de minha pesquisa, quanto de meu crescimento pessoal.

E, finalmente, aos maiores incentivadores dessa jornada, minha família. À Dona Ernesta, minha mãe, pela paciência e imenso apoio e à Julieta, minha irmã, pela ajuda e confiança no potencial de meu trabalho.

“Faça o teu melhor, na condição que você tem, enquanto você não tem condições melhores, para fazer melhor ainda!” (Mário Sérgio Cortella)

Resumo

Margens Continentais Passivas Elevadas (MCPEs) são caracterizadas por apresentarem extensas elevações topográficas, como serras escarpadas, localizadas na transição entre platôs interiores elevados e planícies costeiras estreitas. Entretanto, a localização da escarpa, bem como sua morfologia, pode variar consideravelmente e, em alguns casos, ao longo de uma mesma MCPE. Esta situação é observada na margem Sudeste do Brasil, onde a porção sul exibe as escarpas íngremes das serras do Mar e da Mantiqueira, marcando divisores de drenagem regionais próximos a costa, e a região norte, caracterizada pela ausência do escarpamento proeminente, com divisores regionais posicionados a mais de 100 km no interior continental. Em particular, na região norte da Serra da Mantiqueira, a intepretação de eventos neotectônicos a partir do estudo de sedimentos neogênicos restritos à margem costeira contrasta com a quiescência tectônica pós-miocênica indicada por idades de denudação e soerguimento em porções no interior continental. Neste estudo, exploramos os padrões de topografia e estruturas tectônicas para investigar a evolução geológica pós-rifte e a influência das estruturas rúpteis na evolução topográfica na terminação norte da Serra da Mantiqueira. Para tanto, realizamos análises geomórficas quantitativas para a extração de métricas da topografia, um extensivo levantamento de campo para levantamento de estruturas geológicas rúpteis e análises mineralógicas de materiais de preenchimento em estruturas rúpteis. Os resultados indicam um grande número de estruturas rúpteis orientadas a NE-SW e NW-SE formadas pela concentração de tensões locais desenvolvidas nas descontinuidades do embasamento pré-cambriano. Falhas rúpteis, cujas estrias são marcadas nos materiais de preenchimento, originaram-se após a precipitação mineral (no caso dos óxidos de manganês) ou durante (no caso da illita), com idade máxima de deformação no Mioceno. Três eventos tectônicos pós-rifte foram determinados: uma transcorrência sinistral E-W e uma distensão WNW-ESE, ambos atuantes entre o Mioceno e o Plioceno; e um evento distensivo NE-SW a NNE-SSW, posicionado no Pleistoceno. Os padrões de topografia, de drenagem e a deformação rúptil indicam a presença de uma knickzona de direção NE-SW ancorada em limites estruturais reativados, associada a um rejuvenescimento topográfico mais recente do que a época Mioceno. Contudo, a morfologia da paisagem em grande escala e, em particular, a origem dos divisores de drenagem regionais deve ser anterior à deformação rúptil e ao rejuvenescimento pós-miocênico, implicando que elementos topográficos mais antigos e mais recentes coexistem na paisagem. A terminação norte da Serra da Mantiqueira, uma MCPE não caracterizada por uma escarpa proeminente, sofreu rejuvenescimento topográfico e deformação rúptil relativamente recentes, e estes processos não estão necessariamente ligados à formação ou persistência de uma "Grande Escarpa".

Palavras-Chave: Evolução da paisagem; Margens passivas; Datação relativa; Deformação rúptil; Tectônica cenozoica; Geomorfologia.

Abstract

Elevated Passive Continental Margins (EPCMs) are characterized by extensive topographic elevations, such as sharp escarpments, located at the transition between a low-relief elevated inland plateau and narrow coastal plains. However, the location of the escarpment, as well as its morphology, can vary considerably, and in some cases, along the same EPCM. This situation is observed in Brazil's southeast margin, where the southern region exhibits sharp escarpments of the Mar and Mantiqueira ranges marking regional drainage divides near the coast, and the northern region is marked by the absence of prominent escarpment, with regional divides positioned more than 100 km inland. In particular, on the northern end of the Mantiqueira Range, the interpretation of neotectonic events from the study of Neogene sediments close to the coast contrasts with the post-Miocene tectonic quiescence indicated by ages of denudation and uplift in portions of the continental interior. This study explores the patterns of topography and tectonics to investigate the post-rift geological evolution and the influence of brittle structures on topographic evolution in the northern end of the Mantiqueira Range. To this end, we performed quantitative geomorphic analyses to extract metrics from the topography, an extensive field survey to survey for brittle geological structures and mineralogical analyses of filling materials in brittle structures. The results indicate a large number of NE-SW and NW-SE oriented brittle structures formed by the concentration of local stresses developed in discontinuities of the Precambrian basement. Brittle faults with slickensides marked in the filling materials originated after mineral precipitation (in the case of manganese oxides) or during (in the case of illite), with a maximum age of deformation in the Miocene. We inferred three post-rift tectonic events: an E-W sinistral strike-slip and a WNW-ESE distension, both active between the Miocene and Pliocene; and a NE-SW to NNE-SSW distensive event, positioned in the Pleistocene. Patterns of topography, drainage, and brittle deformation indicate the presence of a NE-SW-oriented knickzone anchored to reactivated structural boundaries, associated with a topographic rejuvenation more recent than the Miocene. However, the large-scale landscape morphology, particularly the origin of the regional drainage divides, must predate post-Miocene brittle deformation and rejuvenation, implying that older and more recent topographic elements coexist in the landscape. The northern termination of the Serra da Mantiqueira, an EPCM not characterized by a prominent escarpment, underwent relatively recent topographic rejuvenation and brittle deformation, and these processes are not necessarily linked to the formation or persistence of a "Great Escarpment".

Keywords: Landscape evolution; Passive margins; Relative dating; Brittle deformation; Cenozoic tectonics; Geomorphology.

Lista de Ilustrações

Capítulo I

Capítulo II

Capítulo III

Capítulo III - Supplementary Figures

Lista de Tabelas

Capítulo II

Lista de Siglas

ALOS	Advanced Land Observation Satellite;
BAP	Brazilian Atlantic Plateau;
CP	Coastal Plain;
CMR	Caparaó Mountain Range;
CRSB	Continental Rift Southeastern Brazil;
DEM	Digital Elevation Model;
EPCM	Elevated Passive Continental Margin;
MCPE	Margem Continental Passiva Elevada;
MMR	Mantiqueira Mountain Range;
MMM	Mar Mountain Range;
PSV	Paraíba do Sul Valley;
QF	Quadrilátero Ferrífero;
RCSB	Rifte Continental do Sudeste do Brasil;
SF	Scarp front.

Lista de Abreviaturas e Símbolos

A	upstream drainage area;
A_0	reference drainage area used in the chi/integral approach of stream-profile analysis;
B	intermediate moment tensor axes;
D	maximum displacement vector;
dx	horizontal derivative;
dz	vertical derivative;
FSC	Fault-slip component diagram;
k_s	channel steepness index;
k_{sn}	channel steepness index normalized to the reference concavity index (θ_{ref});
L	lateral horizontal displacement;
n	sample population;
nf	number of neoformed faults;
NF	pure extensive (stress regime);
nr	number of reactivated faults;
NS	transtensive (stress regime);
nt	number of compatible structural measures;
mm/yr	millimeters per year;
m	meters, a unit of length;
m^2	square meters, a unit of area;
Ma	millions of years ago (date)
R	stress ratio;
P	minimum moment tensor axes;
S	local channel slope;
SS	pure strike-slip (stress regime);
T	maximum moment tensor axes;
T	transversal horizontal displacement;
TF	pure compressive (stress regime);
TS	transpressive (stress regime);
U-Th/He	uranium-thorium/helium thermochronology;
UF	radial extensive / radial compressive (stress regime);
V	vertical displacement;

x	distance along the channel;
x_b	position of the base level used in the chi/integral approach of stream-profile analysis;
χ	the longitudinal coordinate chi used in the chi/integral approach of stream profile analysis, with dimensions of length;
z	channel bed elevation;
$z(x_b)$	elevation at the base level in the chi/integral approach of stream-profile analysis;
$\sigma1$	maximum compressive stress;
$\sigma2$	intermediate compressive stress;
$\sigma3$	minimum compressive stress;
θ	intrinsic concavity index;
θ_{ref}	fixed reference intrinsic concavity index.

Sumário

Capítulo I

Capítulo II

Capítulo III

Capítulo IV

Capítulo I

Introdução

1.1 Contexto da pesquisa

1.1.1 Margens Continentais Passivas Elevadas

Margens passivas ocorrem na transição entre as litosferas continental e oceânica no interior de uma placa tectônica e são originadas por processos de rifteamento seguidos de expansão de fundo oceânico durante a separação continental (Bradley, 2008). De maneira geral, as margens continentais passivas apresentam grande variabilidade na morfologia topográfica, o que reflete em complexas interações entre denudação, padrões de drenagem, controle tectônico e litológico (Gallagher et al., 1998). Em muitas margens passivas ao redor da Terra são encontradas extensas elevações topográficas, como serras escarpadas, marcando a passagem entre platôs interiores elevados (1 a 2 km acima do nível do mar) e planícies litorâneas estreitas (e.g., Japsen et al., 2012a; Summerfield, 2014; Green et al., 2018). As Margens Continentais Passivas Elevadas (MCPE) estão presentes nas regiões Sudeste e Nordeste do Brasil, Sul, Sudoeste e Sudeste da África, África do Sul, Sudoeste da Índia, Sudeste da Austrália, Noruega e Arábia Saudita (e.g., Japsen et al., 2009; Green et al., 2018; Fig. 1.1). A existência de grandes elevações ao longo dessas margens tem sido tema de grandes debates nas últimas décadas. Alguns autores sugerem que essas elevações estão associadas ao recuo da escarpa originada no último episódio de rifteamento (e.g., Brown et al., 2000, 2002; van der Beek et al., 2002; Sacek et al., 2012), enquanto outros indicam que a evolução da paisagem pós-ruptura continental está ligada a seguidos episódios de soterramento e exumação pós-rifte (e.g., Japsen et al., 2006, 2009, 2012a; Green et al., 2013, 2018).

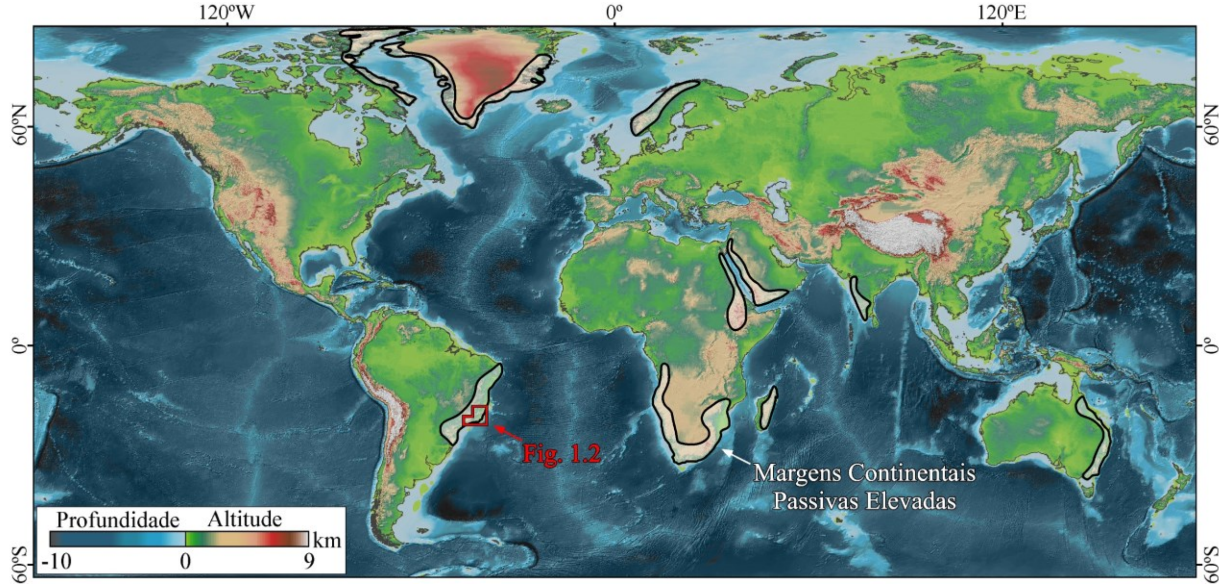

Fig. 1.1: Mapa topográfico da Terra entre as latitudes 62°S e 82°N destacando a localização das MCPEs (topos mais elevados que 2 km acima do nível do mar) e a localização da região Sudeste do Brasil (polígono em vermelho). Os dados de elevação foram extraídos de GEBCO Compilation Group (2020) e a localização das MCPEs baseada em Japsen et al. (2012a) e Summerfield (2014).

Diferentes abordagens são frequentemente utilizadas para a investigação da evolução tectônica e topográfica das paisagens em MCPEs, como: dados sedimentares *offshore* que frequentemente sugerem oscilações nas taxas de erosão e sedimentação ao longo do tempo (e.g., Contreras et al., 2010; Japsen et al., 2012b; Jelinek et al., 2014); dados de nuclídeos cosmogênicos que, em geral, produzem baixas taxas de desnudação em várias MCPEs (e.g., Cockburn et al., 2000; Bierman e Caffee, 2001; Sosa Gonzalez et al., 2016); e dados termocronológicos de baixa temperatura, em particular traço de fissão e datação U-Th/He em apatitas, mostrando que a denudação pós-rifte dos MCPEs não foi lenta e estável no espaço ou no tempo (e.g., Japsen et al., 2006, 2009, 2012b; Cogné et al., 2011, 2012; Wildman et al., 2019; Van Ranst et al., 2020). Apesar de uma gama substancial de dados empíricos, o conhecimento sobre a evolução de MCPEs ainda é incompleto. Em particular, a maioria dos estudos que exploraram a evolução da paisagem em MCPEs foi realizada em margens passivas marcadas por uma escarpa íngreme próximo à costa (e.g., Japsen et al., 2009; Cogné et al., 2011, 2012; Sacek et al., 2012; Braun, 2018; Souza et al., 2020), separando os rios que fluem diretamente para o oceano daqueles que fluem para o interior continental. Entretanto, tal configuração topográfica não é homogênea ao longo da margem continental e, em vários casos, existe uma variabilidade significativa na localização da escarpa, que pode estar posicionada perto da costa ou a mais de 100 km rumo ao interior continental, bem como sua expressão topográfica, que pode ser muito íngreme ou apenas mergulhar suavemente em direção à costa.

A margem continental do sudeste do Brasil apresenta um modelo clássico de variação das características geomórficas ao longo de uma MCPE. Na porção sul da margem, são observadas duas escarpas íngremes e bem definidas (serras do Mar e da Mantiqueira) marcando divisores de drenagem regionais próximos à costa e separadas por um rifte continental cenozoico, conhecido como Rifte Continental do Sudeste do Brasil (RCSB; Riccomini et al., 1989) (Fig. 1.2 e 1.3). Por outro lado, na área de estudos, terminação norte da Serra da Mantiqueira, a escarpa íngreme próxima à costa está ausente, e os divisores de drenagem estão posicionados distantes do litoral, chegando a 150 km rumo ao interior continental (Fig. 1.2 e 1.3). Os mecanismos responsáveis pelo rejuvenescimento e variabilidade topográfica das MCPEs são pouco compreendidos, contudo, a atuação de campo de tensões regionais e/ou a atividade de plumas mantélicas são comumente invocados como possíveis causas (e.g., Jones et al., 2002; Japsen et al., 2012a).

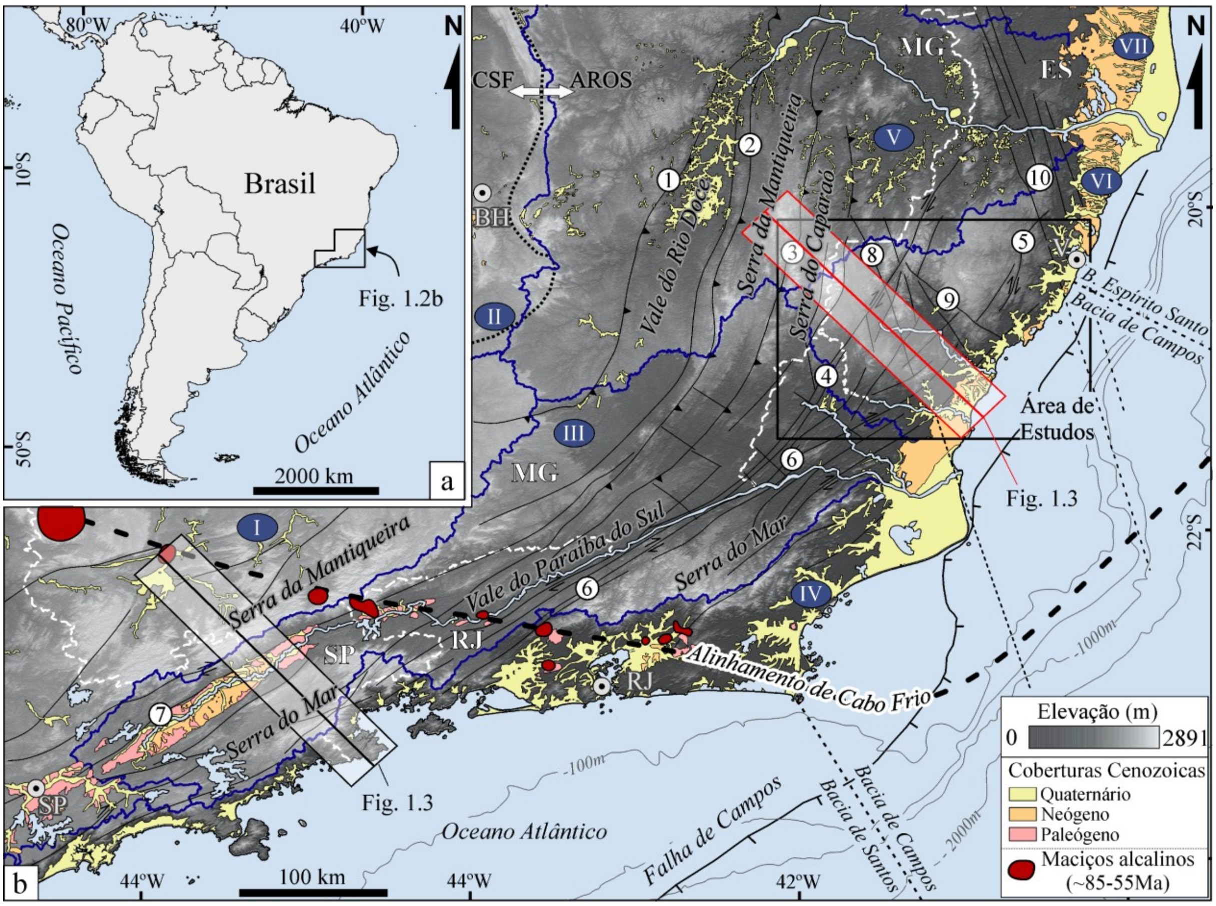

Fig. 1.2: Contexto topográfico e geológico da Margem Continental Sudeste do Brasil (compilado de Cunningham et al., 1998; Thompson et al., 1998; Novais et al., 2003; Leite et

al., 2004a, 2004b; Silva et al., 2004, 2005; Thomaz Filho et al., 2005; Alkmim et al., 2006; Calegari et al., 2016). (a) Localização da área de estudos no contexto da América do Sul e (b) na região Sudeste do Brasil. A área de estudos está localizada na terminação Norte das serras do Mar e da Mantiqueira no contexto das bacias hidrográficas costeiras do Espírito Santo (linhas azuis). Feições topográficas elevadas ocorrem associadas a uma complexa trama estrutural de zonas de cisalhamentos e lineamentos estruturais. Bacias hidrográficas dos rios principais (linhas azuis): I = Paraná; II = São Francisco; III = Paraíba do Sul; IV = Costeira do Rio de Janeiro; V = Doce; VI = Costeira do Espírito Santo; VII = São Mateus e Itanhém. Principais zonas de cisalhamento: 1 = Dom Silvério; 2 = Abre Campo; 3 = Manhuaçu; 4 = Guaçuí; 5 = Batatal; 6 = Além Paraíba; 7 = Itu. Principais lineamentos estruturais: 8 = Alegre; 9 = Piúma; 10 = Colatina. Províncias Geológicas: CSF = Cráton São Francisco; AROS = Sistema Orogênico Araçuaí-Ribeira. Estados (linhas brancas pontilhadas): SP = São Paulo; MG = Minas Gerais; RJ = Rio de Janeiro; ES = Espírito Santo. Capitais: BH = Belo Horizonte; RJ = Rio de Janeiro; SP = São Paulo; V = Vitória.

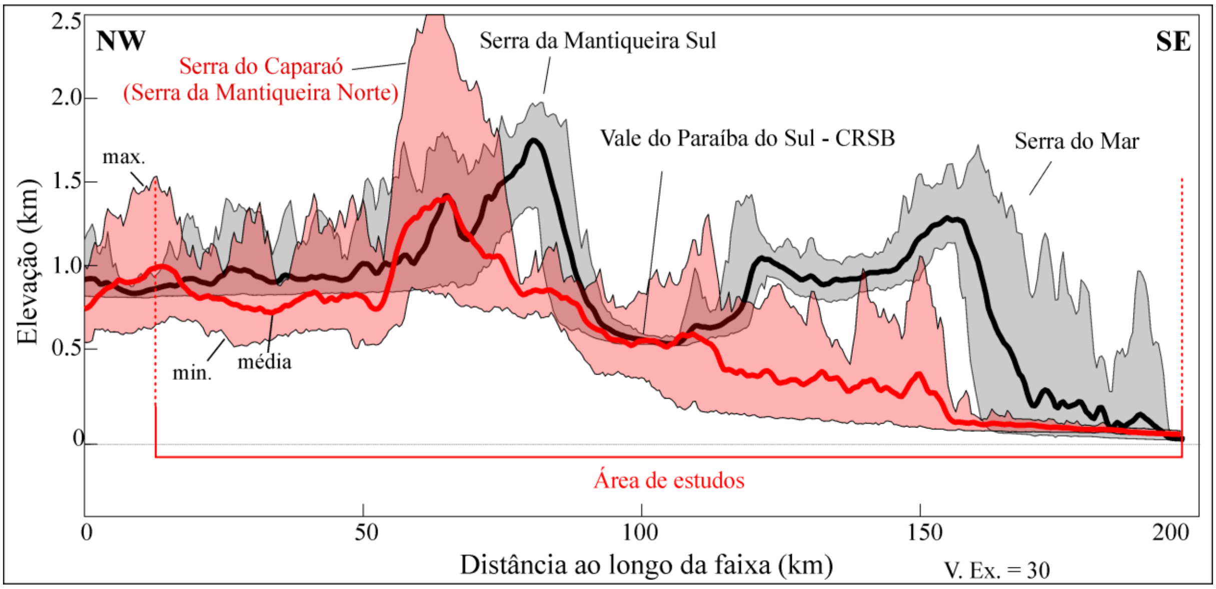

Fig. 1.3: Perfis em faixa da Serra da Mantiqueira (ver localização na Fig. 1.2b). A faixa cinza se refere ao perfil da porção sul e faixa vermelha à terminação norte (área de estudos). O perfil em faixa da porção sul mostra duas escarpas bem definidas, enquanto a região norte da Serra da Mantiqueira exibe quebras contínuas de menor magnitude entre a Serra do Caparaó e a região costeira. Os perfis em faixa, com largura de 40 km, foram feitos com exagero vertical de 30 vezes utilizando a rotina *MakeTopoSwath* inserida no *Topographic Analysis Kit* (Forte e Whipple, 2019), com base no *TopoToolbox* (Schwanghart e Scherler, 2014).

1.1.2 Tectônica pós-rifte na terminação norte da Serra da Mantiqueira

O desenvolvimento e a estruturação das margens continentais são frequentemente associados à reativação de descontinuidades pré-existentes do embasamento, com atuação na concentração das tensões crustais e no controle de depocentros de bacias petrolíferas (e.g., Dixon et al., 1987; Dunbar e Sawyer, 1989; Michon e Sokoutis, 2005; Audet e Bürgmann, 2011; Petersen e Schiffer, 2016; Salazar-Mora et al., 2018). Além do controle estrutural durante o rifteamento, zonas de fraqueza podem influenciar também na configuração topográfica de MCPEs, como no aumento de taxas de recuo das escarpas (e.g., Weissel e Seidl, 1997; Gunnell e Harbor, 2010). Além disso, o desenvolvimento e a formação de estruturas rúpteis ao longo de descontinuidades do embasamento podem gerar respostas nos padrões geomórficos da paisagem, como no soerguimento diferencial de blocos tectônicos (e.g., Quigley et al., 2007; Hiruma et al., 2010; Cogné et al., 2012), no aumento dos processos de erosão fluvial e nas taxas de escorregamento de encostas (e.g., Molnar et al., 2007; Brideau et al., 2009; Clarke e Burbank, 2010), bem como na geometria e confinamento de rios (e.g., Roy et al., 2015; Duvall et al., 2020).

Vários autores interpretam a ocorrência de um ou mais episódios de rápido resfriamento crustal pós-rifte na região Sudeste do Brasil (Fig. 1.2; Tello Saenz et al., 2003, 2005; Hiruma et al., 2010; Cogné et al., 2011, 2012; Karl et al., 2013; Engelmann de Oliveira et al., 2016; Souza et al., 2020; Van Ranst et al., 2020). Diversas causas são abordadas para as variações das taxas de denudação durante o período pós-rifte, entre elas a variação do campo de tensão regional compressivo imposto na Placa Sul-Americana (Hiruma et al., 2010; Cogné et al., 2011, 2012, 2013; Karl et al., 2013) e/ou o enfraquecimento termal da crosta em resposta à passagem da placa sobre a Pluma de Trindade (Cobbold et al., 2001; 2007; Thomaz Filho et al., 2005; Zalán e Oliveira, 2005; Cogné et al., 2011, 2012; Jelinek et al., 2014; Van Ranst et al., 2020; Fig. 1.2b). Na maioria dos casos, a consequência da imposição das tensões atuantes na margem é a deformação rúptil controlada por heterogeneidades do embasamento, como a reativação de zonas de cisalhamento pré-cambrianas (Riccomini et al., 1989; Cogné et al., 2011; Jelinek et al., 2014; Salomon et al., 2015).

Zonas de fraqueza crustal estão vinculadas ao desenvolvimento de descontinuidades rúpteis (e.g., Dunbar e Sawyer, 1989; Sandiford et al., 2004; Gudmundsson et al., 2010), comumente refletidas em superfície na forma de extensas estruturas lineares de expressão topográfica (O' Leary et al., 1976). Na margem sudeste do Brasil, a ocorrência de lineamentos estruturais no embasamento é frequentemente associada ao desenvolvimento de bacias costeiras durante a fase de separação continental (e.g., Guardado et al., 1989; Chang et al., 1992; Novais et al., 2003; Fetter, 2009; Calegari et al., 2016). No entanto, pouco se entende sobre a dinâmica crustal e a assinatura topográfica dessas feições frente aos mecanismos tectônicos atuantes no período pós separação continental. Na porção sul da Serra da Mantiqueira, onde a maioria dos estudos foi realizada, dados sedimentológicos e termocronológicos são geralmente interpretados como indícios de reativação tectônica pós-rifte a partir de dois períodos principais de resfriamento (i. Cretáceo Superior – Paleógeno e ii. Neógeno) (e.g., Hiruma et al., 2010; Cogné et al., 2011, 2012; Franco-Magalhaes et al., 2014; Engelmann de Oliveira et al., 2016; Souza et al., 2020). Por outro lado, poucos estudos exploraram a história tectônica da terminação norte da Serra da Mantiqueira. Em particular, nesta região, os eventos neotectônicos são interpretados a partir da deformação dos sedimentos neogênicos depositados ao longo da costa (Bricalli e Mello, 2013), enquanto os eventos de soerguimento são posicionados no período compreendido entre o Cretáceo Superior e o Paleógeno (Jelinek et al., 2014; Van Ranst et al., 2020; Fonseca et al., 2021). Isto se deve principalmente à ocorrência restrita de coberturas cenozoicas na costa e à inexistência de marcadores estratigráficos no embasamento, o que dificulta a amarração temporal das estruturas rúpteis que controlam a estruturação geológica da margem continental.

1.2 Área de estudo

1.2.1 Contexto fisiográfico

A área de estudos está situada na terminação norte da Serra da Mantiqueira, abrangendo toda a região sul do Estado do Espírito Santo e as regiões do extremo sudeste de Minas Gerais e do extremo nordeste do Rio de Janeiro (Fig. 1.4). A região norte da Serra da Mantiqueira, juntamente com a Serra do Mar, localizada mais ao sul, compõe um conjunto de elevações topográficas que bordejam a costa sudeste do Brasil por aproximadamente 1000 km (Fig. 1.2b). Entre os Estados de São Paulo e Rio de Janeiro, essas feições representam extensos divisores de drenagem alinhados paralelamente à costa, delimitando a Bacia do Rio Paraíba do Sul da Bacia do Rio Paraná a noroeste, e as bacias litorâneas do Rio de Janeiro a sudeste, com distâncias entre 4 e 70 km (Fig. 1.2b). Na área de estudos, os divisores de drenagem das bacias litorâneas do Espírito Santo estão posicionados a distâncias consideravelmente maiores, chegando a 150 km da costa (Fig. 1.3 e 1.4), onde a transição entre a Serra do Caparaó e a região costeira ocorre com uma amplitude altimétrica de 2891 m, a maior da margem continental brasileira. As bacias litorâneas do Espírito Santo (Itabapoana, Itapemirim, Iconha, Benevente, Jucu e Santa Maria) formam um conjunto de bacias alongadas com eixos alinhados a NW-SE/E-W, drenando diretamente para a costa (Fig. 1.4). O conjunto de serras do Mar e da Mantiqueira está sob clima subtropical úmido, variando de Aw a Cfa-Cfb na classificação de Köppen-Geiger (Alvares et al., 2013). A temperatura média anual varia entre 17 e 24° C, e a precipitação média anual varia de 835 a 2109 mm/ano na área de estudo (Karger et al., 2017).

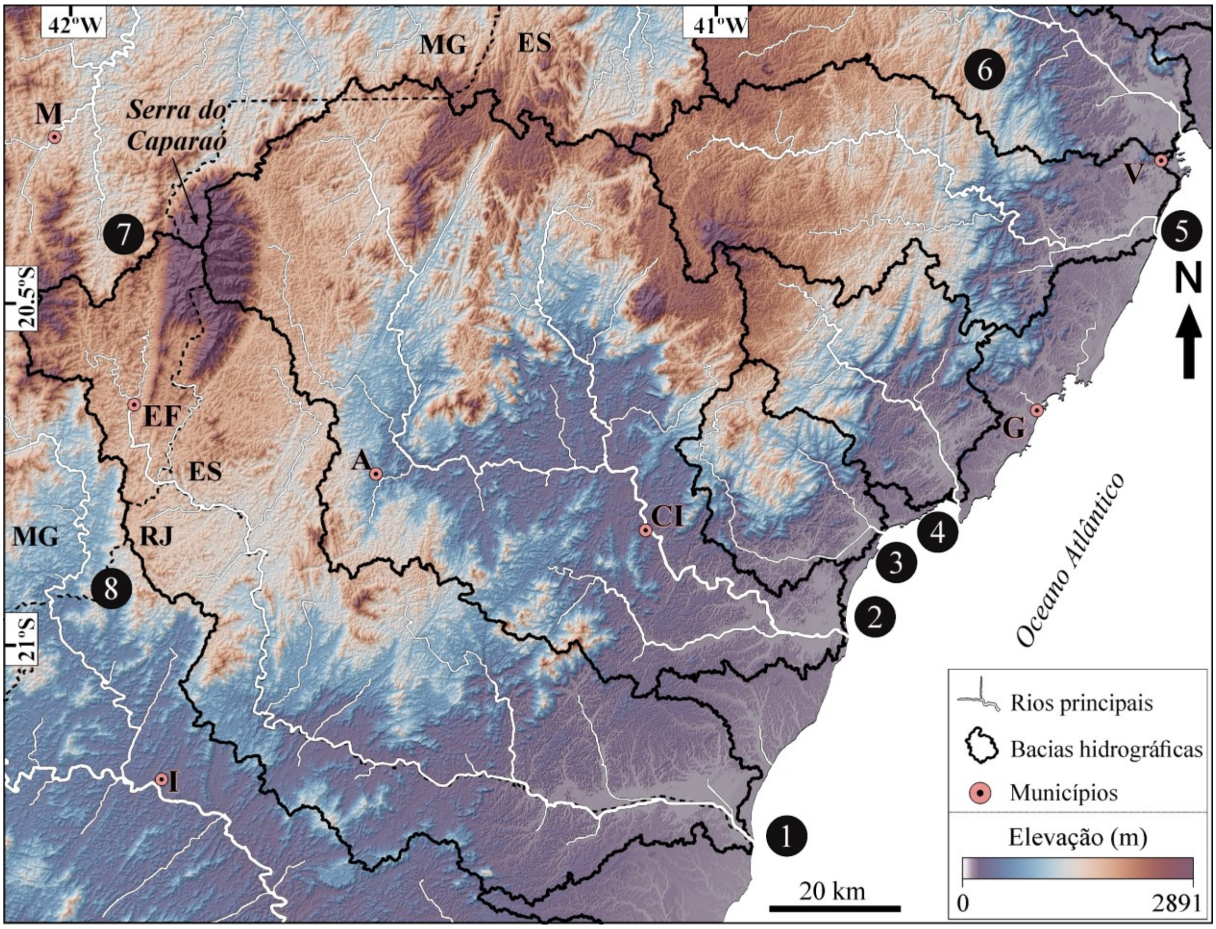

Fig. 1.4: Modelo digital de elevação plotado em relevo sombreado com azimute 315º mostrando a distribuição especial da topografia e das bacias de drenagem. Municípios: A = Alegre; CI = Cachoeiro de Itapemirim; EF = Espera Feliz; G = Guarapari; I = Itaperuna; M = Manhuaçu; V = Vitória. Bacias hidrográficas (linhas pretas): 1 = Itabapoana; 2 = Itapemirim; 3 = Iconha; 4 = Benevente; 5 = Jucu; 6 = Santa Maria; 7 = Paraíba do Sul: 8 = Muriaé. Estados (linhas pretas pontilhadas): ES = Espírito Santo; MG = Minas Gerais; RJ = Rio de Janeiro. Modelo digital de elevação ALOS (Advanced Land Observation Satellite) de 30m (Takaku et al., 2014).

1.2.2 Contexto geotectônico

O substrato rochoso da área estudada constitui unidades geológicas formadas durante a Orogênese Brasiliana /Pan Africana (ca. 630 Ma a 480 Ma) (e.g., Almeida et al., 1981; Silva et al., 2005) em uma complexa trama tectônica de direção NE-SW a N-S (Pedrosa-Soares e Wiedemann-Leonardos, 2000). O embasamento do orógeno aflorante na área é formado por rochas paleoproterozoicas de alto grau metamórfico constituído por ortogranulitos, charnockitos e enderbitos (Noce et al., 2007a; Heilbron et al., 2016). As unidades originadas no estágio pré-orogênico apresentam trama estrutural bem marcada em gnaisses aluminosos intercalados com rochas calcissilicáticas e sequências vulcanossedimentares metamorfizadas, e por tonalitos e granodioritos oriundos de um magmatismo pré-colisional (Pedrosa-Soares et al., 2008; Santiago et al., 2020a). Granitos e leucogranitos tipo S estão associados ao estágio sin-colisional, enquanto rochas pós-colisionais são compostas por gabro-noritos, granitos, charnockitos e enderbitos (Pedrosa-Soares et al., 2008; Vieira e Menezes, 2015; Heilbron et al., 2016). O registro geológico mais jovem na região é composto por sedimentos de idade mio-pliocênica da Fm. Barreiras (Arai, 2006) e por depósitos aluvio-coluvionares e litorâneos de idade quaternária (Vieira e Menezes, 2015).

A trama estrutural é caracterizada pela presença de extensas zonas de cisalhamentos transcorrentes a transpressivas de direção NE-SW a NNE-SSW, originadas no estágio posterior à propagação das frentes de empurrão da Orogênese Brasiliana / Pan-Africana (ca. 560 a 535 Ma) (Cunningham et al., 1998; Alkmim et al., 2006). Essas zonas refletem extensas feições lineares de relevo paralelas às principais elevações topográficas alinhadas à costa (Fig. 1.4 e 1.5). Na área de estudos, destacam-se as zonas de cisalhamento Guaçuí, Batatal e Além Paraíba, que compõem feições lineares bem marcadas no relevo (Fig. 1.5). Juntamente com as estruturas brasilianas, ocorrem lineamentos de direção NW-SE a NNW-SSW relacionados a zonas de fraturas ou a falhas, como os lineamentos Alegre, Colatina e Piúma (Fig. 1.5; Novais et al., 2003; Calegari et al., 2016; Lourenço et al., 2016). Ao longo desses lineamentos, são documentados dois grupos de diques gabroicos: toleíticos e alcalinos (Fig. 1.4; Calegari et al., 2016; Santiago et al., 2020b). O grupo alcalino possui origem cambriana relacionada ao colapso do orógeno, enquanto o grupo toleítico tem sua origem vinculada a reativações de estruturas cretáceas durante a separação do Supercontinente Gondwana Ocidental (Santiago et al., 2020b). Ainda segundo esses autores, os lineamentos NW-SE atuaram como condutores para as duas fontes magmáticas desde o Cambriano até o início do Cenozoico.

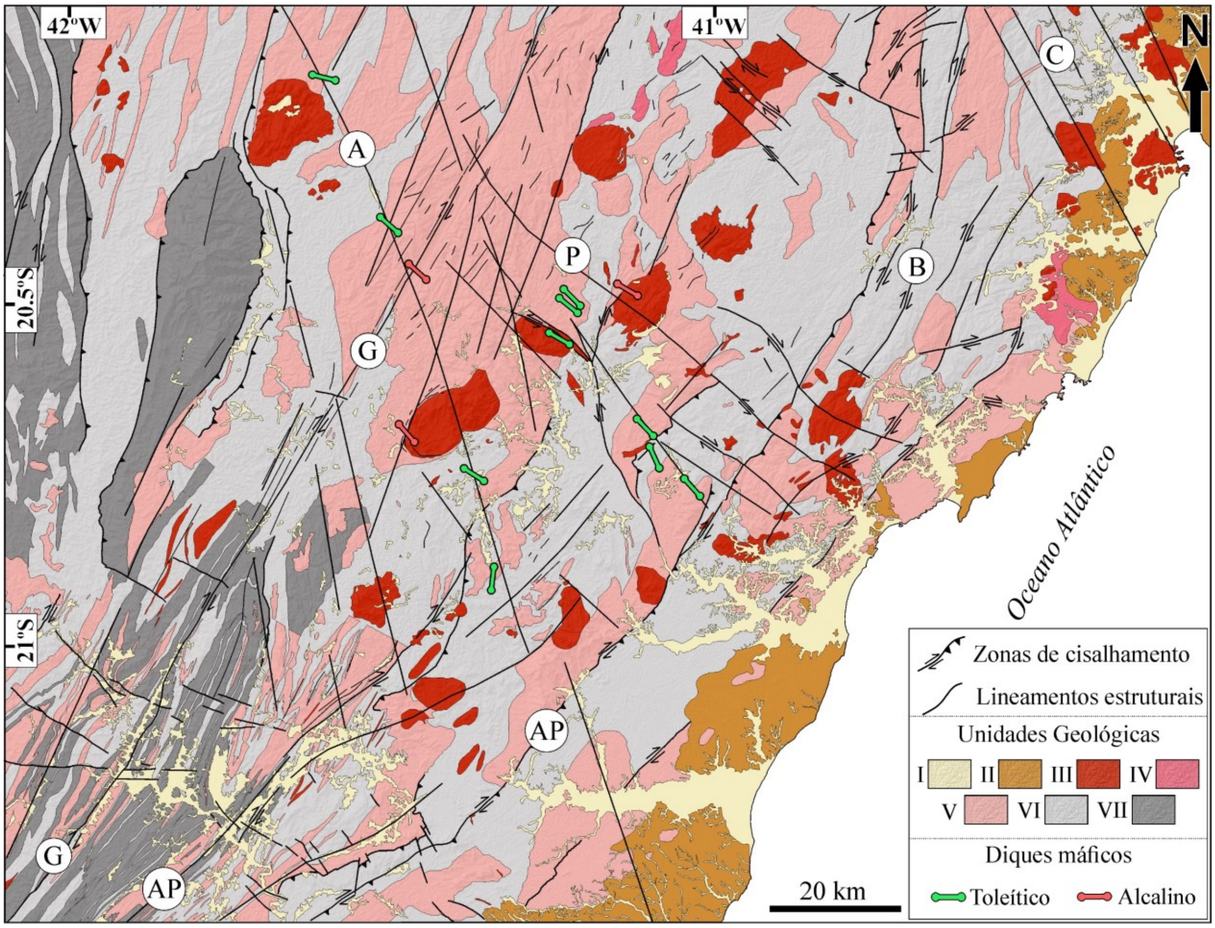

Fig. 1.5: Mapa geológico da área de estudos (modificado de Leite et al., 2004a, 2004b; Silva et al., 2004; Horn et al., 2007; Noce et al., 2007b; Pedrosa-Soares et al., 2011; Novo et al., 2012, 2014; Vieira e Menezes, 2015; Heilbron et al., 2016; Santiago et al., 2020b). Unidades geológicas: I = Depósitos aluvio-coluvionares e costeiros quaternários; II = Depósitos neogênicos da Fm. Barreiras; III = Unidades pós-colisionais cambrianas; IV = Unidades sin-colisionais neoproterozoicas; V = Unidades pré-colisionais neoproterozoicas; VI = Complexos paragnáissicos neoproterozoicos; VII = Embasamento Paleoproterozoico; Zonas de cisalhamentos e lineamentos estruturais: A = Alegre; AP = Além Paraíba; B = Batatal; C = Colatina; G = Guaçuí; P = Piúma.

Os registros geológicos conhecidos na área de estudos que sucedem a Orogênese Brasiliana / Pan Africana estão relacionados à separação do Supercontinente Gondwana Ocidental, que culminou na abertura do Oceano Atlântico Sul. Os eventos extensionais ligados à separação continental foram precedidos por uma fase de anomalia termal durante o Jurássico, que evoluiu para a fase rifte no Cretáceo Inferior sob ação de um tensor distensivo de direção NW-SE a WNW-ESE (Chang et al., 1992; Stanton et al., 2010; Almeida et al., 2013). Nesta fase, estruturas herdadas da Orogênese Brasiliana / Pan Africana atuaram como zonas de instabilidades crustal controlando os principais elementos estruturais e depocentros das bacias costeiras, como as bacias de Campos e Santos (Ojeda, 1982; Guardado et al., 1989; Chang et al., 1992). Já as feições de direção NW-SE a NNW-SSE atuaram como zonas de fraturas e zonas de transferência, segmentando depocentros de sub-bacias e controlando altos e baixos estruturais (Cobbold et al., 2001; Fetter, 2009; Calegari et al., 2016).

A evolução pós-rifte é melhor documentada na porção sul da Serra da Mantiqueira, onde muitos trabalhos utilizando traços de fissão e dados de (U-Th)/He em apatita indicam duas fases principais (Cretáceo Superior - Paleógeno e Neógeno) de resfriamento associadas à exumação regional pós-rifte em escala de km (Hiruma et al., 2010; Cogné et al., 2011, 2012; Franco-Magalhães et al., 2014; Engelmann de Oliveira et al., 2016; Souza et al., 2020). O episódio Cretáceo Superior - Paleógeno está ligado à passagem da placa sobre a Pluma de Trindade, registrada por maciços alcalinos (~ 85-55 Ma) alinhados com o Alinhamento Magmático de Cabo Frio (Fig. 1.3; Thompson et al., 1998; Thomaz Filho et al., 2005). Este evento foi seguido pelo desenvolvimento do RCSB e deposição das primeiras sequências sedimentares nas bacias cenozoicas (e.g., São Paulo, Taubaté, Resende) entre as serras do Mar e da Mantiqueira (Riccomini et al., 1989, 2004; Zalán e Oliveira, 2005). Segundo Riccomini et al. (1989), as bacias cenozoicas do CRSB originaram-se com a reativação de zonas de cisalhamento sob um regime distensivo NNW-SSE. Em contraste, Cogné et al. (2013) indicam que a Bacia de Taubaté se formou como uma bacia *pull-apart* a partir de uma transcorrência sinistral E-W ligada à imposição de um campo de tensão regional compressivo sobre a placa. Na terminação norte da Serra da Mantiqueira, o resfriamento Cretáceo Superior - Paleógeno é interpretado como resultado da reativação de zonas de cisalhamentos pré-cambrianas (Jelinek et al., 2014; Van Ranst et al., 2020; Fonseca et al., 2021). Na região do RCSB, o resfriamento do Neógeno está provavelmente ligado à reativação transpressiva de estruturas herdadas do embasamento (Cobbold et al., 2001; Cogné et al., 2012, 2013), enquanto as idades mais recentes de denudação (< 30 Ma) na extremidade norte da Serra da Mantiqueira, são interpretadas em termos de mudanças climáticas e processos acelerados de erosão (Jelinek et al., 2014).

A quiescência tectônica na extremidade norte da Serra da Mantiqueira durante o Neógeno (Jelinek et al., 2014) contrasta com as idades neotectônicas da margem sul. Por exemplo, no RCSB são propostos pelo menos 3 eventos tectônicos distensivos e transcorrentes entre o Neógeno e o Holoceno (e.g., Riccomini et al., 1989, 2004; Ferrari, 2001; Silva e Mello, 2011; Maciel et al., 2017; Souza et al., 2017). Estes eventos tectônicos também são identificados na área de estudo (Bricalli e Mello, 2013; West e Mello, 2020), entretanto, essas idades são restritas a poucos km da margem, onde ocorrem os sedimentos da Fm. Barreiras

(Fig. 1.5). A Fm. Barreiras constitui um marcador estratigráfico pós-Mioceno amplamente utilizado para balizar os registros neotectônicos no Brasil (e.g., Bezerra et al., 2014; Lima et al., 2014, 2017; Alves et al., 2019) e está presente de forma descontínua ao longo da margem atlântica, desde o Sudeste até o Norte do Brasil (Arai, 2006). Na costa Norte e Nordeste, estudos indicam que a deposição da Fm. Barreiras ocorreu durante uma transgressão marinha entre o Mioceno e o Plioceno (Arai, 2006; Rossetti et al., 2013), enquanto no Sudeste, sua origem está associada a ambiente fluvial (Morais et al., 2006) durante o Plioceno (França et al., 2007).

1.3 Questões

A partir do conhecimento atual sobre os aspectos topográficos, o arranjo estrutural rúptil e a evolução tectônica pós-rifte da margem continental do sudeste do Brasil, as seguintes questões científicas são levantadas:

(i) Qual a origem das estruturas rúpteis e sua relação com as fases de reativação das descontinuidades do embasamento da terminação norte da Serra da Mantiqueira?

(ii) Os padrões de topografia e relevo em MCPEs são controlados por estruturas rúpteis geradas pela atividade tectônica pós-rifte?

(iii) Os processos de evolução topográfica da costa sudeste do Brasil estão necessariamente ligados à formação ou persistência de uma “Grande Escarpa”?

1.4 Objetivos

A presente Tese de Doutorado possui como objetivo geral o estudo das estruturas rúpteis e de suas relações com o desenvolvimento da topografia na terminação norte da Serra da Mantiqueira. Para tanto, são definidos os seguintes objetivos específicos:

(i) Descrever os materiais de preenchimento que ocorrem nas estruturas geológicas rúpteis presentes em rochas alteradas do embasamento cristalino, buscando posicionar sua origem em relação ao contexto evolutivo cenozoico da margem sudeste do Brasil;

(ii) Analisar a geometria e a cinemática das estruturas rúpteis, posicionando-as em relação à evolução tectônica regional na fase pós-rifte;

(iii) Avaliar os efeitos da deformação rúptil na distribuição dos padrões de topografia e relevo no contexto evolutivo de uma MCPE;

1.5 Estrutura da Tese

Este estudo é apresentado sob a forma de capítulos e artigos científicos da seguinte forma:

Capítulo I - Introdução: Apresenta o contexto da pesquisa, as características fisiográficas e geotectônicas da área de estudos, as questões científicas e os objetivos da Tese de Doutorado.

Capítulo II - *Filling materials in brittle structures as indicator of cenozoic tectonic events in Southeastern Brazil*: Exibe a caracterização mineralógica dos materiais de preenchimento em estruturas rúpteis e a análise estrutural rúptil no contexto paleoambiental e paleotectônico cenozoico da região Sudeste do Brasil. Esse capítulo constitui o primeiro artigo da Tese, publicado no periódico Anuário do Instituto de Geociências – UFRJ (ISSN 1982-3908 - Qualis CAPES B1), volume 43-2, páginas 237-254, ano de 2020. http://doi.org/10.11137/2020_2_237_254.

Capítulo III: *Brittle deformation and topographic rejuvenation in an elevated passive continental margin not characterized by a sharp escarpment*: Exibe a análise estrutural rúptil de um extensivo trabalho de campo combinado com análises geomórficas quantitativas sob a perspectiva evolutiva de Margens Continentais Passivas Elevadas, com foco na evolução topográfica da terminação norte da Serra da Mantiqueira, Sudeste do Brasil. Esse capítulo foi submetido ao periódico *Geomorphology* (ISSN 0169-555X - Qualis CAPES A2).

Capítulo IV: Considerações Finais: Exibe a síntese das conclusões encontradas nos estudos apresentados nesta Tese e as perspectivas de futuros estudos na região de acordo com as lacunas ainda não respondidas até o momento.

Capítulo II

Filling materials in brittle structures as indicator of cenozoic tectonic events in Southeastern Brazil

Salomão Silva Calegari[1], Thaís Ruy Aiolfi[2], Mirna Aparecida Neves[3], Caroline Cibele Vieira Soares[3], Rodson de Abreu Marques[3], Fabrício de Andrade Caxito[1].

[1] Centro de Pesquisa Professor Manoel Teixeira da Costa, Instituto de Geociências, Universidade Federal de Minas Gerais, Belo Horizonte, Brazil
[2] Centro de Ciência e Tecnologia, Universidade Estadual do Norte Fluminense Darcy Ribeiro, Campos dos Goytacazes, Brazil
[3] Departamento de Geologia, Universidade Federal do Espírito Santo, Alegre, Brazil

2.1 Abstract

The filling materials in brittle structures can provide useful information about the Cenozoic evolution developed over proterozoic terrains. When these materials are affected by faults, they record deformation phases that can be determined chronologically, and in the occurrence of lateritic materials, it is possible to infer the paleoenvironmental conditions during the mineral formation. This work aimed to identify crystalline phases of brittle structure filling materials and to propose evolutionary interpretations for Cenozoic tectonic reactivation based on literature data. The study area is located in the Southern part of the Espírito Santo State, near the Brazilian Southeastern Continental Margin, where proterozoic geological structures have been reactivated since the mesozoic rift phase, up to the Holocene. The mineral assemblage found in the filling materials includes primary minerals such as quartz, muscovite, microcline, rutile, titanite, and bannisterite; and the weathering minerals such as kaolinite, illite, hematite, goethite, hydrobiotite, lithiophorite and, birnessite. The mineralogical association found in the filling materials denotes the action of fluid phases with mineral precipitation at the brittle discontinuities during the weathering processes that occurred during the Cenozoic, probably between the Miocene and the Pleistocene. The faults, which striations are marked on the filling materials, originated after (in the case of the manganese oxides) or during (in the case of the illite) the mineral formation, indicating that the maximum age of these faults is in the Miocene. The origin of the brittle structures that affected the filling materials studied here is linked to the uplifting of the Continental Brazilian Margin when ancient geological structures were reactivated as normal faults due to the local action of an extensional regime.

Keywords: Brittle Structures; Relative Dating; Cenozoic.

2.2 Introduction

The mobilization of material through the weathering profile, carrying substances to a deeper level of the substrate, can occur along discontinuities, where mineral precipitation is favored. These discontinuities generally are brittle structures, such as joints and faults, which control fluid flow in low permeable rocks. Depending on their nature, distribution, continuity, and connectivity, these structures allow the transport of mineralizing fluids (Kurz et al., 2008; Faulkner et al., 2010; Balsamo et al., 2013), as they generate ducts and sites for mixing of fluids and mineral precipitation (Zhang et al., 2008).

The study of weathering profiles and lateritic materials can help understand the Cenozoic geological events, as they give information about climate and relief evolution, environmental conditions, weathering intensity, and Neotectonic phases (Costa, 1991; Romano and Castañeda, 2006; Santos and Ladeira, 2006; Modenesi-Gauttieri et al., 2011; Augustin et al., 2013). Here, we use the term laterite as referring to the weathering material composed mainly of oxides and hydroxides of Aluminum and Iron, clay minerals and some silicates, commonly originated under hot and wet climate (Allaby, 2008).

According to Monteiro et al. (2014), the rocks and laterites exposed at the atmosphere-hydrosphere-lithosphere-biosphere interface are constantly reworked by mineral dissolution and re-precipitation. Supergene deposits with manganese oxides are formed due to strong and prolonged weathering processes, resulting in a thick cover of weathered rock under wet and hot climate, favorable geomorphologic conditions, and relatively stable tectonic environment (Deng and Li, 2013).

The compositional study of brittle structure filling material made it possible, according to Carmo and Vasconcelos (2004) and De Putter et al. (2015), to access information about climate, tectonic environment, and geomorphology at the time of mineral formation. Lateritic material that fills the space between the rock discontinuities is called, by Costa (1991), as “fissure ferruginous rock”, that compose thin goethite laminas accumulated on the fracture walls. Some supergene manganese minerals that fill brittle structures can be dated using isotopic and paleoclimate data (Carmo and Vasconcelos, 2004, 2006; De Putter et al., 2015).

In the State of Espírito Santo, Southeastern Brazil, Calegari et al. (2016) identified brittle structures with lateritic materials and clay minerals that fill or cover planar joint and fault surfaces. The mineralogical characterization of these materials can give relevant information about the poorly understood Cenozoic tectonic evolution and weathering processes of this region. In this work, we selected eight outcrops where brittle structures with filling material occur, seven of them located in Southern Espírito Santo and one in the Southeastern of Minas Gerais State (Fig. 2.1). The aim is to identify the crystalline phases of filling materials and analyze the structures for kinematic interpretations of the Cenozoic tectonic tying up with literature data.

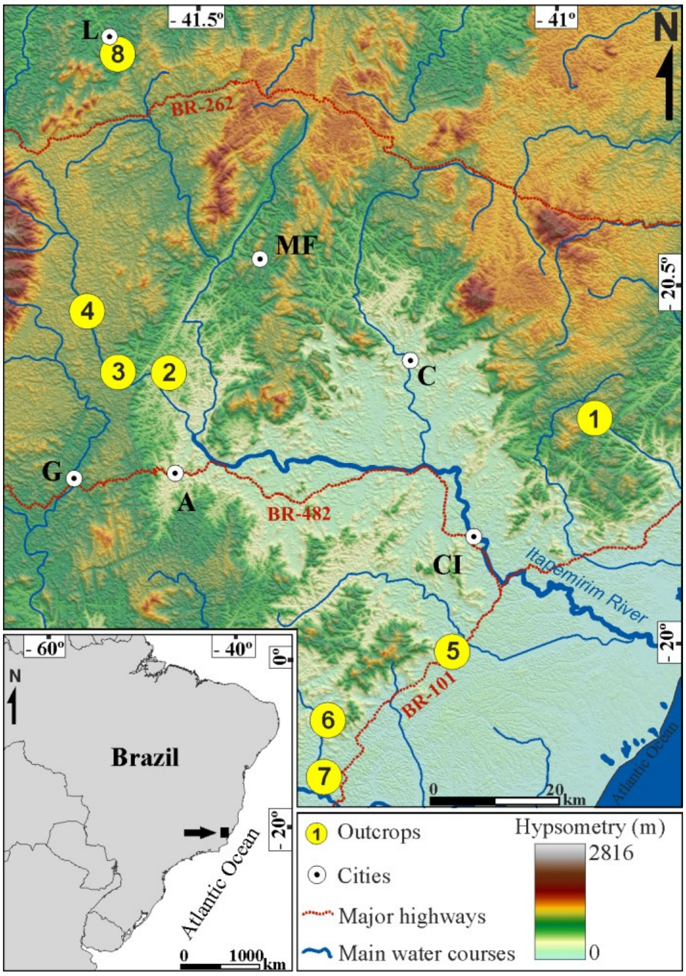

Fig. 2.1. Outcrops location map. Cities: A = Alegre, C = Castelo, CI = Cachoeiro de Itapemirim, G = Guaçuí, L = Lajinha, MF = Muniz Freire. Vetorial map data from GEOBASES (2002).

2.3 Methods

During the field works, after the detailed description and photographic register of the outcrops, samples of filling materials and host rocks were collected, also the attitude of geological structures was measured. For the identification of the mineral phases, the material was analyzed macroscopically with the naked eye, with a hand magnifier (20-times magnification), and a binocular loupe (10, 15, 20, 30, and 40-times magnification). The samples with black color were submitted to the peroxide hydrogen reaction test in order to verify the eventual presence of manganese oxides.

Twenty samples were prepared for diffractometric analysis by trituration using an agate mortar, up to reach granulation minor than a 350-mesh screen (0,044 millimeters). The diffractograms were constructed using a goniometer with cooper anode x-ray tubes, K-alfa radiation with 1,45418 Angstrom wavelengths, scanning speed of 0,3° 2 theta/min, and 2 theta angle varying from 5 to 75º. The diffractograms were interpreted using the software X'Pert HighScore Plus v. 2.0.1 and known patterns from the literature (Brindley and Brown, 1980).

The structural data were analyzed using the software OpenStereo v. 0.1.2f (Grohmann et al., 2011) and WinTensor v. 5.8.9 (Delvaux and Sperner, 2003). The joint data were plotted on density stereograms, and the fault data were inverted by the "Right Dihedron Method" (Angelier and Mechler, 1977), in order to obtain four classifications of the reduced stress tensor: the main stress axes: $\sigma1$, $\sigma2$, and $\sigma3$ (maximum, intermediate, and minimum compression) and the stress ratio R ($R = \sigma2 - \sigma3 / \sigma1 - \sigma3$). To obtain the stress regime, we used the values of R according to the classification defined by (Delvaux et al., 1997): radial extensive (UF; vertical $\sigma1$, $0 < R < 0.25$); pure extensive (NF; $\sigma1$ vertical, $0.25 < R < 0.75$), transtensive (NS; $\sigma1$ vertical, $0.75 < R < 1$ or $\sigma2$ vertical, $1 < R < 0.75$); pure strike-slip (SS; $\sigma2$ vertical, $0.75 < R < 0.25$); transpressive (TS; $\sigma2$ vertical, $0.25 < R < 0$ or $\sigma3$ vertical, $0 < R < 0.25$); pure compressive (TF; $\sigma3$ vertical, $0,25 < R < 0,75$), and radial compressive (UF; $\sigma3$ vertical, $0,75 < R < 1$). Kinematic data were plotted on Frohlich's Triangular Diagram (Frohlich, 1992) to assess the distribution of the stress regime in the area. Finally, for the deformation analysis, we used the values acquired by the fault data inversion to obtain the paleotension fields by the "Rotational Optimization" procedure using the F5 function in the Win-Tensor software.

2.4 Geological setting

The study area is located in the Araçuaí Belt domain, Northern part of the Mantiqueira Province (Almeida et al., 1981; Heilbron et al., 2004; Fuck et al., 2008). The Mantiqueira Province is a segment of the Brazilian-Pan African Orogenic System developed during the Neoproterozoic and the beginning of the Paleozoic (Almeida et al., 1981; Brito Neves et al., 1999). The collisional event that generated this orogenic system registered in the Atlantic Margin of South America and Africa is called Brazilian-Pan African orogeny.

The Araçuaí Belt extends between the parallels 15º e 21º south, from the eastern limit of the São Francisco Craton up to the South Atlantic Coast. The Araçuaí Belt Southern limit is considered as a transition zone where the foliation trend changes from N-S to NE-SW, near the 21º parallel, at the very beginning of the Ribeira Belt, belonging to the central segment of the Mantiqueira Province (Pedrosa-Soares and Wiedemann-Leonardos, 2000).

The study area is located at the Crystalline Nucleus of the Orogenic System, comprised of a Paleoproterozoic substrate, metamorphosed in high-amphibolite to granulite facies; metasedimentary – metavolcanosedimentary assemblage (paragneiss complexes), and pre to post-collisional granitic suites (G1 to G5; Alkmim et al., 2006; Fig. 2.2).

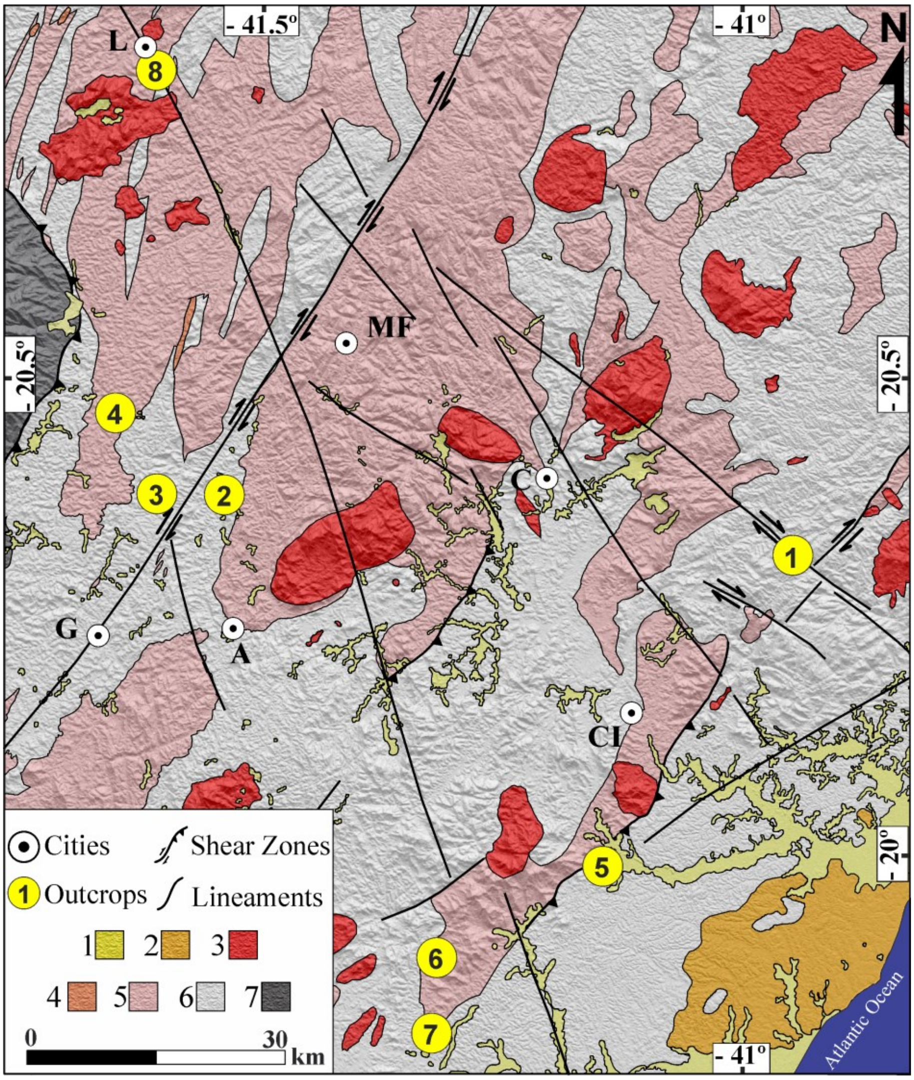

Fig. 2.2: Regional geological map showing lithotypes and geological framework of study area (modified from Horn et al. (2007); Novo et al. (2014) and Vieira and Menezes (2015), with location of sampling outcrops. ASTER GDEM image from ERSDAC (2013). Lithological units: 1 = Alluvial-colluvial/coastal deposits, 2 = Barreiras Formation, 3 = G5 Supersuite, 4 = G2 Supersuite, 5 = G1 Supersuite, 6 = Metasedimentary and metavolcanosedimentary rocks, 7 = Basement complexes. Shear zones: G = Guaçuí, B = Batatal. Lineaments: A = Alegre, I = Itaoca, P = Piúma. Cities: A = Alegre, CI = Cachoeiro de Itapemirim, G = Guaçuí, L = Lajinha, MF = Muniz Freire, C = Castelo.

The Caparaó Suite, a Paleoproterozoic remaining unit, is a granulitic association with enderbites, charnockites, diorites, and gabbroic rocks, which occurs in the core of a large antiformal structure at the homonymous mountain range (Noce et al., 2007a).

The metasedimentary and metavolcanosedimentary rocks, metamorphosed in the pre-orogenic stage, are aluminous gneisses derived from calcium-silicate rocks and volcano-sedimentary sequences, with basics and felsic volcanic rocks (Féboli, 1983; Pedrosa-Soares et al., 2008). This association is included in the Paraíba do Sul Complex (Féboli, 1983) or in the Undivided Paragneisses Complex (Pedrosa-Soares et al., 2008), and the provenance of these rocks can be related to passive margin sequences or arc complexes (Pedrosa-Soares and Wiedemann-Leonardos, 2000).

The magmatic suites are 630 to 460 Ma in age and register the various orogenic stages of the Brazilian-Pan African event (Pedrosa-Soares et al., 2001, 2007, 2008; Pedrosa-Soares and Wiedemann-Leonardos, 2000; Silva et al., 2005; Fig. 2.2). The G1-Supersuite, pre-collisional, is related to the edification of the Araçuaí Orogen magmatic arc and is composed mainly by ortho-derivative rocks of tonalitic and granodiorite protoliths (Pedrosa-Soares and Wiedemann-Leonardos, 2000; Pedrosa-Soares et al., 2008, 2011). The G2-Supersuite, sin-collisional, is related to deformation and regional metamorphism and involves Type-S granitic protoliths, such as peraluminous, sub-alkaline, and calcium-alkaline granites (Pedrosa-Soares et al., 2008, 2011). In the post-collisional stage, the plutons of G5-Supersuite formed, characterized as Type-I, with granite and charnockite, besides gabbro (De Campos et al., 2004; Pedrosa-Soares et al., 2008).

The gneissic foliation, also related to the Brazilian-Pan African Cycle, has a main trend in the NE-SW to N-S striking (Wiedemann et al., 2002), while the mylonitic foliation occurs along the shear zones with NE-SW to NNE-SSW striking. These shear zones, such as the Guaçuí Shear Zone (GSZ) and the Batatal Shear Zone (BSZ) (Fig. 2.2) are related to an orogenic lateral escape at the final collisional phase (Cunningham et al., 1998; Alkmim et al., 2006).

The Alegre Lineament, with NNW-SSE striking, reflects a regional fault zone that reaches the Campos coastal basin (Calegari et al., 2016). It is considered of Cambrian age, but with distensive reactivation movements that occurred during the rift phase and at the Cenozoic. The Piúma Lineament, another structure that is prominent in the area, was described as a brittle shear zone, with NW-SE striking dipping to SW (Lourenço et al., 2016). According to these authors, it was originated in a post-Brazilian event that promoted NNE-SSW distension and was reactivated most probably in the South Atlantic opening as a normal dextral to transtensional dextral shear zone.

The Cenozoic lithostratigraphic units present in the area are the Miocene siliciclastic sediments of the Barreiras Formation and the quaternary alluvial-coastal deposits (Silva et al., 2004; Vieira and Menezes, 2015; Fig. 2.2).

In this region, there are few studies on the Meso-Cenozoic geological evolution. Relevant studies have been developed in Southeastern Brazil, indicating periods of denudation during the Late Cretaceous, at the Paleogene and the Neogene, linked to the rupture of the Gondwana and the evolution of the coastal basin (e.g., Hackspacher et al., 2004; Cogné et al., 2012; Karl et al., 2013). Further north of the study area, Jelinek et al. (2014) identified three denudation episodes at different periods: Early Cretaceous, Late Cretaceous-Paleocene, and Neogene. Other studies developed in the same region also point out episodes of denudation in the Late Cretaceous and Neogene (Morais Neto et al., 2009) and in the Early Cretaceous and Late Cretaceous-Paleocene (Harman et al., 1998). Jelinek et al. (2014) and Harman et al. (1998) associate the Early Cretaceous denudation to the changing of local base level related to rifting and initial opening of the South Atlantic Ocean. The Late Cretaceous denudation has been associated with mantle anomalies and thermal isostasy, which caused a broad crustal lifting; and the Neogene denudation may have occurred due to climatic change, with a transition to a semi-arid climate (Morais Neto et al., 2009; Jelinek et al., 2014).

2.5 Results

2.5.1 Macroscopic analysis

In the studied outcrops, gneisses, migmatites, and mylonites predominate, with local occurrences of mafic dikes and quartz veins (Fig. 2.2 and 2.3a to c). Gneisses (outcrops 1 and 4-7), migmatites (outcrop 8) and mylonites (outcrops 2 and 3) occur as weathered rocks from reddish to whitish in color. The minerals macroscopically identified in the filling materials are quartz, feldspars, white mica, biotite, white clay and, occasionally, red and orange clay. Most samples of filling materials in brittle structures developed in gneisses show manganese oxide in the form of a black clayey material, which compounds millimetric pellicles over discontinuity planes, such as foliation and fractures. Occasionally, oxide pellicles in planes show striations, indicating kinematics (Fig. 2.4a to c).

One of the samples (outcrop 1) is from a quartz vein that contains white mica, white clay, and manganese oxide with botryoidal habit and dendritic structure; the oxide composes thin black pellicles that fill fissures (Fig. 2.4d to f). The diabase dikes are generally weathered and occur in outcrops 1, 5, 7, and 8. Macroscopically it is possible to observe orange, red and white clays, quartz, besides feldspars and black oxide. The oxide is on discontinuity planes, mainly in the contact between the dike and the host rock and also in striated plans (Fig. 2.4g to h).

Fig. 2.3: Field characteristics of some studied outcrops: (a) weathered gneiss (Outcrop 1, sample 1-A); quartz vein with black oxide (Sample 1-B) and diabase dike (Sample 1-D); (b) Mylonitic gneiss with foliation to N10E/85SE (Outcrop 2, sample 2-B) and (c) Weathered gneiss (Outcrop 7).

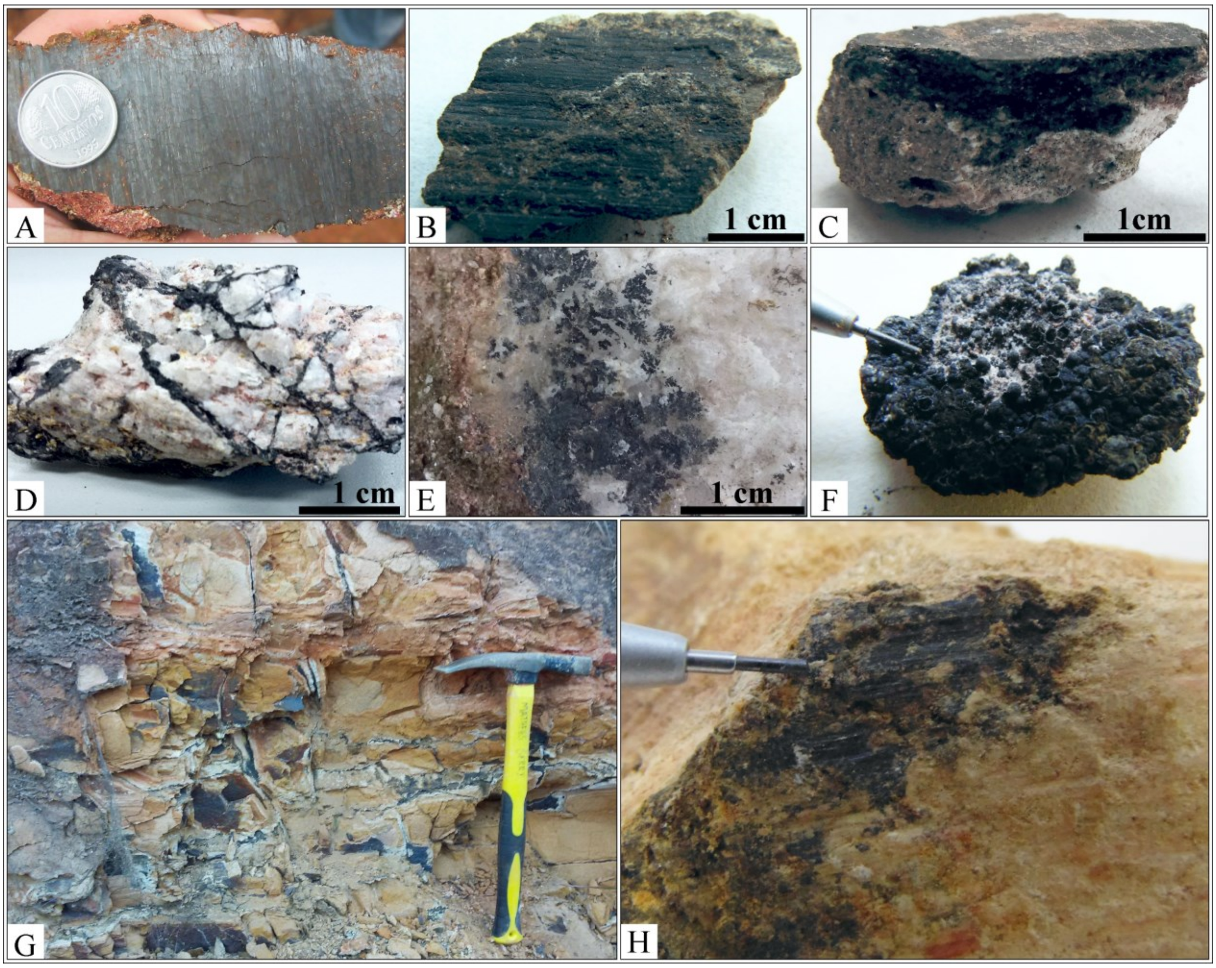

Fig. 2.4: Manganese oxide pellicles on discontinuity planes showing fault striations: (a) Sample 3-A, Outcrop 3; (b) Frontal and (c) lateral view of the Sample 8-A, Outcrop 8. Manganese oxides collected in quartz vein: (d) filling fissures; (e) composing dendritic forms and (f) showing botryoidal habit (Sample 1-B, Outcrop 1). (g) Fractured diabase dike with manganese oxide filling the discontinuities (Outcrop 8) and (h) striations marked on this material (Sample 8-E).

2.5.2 Diffractometric Analysis

The samples analyzed by x-ray diffractometry are representative of the black and clayey filling material in gneisses, quartz vein, and mafic dikes. The chemical composition of the primary and weathering minerals found in these samples are shown in Tab. 2.1.

	Mineral	Chemical Composition
Primary Minerals	bannisterite	$KCa(Mn^{2+}, Fe^{2+}, Zn, Mg)_{20}(Si, Al)_{32}O_{76}(OH)_{16}.4\text{-}12H_2O$
	microcline	$KAlSi_3O_8$
	muscovite	$KAl_2(Si_3Al)O_{10}(OH,F)_2$
	quartz	SiO_2
	rutile	TiO_2
	titanite	$CaTiSiO_5$
Weathering Minerals	birnessite	$(Na, Ca)_{0.5}(Mn^{4+}, Mn^{3+})_2O_4.1.5H_2O$
	goethite	$\alpha\text{-}Fe^{3+}O(OH)$
	hematite	$\alpha\text{-}Fe_2O_3$
	hydrobiotite	$[K(Mg, Fe^{2+})_3(Al, Fe^{3+})Si_3O_{10}(OH, F)_2].[(Mg, Fe^{2+}, Al)_3(Si, Al)_4O_{10}(OH)_2.4H_2O]$
	illite	$(K, H_3O)(Al, Mg, Fe)_2(Si, Al)_4O_{10}[(OH)_2,(H_2O)]$
	kaolinite	$Al_2Si_2O_5(OH)_4$
	lithiophorite	$(Al, Li)Mn^{4+}O_2(OH)_2$

Tab. 2.1: Primary and weathering minerals found in the samples by XRD analysis (chemical composition from Anthony et al., 2001).

In gneisses filling materials, it's observed the characteristic peaks of quartz, muscovite and microcline, and the weathering minerals kaolinite, illite, hydrobiotite, and hematite; in one of the samples, the goethite occurs, and two of them display bannisterite (Fig. 2.5).

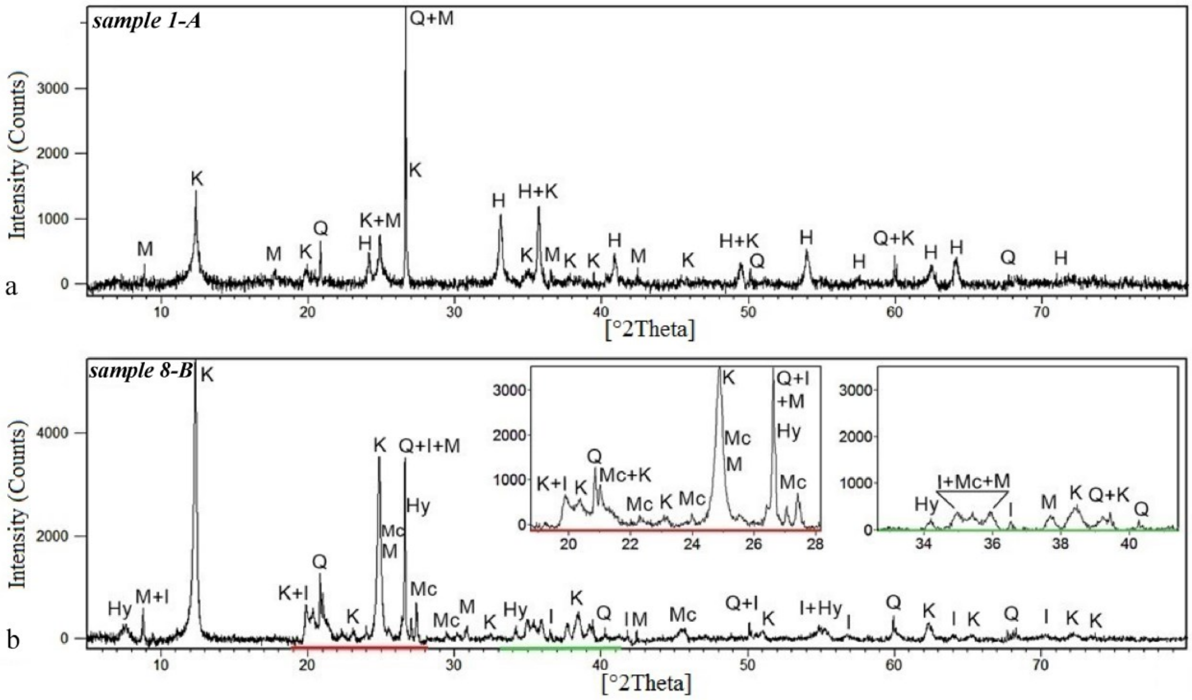

Fig. 2.5: Diffractograms of gneisses: samples (a) 1-A (see Fig. 2.3b) and (b) 8-B (H = hematite, Hy = hydrobiotite, I = illite, K = kaolinite, Mc = microcline, M = muscovite, Q = quartz).

The kaolinite (Fig. 2.5a and b) and illite (Fig. 2.5b) are clay minerals common in soils (Velde and Meunier, 2008). The hydrobiotite (Fig. 2.5b) is a phyllosilicate formed in the initial stages of weathering (Anthony et al., 2001). The iron oxide and hydroxide identified in several samples are hematite (Fig. 2.5a) and goethite. These minerals indicate different stages of iron oxidation, different humidity conditions, pH, Eh, and microbial activity during the weathering (Velde and Meunier, 2008).

The manganese minerals lithiophorite and birnessite occur on the fault planes, foliation, and fractures of gneisses (Fig. 2.6). These minerals give a typical black color to the hand samples and are commonly associated with the presence of iron oxides (Velde and Meunier, 2008).

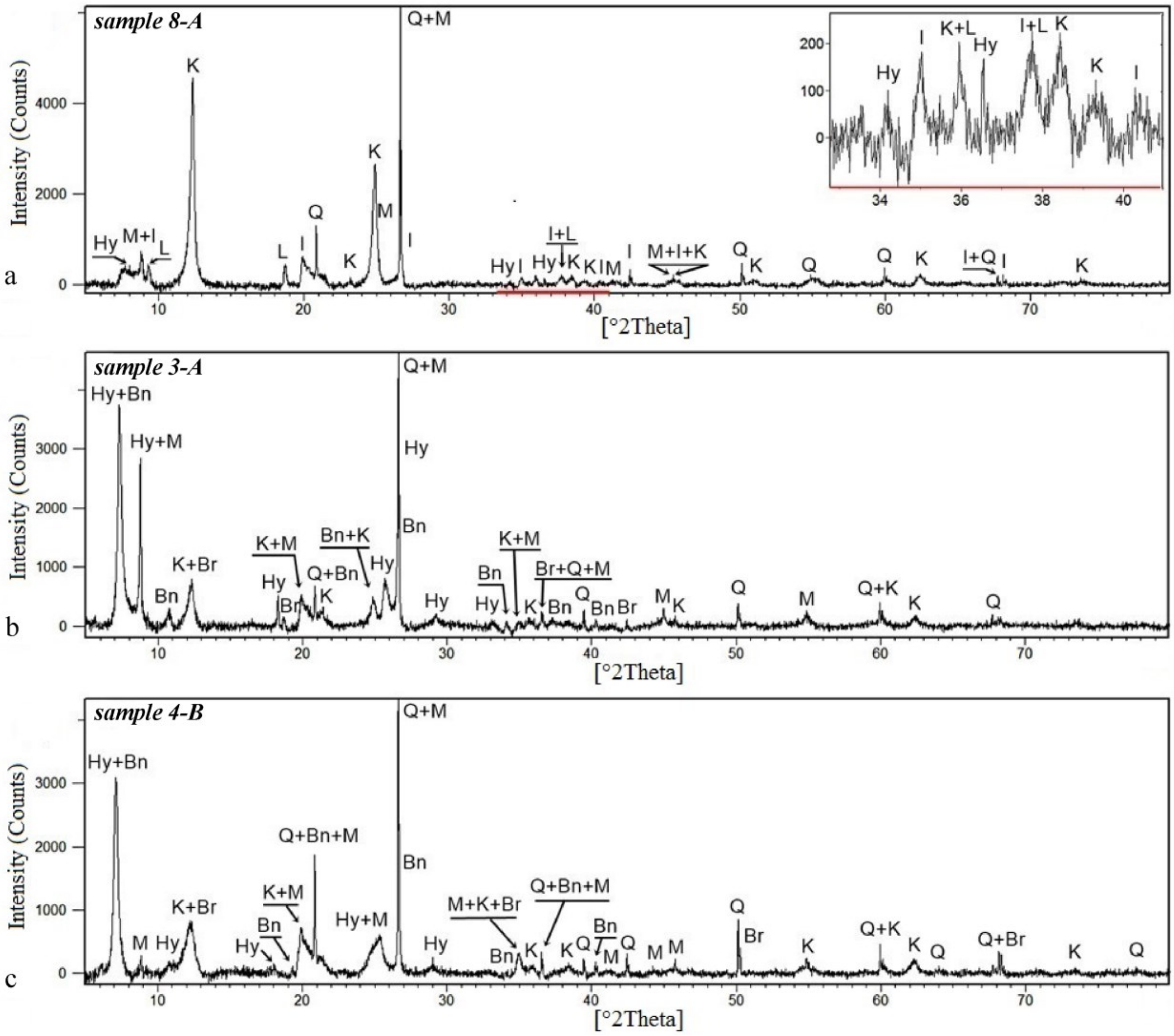

Fig. 2.6: Diffractograms of the black filling material found on fault planes, foliation and fractures of gneisses. Samples: (a) 8-A (see Fig. 2.4b and c); (b) 3-A (see Fig. 2.4a) and (c) 4-

B. (Bn = bannisterite, Br = birnessite, Hy = hydrobiotite, I = illite, K = kaolinite, L = lithiophorite, M = muscovite, Q = quartz).

The bannisterite was also identified (Fig. 2.6b and c). It is a primary mineral with manganese as the main cation (Dunn et al., 1981) and occurs in manganese and zinc-bearing metamorphosed rocks (Anthony et al., 2001). This mineral can be related to the manganese field that occurs in the region of the Caparaó Mountain Range, according to Vieira and Menezes (2015). The other primary minerals identified are remnants that were not affected by weathering.

The quartz vein presents the peaks of quartz, muscovite, kaolinite, and lithiophorite appear (Fig. 2.7a), while the clayey filling material in the fractures presents peaks of quartz, illite, and kaolinite (Fig. 2.7b).

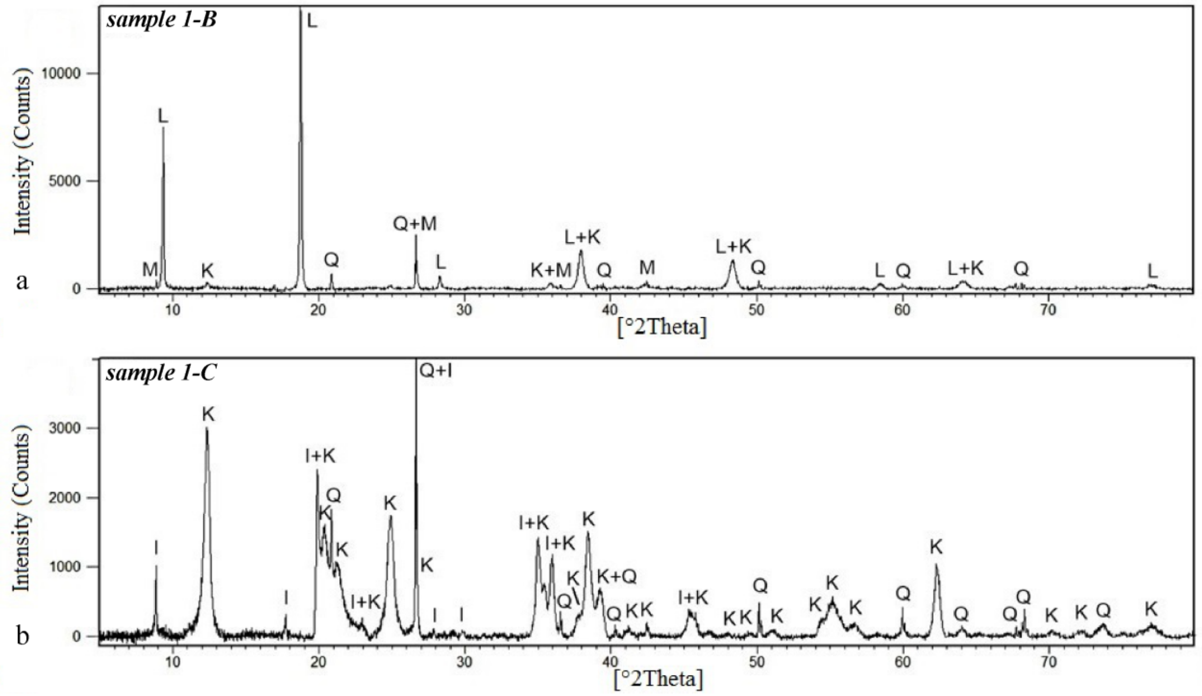

Fig. 2.7: Diffractograms of the materials collected in the quartz vein. (a) Black manganese material (sample 1-B, see Fig. 2.3a and d to f) and (b) fracture filling material in the quartz vein (Sample 1-C) (I = illite; K = kaolinite; L = lithiophorite; M = muscovite; Q = quartz).

The mafic dikes have quartz, kaolinite, goethite, and titanite (as shown in Fig. 2.8a), besides rutile, hydrobiotite, and illite. Peaks of lithiophorite, quartz, kaolinite, goethite, illite, and hematite appear in the black filling material of striated fault planes that occur in these dikes, while the birnessite and muscovite were found in a discontinuity plane existent between the dike and the host rock (The mafic dikes have quartz, kaolinite, goethite, and titanite, (as shown in Fig. 2.8b and c).

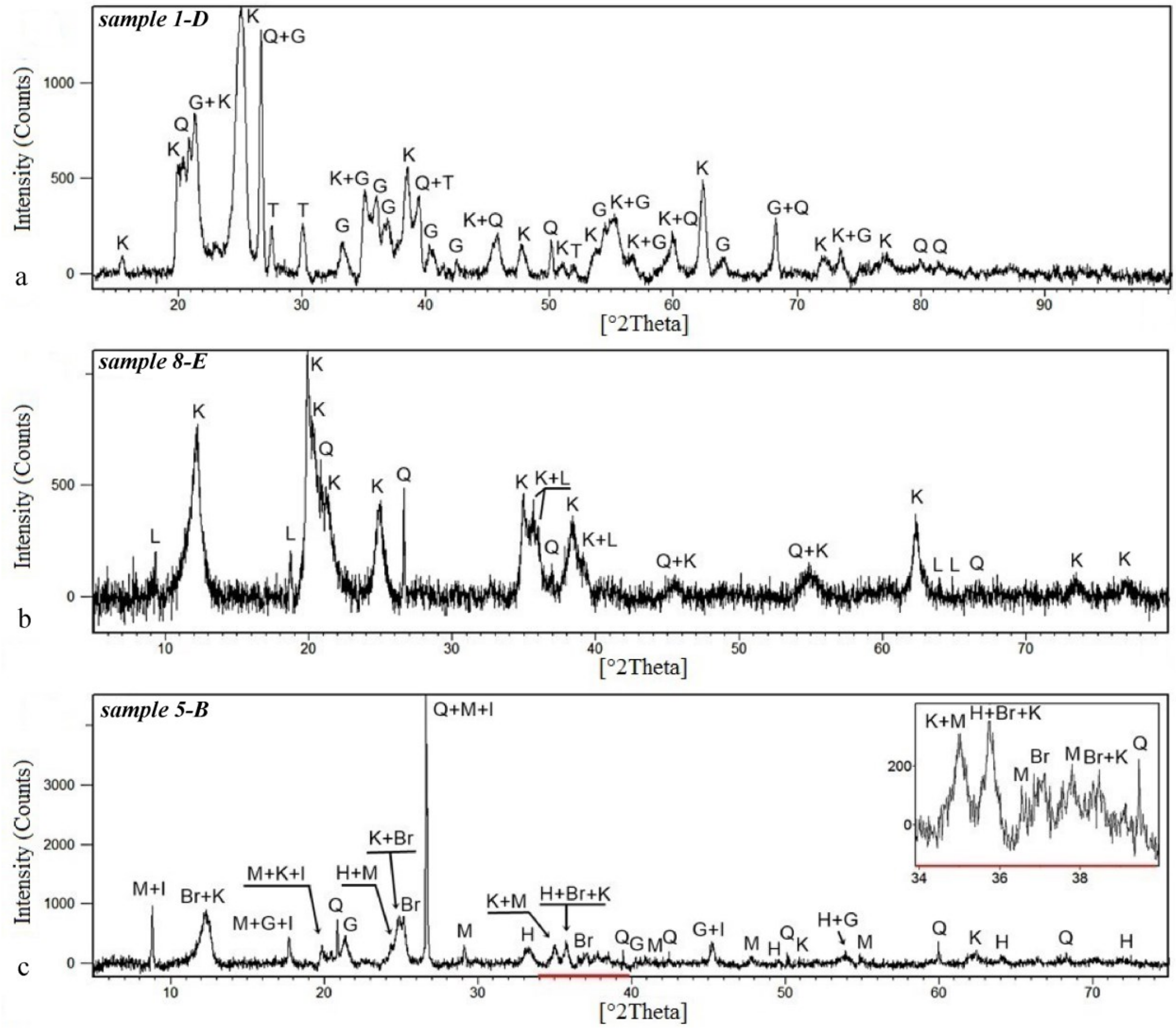

Fig. 2.8: Diffractograms of (a) mafic dike (Sample 1-D, see Fig. 2.3a); (b) and (c) filling material in the mafic dike (Sample 8-E, see Fig. 2.4g and h) and (Sample 5-B) (Br = birnessite; G = goethite; H = hematite; I = illite; K = kaolinite; L = lithiophorite; M = muscovite; T = titanite; Q = quartz).

2.5.3 Geological structures and kinematics

In the studied outcrops, 73 joints measurements and 75 brittle faults measurements were collected. The joints are distributed into three main families, one main striking NW-SE, with a high dip angle, and two other families oriented to N52E/82NW and N38W/38SW (Fig. 2.9a). In Outcrops – 1 and 2, joints with NW-SE striking are predominant, although NE-SW striking also occurs. In Outcrop-3, there are NE-SW joints, and in Outcrops 4 and 6, preferential trends are absent.

The brittle faults occur in weathered rocks (gneisses and mafic dikes) and have fault striations marked in thin layers of the filling materials. These rupture plans are associated with normal, normal oblique and transcurrent movements; approximately 47% is related to a pure extensional tectonic regime, 23% related to a transtentional tectonic regime, 20% to a radial extensional tectonic regime, and 11% to a pure transcurrent tectonic regime (Fig. 2.9b). The pure extensional regime is composed of mid-angle normal faults, mainly in the NE-SW and NW-SE directions, and are found in outcrops 1 to 6 and 8 (Fig. 2.9c). Oblique faults, related to a transtensional regime, have no apparent uniform orientation and are found in outcrops 1 to 4, 6 and 8 (Fig. 2.9d). On the other hand, normal faults that occur under the extensional radial regime have preferential NE-SW direction with a high dip angle in outcrops 2, 3, 5, and 8 (Fig. 2.9e). The faults associated with a pure transcurrent regime, represented in outcrops 1, 2, 6, and 8, have E-W and N-S direction with a high dip angle (Fig. 2.9f).

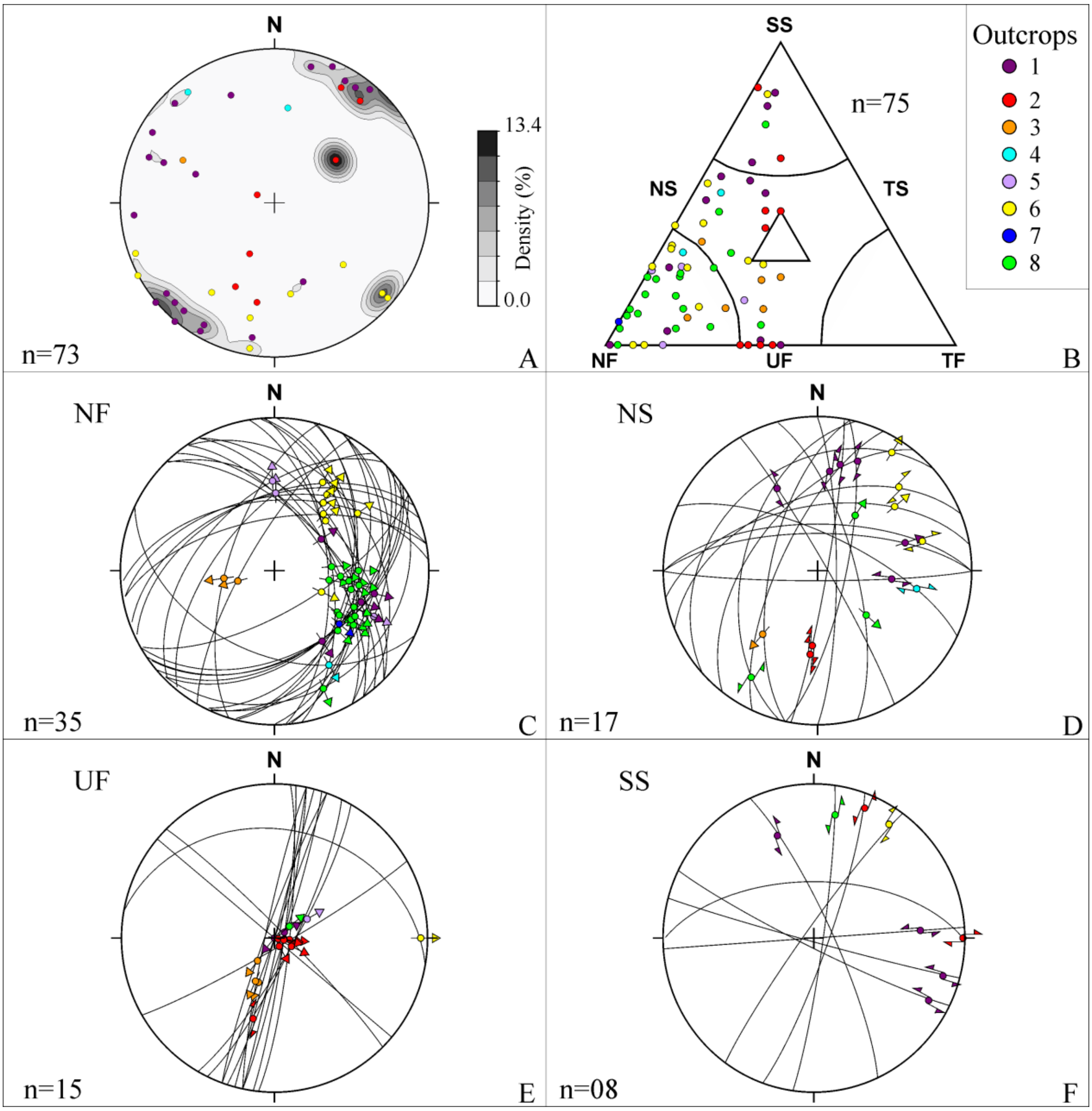

Fig. 2.9: (a) Stereogram of poles of joints, (b) Frohlich Triangle Diagram of fault data, stereograms of the fault data according to the tectonic regime: (c) NF – pure extensive, (d) NS – transtensive, (e) UF – radial extensive and (f) SS – pure strike-slip. (projections in low hemisphere of equal area; striations are represented by colored symbols according to the outcrop; n = number of measures).

The inversion and sectorization of the 75 mapped faults resulted in two different extension paleostress fields, one with NW-SE direction and the other one with NE-SW direction (Fig. 2.10a and b). The NW-SE extensional regime is related to high-angle NE-SW normal faults, measured in outcrops 2, 3 and 8. The NE-SW regime is evidenced by oblique and transcurrent faults in the NE-SW and NW-SE directions, with striations dipping towards NE and SE, found in outcrops 1, 4 to 6, and 8.

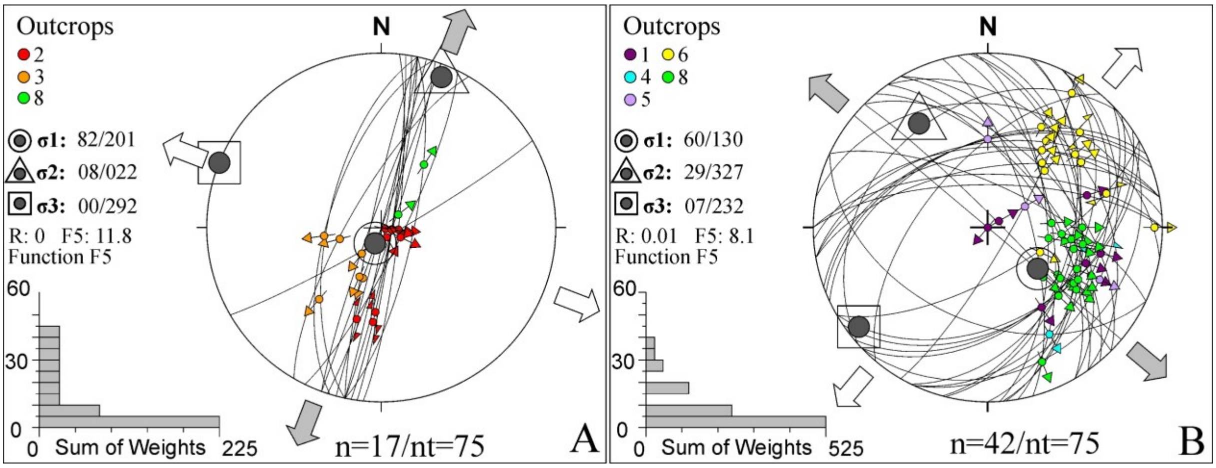

Fig. 2.10: Paleostress regimes obtained by inversion of fault data. (a) Fault data indicate extensional effort in the NW-SE and (b) extensional effort in the NE-SW. (Striations are represented by colored symbols according to the outcrop; stress axis: $\sigma_1 > \sigma_2 > \sigma_3$; n/nt = number of compatible measures/total number of measures).

2.6 Discussion

Field descriptions coupled with DRX analyses allow identifying birnessite, goethite, hematite, hydrobiotite, illite, kaolinite, and lithiophorite as filling materials within brittle structures, generated from weathering processes in gneisses, quartz veins and mafic dikes (Tab. 2.2).

The origin of kaolinite is closely linked to the chemical weathering of feldspars (Oberlin and Couty, 1970; Anthony et al., 2001), while illite originates by weathering of primary muscovite, as from the breaking of mica films in minuscule particles by physical processes until it reaches the clay-size when the primary mineral loses potassium (Velde and Meunier, 2008). Another process of illite formation is from pseudomorphic transformation of K-feldspar during the primary stages of physical weathering (Meunier, 1980, by Velde and Meunier, 2008, p. 248). The hydrobiotite is formed in the initial stages of weathering, originated from the biotite transformation into vermiculite (Anthony et al., 2001; Velde and Meunier, 2008). The Fe-oxyhydroxides originate throughout the weathering process and are formed from the iron extraction of the silicate structure containing the element during the mineral oxidation (Velde and Meunier, 2008). The presence of Mn oxides in soils indicates oxidative conditions of high pH and are commonly associated with iron oxides such as hematite (Vodyanitskii et al., 2004; Churchman and Lowe, 2012). The birnessite and lithiophorite are phyllomanganates (layer structures) that can be associated with the formation of lateritic soils, forming in the initial weathering phases of Mn-rich silicates, like the bannisterite (Anthony et al., 2001; Scheinost, 2004).

		Gneiss	Quartz vein	Mafic dike
		Wall-rock		
Primary Minerals	bannisterite	x		
	microcline	x		x
	muscovite	x	x	
	quartz	x	x	x
	rutile			x
	titanite			x
		Filling material		
Weathering Minerals	birnessite	x		x
	goethite	x		x
	hematite	x		x
	hydrobiotite	x		x
	illite	x	x	x
	kaolinite	x	x	x
	lithiophorite	x	x	x

Tab. 2.2: Minerals found in the filling materials and in the respective wall-rock.

The weathering minerals found in this study commonly occur distributed at different zones of a typical crystalline rock weathering profile (Righi and Meunier, 1995). The clay minerals, such as illite and kaolinite, are concentrated in the saprolite pedoplasma zone (clay-rich), although kaolinite also occurs distributed in the whole profile (Velde and Meunier, 2008). The concentration of Fe-oxyhydroxides, and consequently of Mn oxides, tends to increase towards the top of the profile as the degree of weathering rises (Anand and Paine, 2002; Churchman and Lowe, 2012).

During the weathering processes, the accumulation of secondary minerals along brittle structures occurs from the dissolution of primary minerals by oxygenated waters and subsequent precipitation of different mineral phases in lower portions of the weathered profile. In the crystalline rock weathering profiles, these structures are found at any point of the profile (slightly altered rock, saprock, saprolite), frequently with the association of kaolinite, as the first mineral to form, and the iron oxides that precipitate after the percolation of the fluid (Righi and Meunier, 1995). The filling materials that occur in the fault planes described here belong to this evolutionary scenario and are considered, according to the proposition of Costa (1991), as “fissure ferruginous crusts”.

In the Southern Espírito Santo State, where sedimentary deposits are rare (Fig. 2.2), the difficulties for temporal tying in studies of Cenozoic tectonics can be overcome by correlating the formation of weathering profiles in near regions, where weathering profiles have been dated. In Southeastern Brazil, some authors have dated the weathering profiles distributed along large geomorphological provinces, with decreasing ages from the central region of the state of Minas Gerais to the coastal region of Rio de Janeiro (Carmo and Vasconcelos, 2004; Vasconcelos and Carmo, 2018; Fig. 2.11).

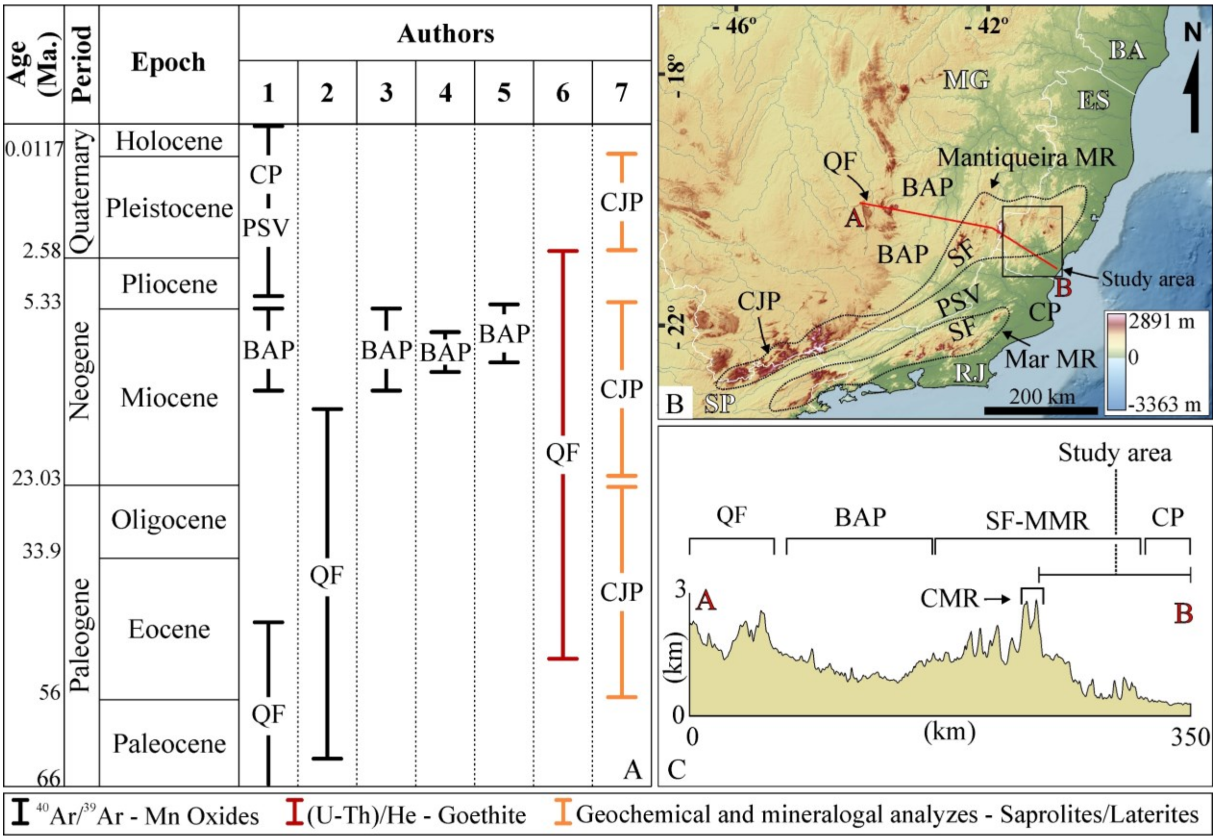

Fig. 2.11: (a) Summary table of ages attributed by previous authors for weathering profiles in the SE Brazil. 1 = Vasconcelos and Carmo (2018); 2 = Spier et al. (2006); 3 = Carmo and Vasconcelos (2006); 4 = Carmo and Vasconcelos (2004); 5 = Vasconcelos et al. (1992); 6 = Monteiro et al. (2014); 7 = Modenesi-Gauttieri et al. (2011). (b) Study area and (c) topographic profile in the context the main geomorphological provinces of SE Brazil. Legend: QF = *Quadrilátero Ferrífero*; BAP = Brazilian Atlantic Plateau; SF = Scarp front; MMR = Mantiqueira Mountain Range; PSV = Paraíba do Sul Valley; CP = Coastal Plain; CMR = Caparaó Mountain Range. States: SP = São Paulo; RJ = Rio de Janeiro; ES = Espírito Santo;

MG = Minas Gerais; BA= Bahia. Digital elevation mode and bathymetry from GEBCO Compilation Group (2020) and geomorphological provinces from Gatto et al. (1983), Carmo and Vasconcelos (2004) and Ross (2011).

Applying the $^{40}Ar/^{39}Ar$ method for dating Mn oxides in duricrusts and laterite deposits at Quadrilátero Ferrífero, Vasconcelos and Carmo (2018) and Spier et al. (2006) obtained ages for the mineral precipitation between 70 to 14 Ma, defining a long and well-marked history of chemical weathering favored by climatic conditions (Fig. 2.11a and b). Monteiro et al. (2014), also in Quadrilátero Ferrífero, used the (U-Th)/He geochronological method in goethite, indicating a historical process of mineral dissolution and precipitation that would be initiated in the Eocene (48 Ma) and continued up to the Pleistocene (2 Ma). Another important Iron field in North Brazil is the Carajás Province, in which Shuster et al. (2012) dated multiple goethite formations through the (U-Th)/He method, in which precipitation occurred between the Eocene (41 Ma) and the Pleistocene (0.7 Ma).

On the Brazilian Atlantic Plateau, Vasconcelos et al. (1992), Carmo and Vasconcelos (2004; 2006) and Vasconcelos and Carmo (2018), also using the $^{40}Ar/^{39}Ar$ method in Mn oxides obtained ages for the formation of weathering profiles in saprolites between the Mid and Neo Miocene (13 to 5 Ma). On the Mantiqueira Mountain Range, at Campos do Jordão Plateau (São Paulo State), Modenesi-Gauttieri et al. (2011) consider three periods of lateritic mantle formation in saprolitic rocks: an alitization and laterite formation phase (Eocene to Late Oligocene), a monosiallitization phase (Miocene), and a podzolization phase (Pleistocene). On the Paraíba do Sul Valley and the Coastal Plain, which are close to the study area, Vasconcelos and Carmo (2018) obtained ages from weathering profiles between 4 Ma to the Present.

Cryptomelane and hollandite are the main datable minerals by the $^{40}Ar/^{39}Ar$ method in the above-cited studies. These minerals were not found in the study area; however, Carmo and Vasconcelos (2006) report that lithiophorite, a mineral identified in the filling materials, occurs as microbands coating crystals of cryptomelane. Therefore, it is possible to consider that the formation of those materials, mainly in Brazilian Atlantic Plateau, Paraíba do Sul Valley and Coastal Plain, is correlated to the evolution of weathering profiles in Espírito Santo State, once the climatic conditions were supposedly similar due to the geographic proximity and the physiographic framework (Fig. 2.11c).

Along this line of thinking, correlating the datable manganese oxides precipitation encountered in the literature - cryptomelane and hollandite - Carmo and Vasconcelos (2004; 2006), Vasconcelos et al. (1992), Vasconcelos and Carmo (2018); to the formation of manganese oxides found in the study area - lithiophorite and birnessite - we consider that the formation of these minerals occurred between the Miocene and the Pleistocene. Similarly, the hematite and goethite precipitation in the filling materials can be correlated to the lateritic process identified by Modenesi-Gauttieri et al. (2011) in São Paulo State, more probably to the phases of the lesser intensity of alteration, between the Miocene and the Pleistocene.

The weathering lateritic materials are usually considered as markers of tectonic stability phases. Tectonic movements that occurred after these phases and printed fault marks on these materials are newer than the lateritic materials. Then, these materials could be considered important chronological markers for the relative dating of faults.

The structural analysis of the described faults, acting after the weathering process, indicates two distensional tectonic regimes: one with the minor horizontal axis directed to NW-SE and other with this axis to NE-SW (Fig. 2.10). This proposition fits some models from previous researchers for the Southeastern Region of Brazil. The minor tension axis to NW-SE can be related to the E-W sinistral transcurrence, acting in the Neogene, and to the NW-SE distension that occurred in the Quaternary (as proposed by Riccomini et al., 1989; Salvador and Riccomini, 1995; Silva and Mello, 2011). Another possibility is that these faults were generated by the gravitational collapse, proposed by Zalán and Oliveira (2005), which would generate a sinistral transtension with the minor axis oriented to NW-SE, between 58 and 20 Ma. The NE-SW distension can be related to a dextral transcurrence that probably acted in the Pleistocene (according to Riccomini et al., 1989; Salvador and Riccomini, 1995; Silva and Mello, 2011 models). We highlight the findings of Calegari et al. (2016), which affirm that, from the Neogene, ancient structures in this area were reactivated as a set of normal faults, subjected to local tension relief. These authors detach, in unison with other authors (such as Bezerra and Vita-Finzi, 2000), that the maximum horizontal axis recovered from reactivated structures can be quite different from the paleostress acting regionally.

Considering that the studied filling materials have been crystallized during the times cited above (Fig. 2.11a) and are marked by the fault striations, we deduce that these faults were generated after the mineral precipitation, namely, after the beginning of Miocene. Probably those events occurred in tectonic pulses, with brittle structures formed in one or more extensional events. Fractures were formed and later filled with minerals newly formed by weathering; the fault striations were posteriorly printed on these filling materials in response to the movements of blocks by, at least, one subsequent extensional event. The displacement of rocky blocks would be facilitated by preexistent discontinuities and clay minerals such as illite, could be formed by dynamic metamorphism, due to the comminution of the original material (muscovite) in the brittle planes, according to Velde and Meunier (2008).

These events are connected to the evolution of the Brazilian Atlantic Margin that developed since the Gondwana fragmentation, as previously studied by several authors that described the lifting and denudation processes of the Brazilian coastal margin. Some authors (e.g., Hackspacher et al., 2004; Cogné et al., 2012; Karl et al., 2013) affirm that such processes initiated in the Late Cretaceous and lasted until the Neogene. Similarly, in Northeastern Brazil, other authors (Harman et al., 1998; Morais Neto et al., 2009; Jelinek et al., 2014) placed the beginning of these events in the Early Cretaceous, persisting up to the Neogene. Anyway, the crustal lifting along the Atlantic margin led to the removal of the more ancient surficial sedimentary covers, which corroborates the idea that the weathered materials analyzed here formed with the maximum age in Miocene, as well as the faults that affected them.

2.7 Conclusions

The data obtained in this work permit to reach the following conclusions:

- The filling material of brittle structures found in the study area consists of primary minerals from the fresh rock and secondary minerals formed by weathering processes.

- The secondary minerals identified, the hydrobiotite, kaolinite, hematite, goethite, lithiophorite, birnessite, and the illite originated by chemical weathering. The illite also can be formed by physical weathering due to the comminution by attrition that occurs during the fault development. The mineralogical association found in the filling materials denotes the action of fluid phases with mineral precipitation at the brittle discontinuities during the weathering processes.

- The formation of the weathering minerals occurred during the Cenozoic, probably between the Miocene and the Pleistocene.

- The faults, which striations are marked on the filling materials, originated after (in the case of the manganese oxides) or during (in the case of the illite) the mineral formation, indicating that the maximum age of these faults is in the Miocene.

- The origin of the brittle structures that affected the filling materials studied here is linked to the uplifting of the Continental Brazilian Margin when ancient geological structures were reactivated as normal faults due to the local action of an extensional regime.

2.8 Acknowledgments

We acknowledge National Council for Scientific and Technological Development (*Conselho Nacional de Desenvolvimento Científico e Tecnológico* - CNPq, project number 870103/2001-6, process number 141700/2018-1) for the scholarship granted to the first author, and Financier of Studies and Projects (*Financiadora de Estudos e Projetos* - FINEP, contract number 01.10.0808.00), for financial support to field works. The scientific results were obtained using Win-Tensor, software developed by Dr. Damien Delvaux, Royal Museum for Central Africa, Tervuren, Belgium. We also thanks to Prof. Dr. Adilson Viana Soares Jr, Prof. Dr. Gustavo Luiz Campos Pires and to the anonymous reviewer of Anuário do Instituto de Geociências - UFRJ for the relevant suggestions that improved this work.

Capítulo III

Brittle deformation and topographic rejuvenation in an elevated passive continental margin not characterized by a sharp escarpment

Salomão Silva Calegari[1], Daniel Peifer[1], Mirna Aparecida Neves[2], Fabrício de Andrade Caxito[1]

[1] Centro de Pesquisa Professor Manoel Teixeira da Costa, Instituto de Geociências, Universidade Federal de Minas Gerais, Belo Horizonte, Brazil
[2] Departamento de Geologia, Universidade Federal do Espírito Santo, Alegre, Brazil

3.1 Abstract

A sharp escarpment lying close to the coast or more in the continental interior defines the morphology of Elevated Passive Continental Margins (EPCMs). Most studies on the dynamics and evolution of EPCMs, including numerical modeling exercises, concentrate on the geometry and evolution of escarpments located at or near a continental drainage divide. However, topographic relief varies considerably along the length of an EPCM, as one can observe in southeastern Brazil and southeastern Australia, and in some cases, the steep, wall-like escarpment may not be present. Here we explore the post-rift brittle tectonic evolution and its influence on channel steepness and drainage network geometry in one such EPCM not characterized by a sharp escarpment (southeastern Brazil). We show a relatively large number of NE-SW and NW-SE oriented brittle structures with slickensides recorded on filling materials following the orientation of pre-existing basement structures, suggesting a multiphase brittle deformation with at least two main paleostress tectonic regimes between the Miocene and Pleistocene. Topography in the landscape is characterized by a regional zone of high channel steepness and local relief extending continuously through the middle part of all seaward-dipping catchments. In this regional "belt" of high topography lies many knickpoints, and all rivers crossing it are marked by non-linear shapes in χ-elevation space. We interpret this "belt" as a regional knickzone anchored in reactivated pre-existing structures. Our results indicate post-Miocene brittle deformation and topographic rejuvenation. However, the origin of the regional drainage divide and adjacent areas located considerably upstream of the regional knickzone must predate the topographic resurgence we infer, implying that older and more recent topographic elements coexist in the landscape. An EPCM not characterized by a prominent escarpment underwent relatively recent topographic rejuvenation and brittle deformation, and these processes are not necessarily linked to the formation or persistence of a "Great Escarpment".

Keywords: Landscape evolution; Passive margin; Brittle deformation; Cenozoic tectonics; Geomorphology.

3.2 Introduction

Passive margins mark the transition between the continental and oceanic lithosphere, forming where rifting processes were followed by oceanic opening during the continental breakup (Bradley, 2008). The present-day morphology of many passive margins is characterized by a prominent escarpment separating a low-relief elevated inland plateau, with elevations ranging from 1-2 km above mean sea level, from a coastal plain (e.g., Japsen et al., 2012a; Green et al., 2013; Summerfield, 2014). Examples of elevated passive continental margins (EPCMs) showing such topographic configuration include southern Africa, eastern Australia, southeastern and northeastern Brazil, western India, Greenland, and Scandinavia. The origin of high topography in EPCMs is enigmatic due to the period since the continental breakup, and many reasons have been proposed to explain its presence and apparent longevity. In most studies, the origin of the high topography in EPCMs is assumed to be related to the rifting process and/or the continental breakup, surviving due to the operation of various mechanisms and interactions capable of driving persistent uplift long after the breakup (e.g., Royden and Keen, 1980; Braun and Beaumont, 1989; Weissel and Karner, 1989; Gilchrist and Summerfield, 1990; Brown et al., 2002). In contrast, other authors argued that the topographic configuration of EPCMs is considerably younger than rifting and breakup and not a direct consequence of these processes, being, instead, an expression of a complex post-breakup history involving episodes of subsidence and burial followed by km-scale exhumation in continental margins (e.g., Japsen et al., 2006, 2009, 2012a; Green et al., 2013, 2018). However, mechanisms for such post-rift topographic rejuvenation are relatively poorly understood, with compressional far-field stresses or mantle plumes invoked as possible causes (e.g., Jones et al., 2002; Japsen et al., 2012a).

Many approaches have been used to investigate the landscape dynamics and evolution of EPCMs, resulting in an extensive body of observational constraints supporting different views on how these landscapes develop. These empirical constraints include offshore sedimentary data, which often suggest oscillations in erosion and sedimentation rates through time (e.g., Gunnell and Fleitout, 1998; Sugden and Denton, 2004; Contreras et al., 2010; Japsen et al., 2012b); cosmogenic nuclide inventories that, in general, imply low denudation rates in various EPCMs (e.g., Cockburn et al., 2000; Portenga and Bierman, 2011; Sosa Gonzalez et al., 2016); and low-temperature thermochronological data, in particular, fission track dating and (U-Th)/He dating in apatite, showing that the post-rift denudation of EPCMs was not slow and steady through space or time (Japsen et al., 2006, 2009, 2012b; Cogné et al., 2011, 2012; Wildman et al., 2019). Furthermore, various numerical modeling studies simulated passive margin escarpments' evolution in the last few decades, which deepened, particularly when combined with empirical constraints, our understanding of the timing, style, and controlling factors of uplift and erosion in these settings (e.g., Gilchrist and Summerfield, 1990; van der Beek et al., 2002; Braun and van der Beek, 2004; Sacek et al., 2012). Nonetheless, there are many unresolved questions about the dynamics and geomorphic history of EPCMs (Braun, 2018).

A sharp escarpment defines the large-scale morphology of an EPCM. However, there is significant variability in the location of the escarpment, which might be placed close to the coast (e.g., Mar Range, Brazil) or more than 100 km in the continental interior (e.g., the southwestern African margin), as well as in its topographic expression, that can be very steep or only dip gently towards the coast. In particular, topographic relief is not homogeneous along a single passive margin, which shows, instead, substantial along-strike variations in morphology (see Fig. 3.1 in Braun, 2018). Nevertheless, most studies investigating landscape evolution in EPCMs were carried out in study areas marked by a prominent escarpment located close to regional drainage divides (e.g., Brown et al., 2000; Japsen et al., 2012a; Sacek et al., 2012; Braun, 2018), whereas few studies explored topographic development in passive margins not defined by a sharp escarpment.

We investigated one such EPCM, the northern end of the Mantiqueira Range (Brazil), where the regional drainage divide and adjacent areas are relatively flat, and they distinguish a gently seaward-dipping region. The prominent escarpment that characterizes the southern portion of the Mantiqueira Range is not present in this northern counterpart (Fig. 3.1), and neither is the continental Cenozoic rift system referred to as Continental Rift of Southeastern Brazil (Riccomini et al., 1989). In the well-studied southern part of the Mantiqueira Range, a wealth of sedimentological and thermochronological data are generally interpreted as indicative of post-rift tectonic reactivation, with two main phases of cooling (i. Upper-Cretaceous-Paleogene and ii. Neogene) and km-scale post-rift exhumation (e.g., Hiruma et al., 2010; Cogné et al., 2011, 2012; Franco-Magalhaes et al., 2014; Engelmann de Oliveira et al., 2016a; Souza et al., 2020), whereas fewer studies explored the tectonic history of the northern termination of the Mantiqueira Range. Yet some authors argue that the northern end of the Mantiqueira Range also experienced post-rift tectonic reactivation based on the deformation of neogenic sediments near the coast (Bricalli and Mello, 2013) and thermochronological data (Jelinek et al., 2014), although the timing, nature, and topographic expression of such reactivation are poorly understood.

Here, we take advantage of modern techniques to perform channel profile analysis, extract knickpoints and patterns of river network orientation from a digital elevation model (DEM), integrated with detailed structural fieldwork on the geometry and kinematics of brittle structures to explore the post-rift brittle tectonic evolution of an EPCM that is not characterized by a sharp escarpment.

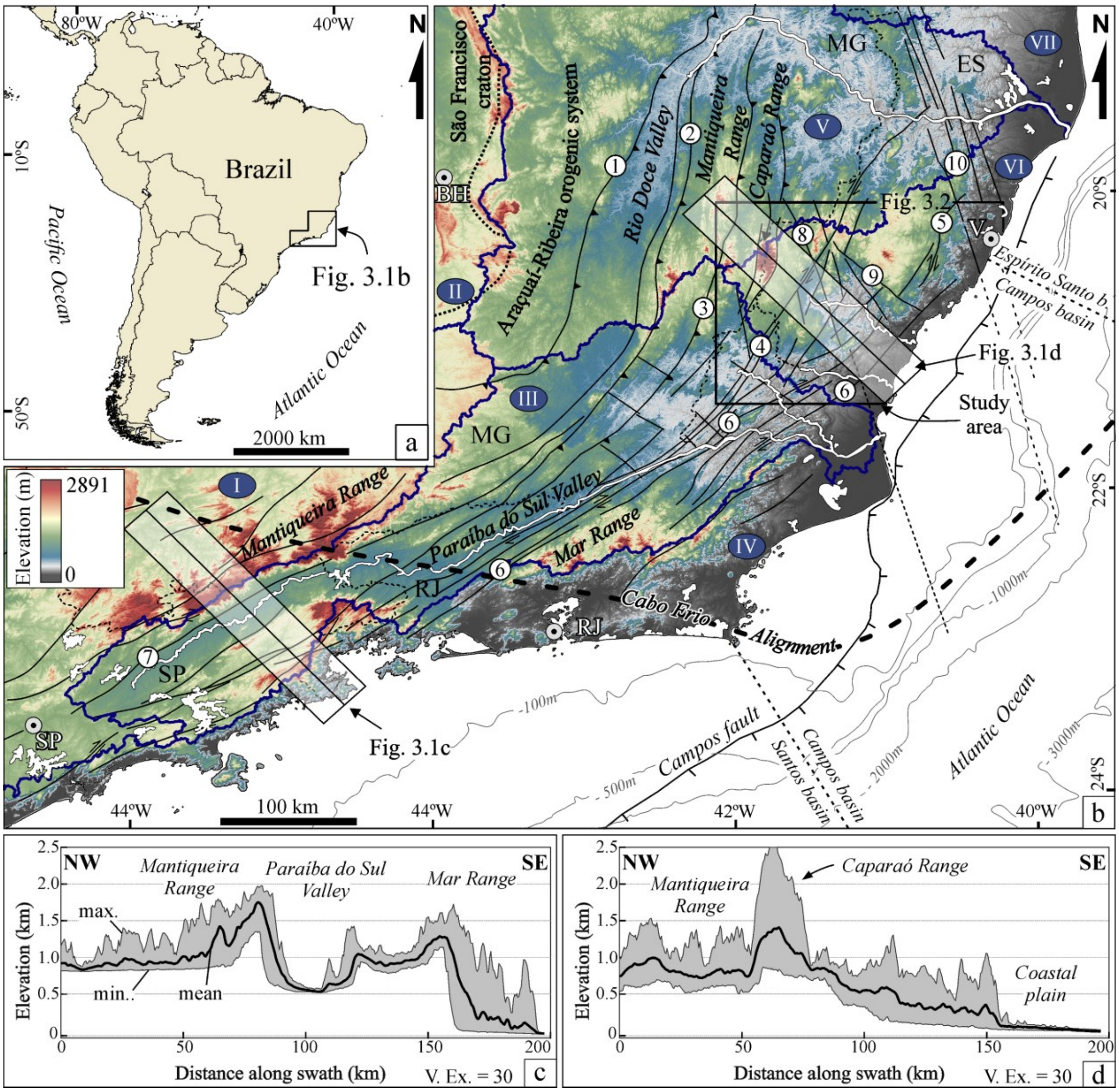

Fig 3.1: Topographic configuration and tectonic features of the continental margin southeastern Brazil. (a) Location of the study area in South America and (b) southeastern Brazil. The study area is located at the northern end of the Mantiqueira Range in the Espírito Santo state. (c) Swath profiles showing the well-defined escarpments in the Mantiqueira and Mar mountain ranges and in (d) a relatively gently dipping surface towards the coast. Swath profiles were made with a 30x vertical exaggeration and 40 km width employing routines in the Topographic Analysis Kit (Forte and Whipple, 2019). Main river catchments: I = Paraná; II = São Francisco; III = Paraíba do Sul; IV = Rio de Janeiro seaward-dipping catchments; V = Doce; VI = Espírito Santo seaward-dipping catchments; VII = São Mateus and Itanhém. Major shear zones: 1 = Dom Silvério; 2 = Abre Campo; 3 = Manhuaçu; 4 = Guaçuí; 5 = Batatal; 6 = Além Paraíba; 7 = Itu. Major structural lineaments: 8 = Alegre; 9 = Piúma; 10 = Colatina.

3.3 Geological setting

The study area is located at the northern end of the Mantiqueira Range, which forms, together with the Mar Range further south, a set of prominent topographic features approximately 1000 km long bordering Brazil´s southeast coast (Fig. 3.1). These mountain ranges configure the transition between the narrow coastal plain and the elevated, low-relief continental interior of the Brazilian Atlantic Plateau, in a typical EPCM setting. However, the topographic relief varies considerably over the Mar-Mantiqueira Range System. In the southern portion of the EPCM, between São Paulo and Rio de Janeiro states, one can observe two steep, well-defined escarpments (Mar and Mantiqueira ranges) oriented parallel to the coast, separated by the CRSB (Fig. 3.1c). In contrast, there is no sharp escarpment associated with the regional drainage divides in the study area, even though there is a substantial elevation drop of 2891 m between the Caparaó Range and the baselevel (Fig. 3.1d). Regional drainage divides are located between 4-70 km away from the coast in the southern part of the EPCM, whereas seaward-dipping catchments extend further into the continental interior in the northern end of the Mantiqueira Range, with regional divides located up to 150 km away from the coast (Fig. 3.1). These catchments in the study area are elongated in the NW-SE direction, extending from the inland regional drainage divide and draining directly to the coast (Fig. 3.2). The Mar-Mantiqueira Range System's regional climate is humid subtropical, ranging from Aw to Cfa-Cfb in Köppen-Geiger's classification (Alvares et al., 2013). Mean annual temperature varies between 17 and 24 °C, and mean annual precipitation varies from 835 to 2109 mm/yr in the study area (Fig. 3.S1; Karger et al., 2017).

The bedrock of these mountain ranges constitutes part of the Araçuaí-Ribeira Orogenic System (Fig. 3.1), formed during the Brasiliano/Pan-African Orogeny (ca. 630 Ma to 480 Ma) (Almeida et al., 1981; Silva et al., 2005; Tedeschi et al., 2016). The oldest units cropping out in the study area are Paleoproterozoic high-grade metamorphic rocks consisting of orthogranulites, charnockites, and enderbites, which compose the orogen basement (Fig. 3.2; Noce et al., 2007a; Heilbron et al., 2016). The Neoproterozoic units from the pre-orogenic stage have a well-marked structural trend, consisting of aluminous gneisses intercalated with calci-siliciclastic rocks and metamorphic volcano-sedimentary sequences, as well as tonalite and granodiorite from the pre-collisional magmatic settings (Pedrosa-Soares et al., 2008; Santiago et al., 2020a). Neoproterozoic S-type granites and leucogranites are associated with the syn-collisional stage, while post-collisional rocks consist of Cambrian gabbro-norites, granites, charnockites, and enderbites (Pedrosa-Soares et al., 2011; Vieira and Menezes, 2015; Heilbron et al., 2016). Semi-consolidated Neogenic sediments from the Barreiras Fm. are exposed in the coastal region (Fig. 3.2). The Barreiras Fm. constitutes a post-Miocene stratigraphic marker widely used to study neotectonics in Brazil (e.g., Bezerra et al., 2014; Lima et al., 2014, 2017; Alves et al., 2019) and is present in a large portion of the Brazilian Atlantic coast. Finally, quaternary alluvial-colluvial and coastal deposits occur in the study area (Fig. 3.2).

Extensive strike-slip to compressive shear zones following roughly a NE-SW to NNE-SSW orientation resulting from the Brasiliano/Pan-African Orogeny characterize southern and southeastern Brazil's morphology (Fig. 3.1; Cunningham et al., 1998; Alkmim et al., 2006). In the study area, NE-SW to NNE-SSW shear zones are present, most notably the Guaçuí, Batatal, and Além Paraíba shear zones (Fig. 3.2), and they form pronounced linear features parallel to the coast (Fig. 3.1). NW-SE to NNW-SSW morphostructural lineaments related to fracture zones or brittle faults such as the Alegre, Colatina, and Piúma lineaments, crosscut the main Brasiliano shear zones (Fig. 3.2; Novais et al., 2003; Calegari et al., 2016; Lourenço et al., 2016). Cambrian to Mesozoic basic dykes occurs in the study area, aligned to the transverse lineaments, suggesting that these have been active since the termination of the Brasiliano orogeny (Fig. 3.2; Santiago et al., 2020b).

The post-breakup geologic evolution of the Brazilian southeastern continental margin is linked to a complex history of uplift events, interactions with pre-existing tectonic structures, and erosional feedbacks (e.g., Gallagher et al., 1994; Tello Saenz et al., 2003). The post-breakup evolution is best studied in the southern part of the Mantiqueira Range, where a large set of apatite fission-track and (U–Th)/He data suggest two main phases of accelerated cooling (Upper-Cretaceous-Paleogene and Neogene) that are interpreted as resulting from tectonic uplift (e.g., Tello Saenz et al., 2003; Hiruma et al., 2010; Cogné et al., 2011, 2012; Franco-Magalhaes et al., 2014; Souza et al., 2020). Such an interpretation is further supported by various geological data, particularly sedimentological and geochronological data on onshore, Cenozoic basins, and Late Cretaceous/Paleogene intrusions (e.g., Riccomini et al., 1989; Cobbold et al., 2001; Contreras et al., 2010; Cogné et al., 2012, 2013).

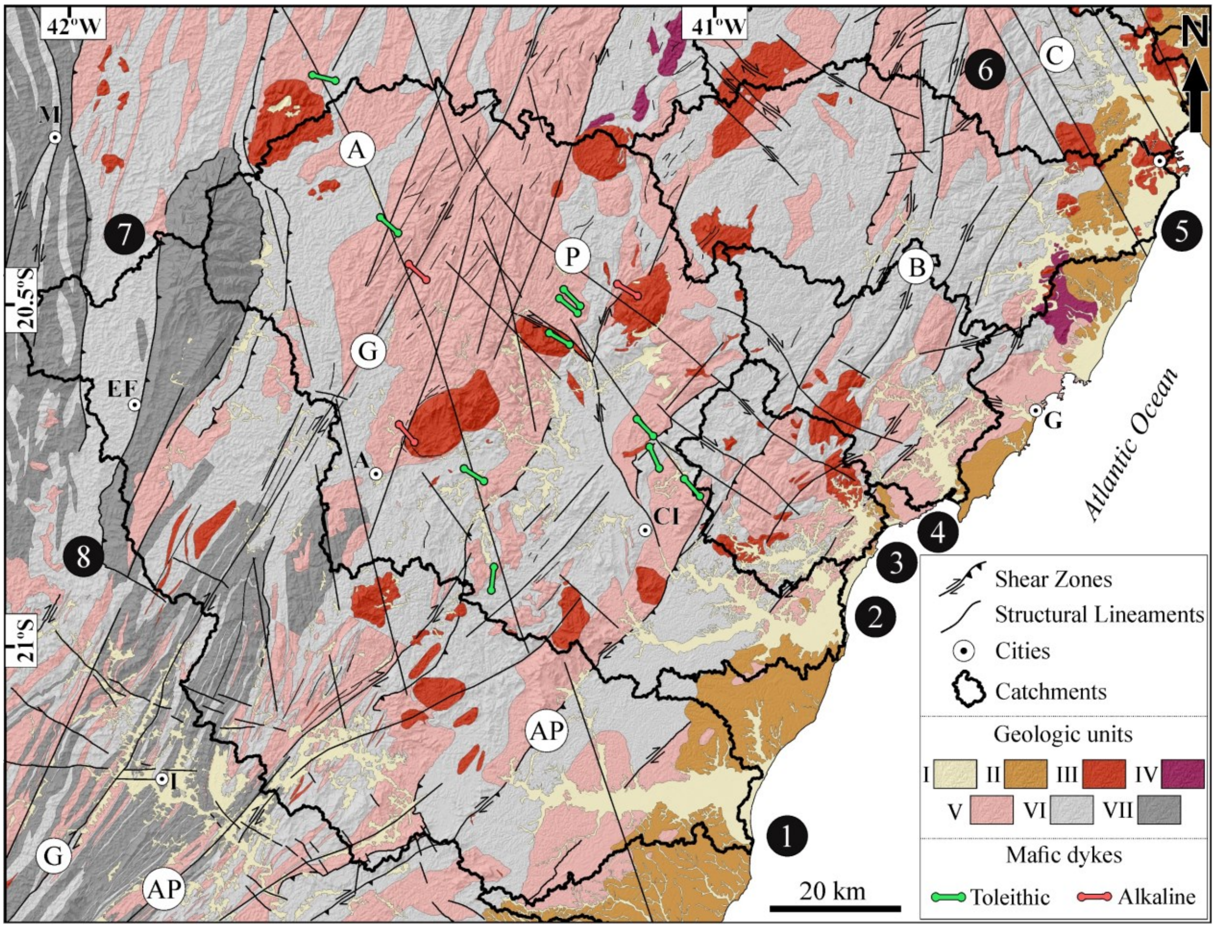

Fig 3.2: Simplified bedrock geology in the study area. Cenozoic covers (I = Alluvial-colluvial/coastal Quaternary deposits and II = Neogene siliciclastic sediments of Barreiras Formation) composes 13% of the geologic units in the study area, whereas crystalline rocks (III = Post-collisional units; IV = Syn-collisional units; V = Pre-collisional units; VI = Neoproterozoic paragneiss complexes; VII = Paleoproterozoic basement) composes 87% of the outcropping rock units. Shear zones and structural lineaments: A = Alegre; AP = Além Paraíba; B = Batatal; C = Colatina; G = Guaçuí; P = Piúma. Cities: A = Alegre; CI = Cachoeiro de Itapemirim; EF = Espera Feliz; G = Guarapari; I = Itaperuna; M = Manhuaçu; V = Vitória. Espírito Santo seaward-dipping catchments: 1 = Itabapoana; 2 = Itapemirim; 3 = Iconha; 4 = Benevente; 5 = Jucu; 6 = Santa Maria. Sub-Catchments of the Doce River: 7 = Manhuaçu. Sub-Catchment of the Paraíba do Sul River: 8 = Muriaé. See location in Fig. 3.1.

The Upper-Cretaceous-Paleogene episode is likely related to the plate's passage over the Trindade Plume, which is recorded by the presence of alkaline massifs (ca. 85-55 Ma) aligned with the Cabo Frio Magmatic Alignment (Fig. 3.1; Thompson et al., 1998; Thomaz Filho et al., 2005). This event was followed by the tectonic development of the Continental Rift of Southeastern Brazil (CRSB) and the deposition of the first sedimentary sequences in the

Cenozoic basins (e.g., São Paulo, Taubaté, Resende) between the Mar and Mantiqueira ranges (Riccomini et al., 1989, 2004; Zalán and Oliveira, 2005). The Neogene cooling recorded in the CRSB region is likely linked to the transpressional reactivation of pre-existing tectonic structures due to far-field stresses (Cobbold et al., 2001; Cogné et al., 2012, 2013). In the northern termination of the Mantiqueira Range, existing low-temperature thermochronological data recorded the Upper-Cretaceous-Paleogene rapid cooling episode, which is also interpreted as an expression of far-field-driven tectonic reactivation of inherited structures (Jelinek et al., 2014; Van Ranst et al., 2020; Fonseca et al., 2021). The Neogene cooling is also recorded, but the explanation for such recent cooling is unresolved, with a high likelihood that it represents an artifact of the numerical inversion of the data (Van Ranst et al., 2020). Nonetheless, some authors proposed, based on brittle deformation affecting the Barreiras Fm., that neotectonics affect the study area, at least where the Barreiras Fm. occur (Bricalli and Mello, 2013; West and Mello, 2020).

3.4 Methods

3.4.1 Field data analysis

The tectonic processes acting on the upper crust are linked to brittle structures' origin, geometry, and kinematics (Faulkner et al., 2010). We carried out field surveys of 487 outcrops to assess the role of brittle deformation in the development of the continental margin in southern Espírito Santo (Fig. 3.S2). The field survey yielded data on 2019 joints (i.e., open fractures), 321 brittle faults, and 444 foliation and banding measurements.

In general, brittle faults can start in three different ways, (i) from pre-existing ductile structures (i.e., foliations and folds), (ii) from pre-existing brittle structures (e.g., joints, veins), or (iii) as new faults within a homogeneous rocky body (Sibson, 1977; Caine et al., 1996; Crider and Peacock, 2004; Collettini et al., 2009; Faulkner et al., 2010; Sperner and Zweigel, 2010). Faults were classified according to their precursor mechanism to evaluate the role of basement anisotropies, as follows: reactivated faults resulting from the reactivation of foliation planes or neoformed faults resulting from either a homogeneous rocky body or pre-existing brittle structures such as precursor joints with the same direction. Furthermore, faults were separated according to the rocky substrate between those affecting the pre-Ordovician basement and those affecting the Barreiras Fm. to establish a hierarchical relationship for the region's observed deformation.

The geometric analysis of the faults was carried out using the fault-slip component diagram (FSC; (Costa et al., 1997) with the Orient software (Vollmer, 2015). The FSC diagram uses the normalized values of *L* (lateral horizontal displacement), *T* (transversal horizontal displacement), and *V* (vertical displacement) originating from the decomposition of the maximum displacement vector (*D*), which coincides with the maximum direction of the shear stress of the fault plane indicated by slickensides. Further details on the method concepts can be found in Costa et al. (1997). The structural data distribution and orientation were also treated using rosette diagrams and density stereograms in the OpenStereo software (Grohmann and Campanha, 2010).

We inverted the fault-slip data using the “Right Dihedron Method” (Angelier and Mechler, 1977) to estimate the four parameters of the reduced stress tensor: the principal stress axes, σ1, σ2, and σ3 (maximum, intermediate, and minimum compression), and the stress ratio R (R = σ2 - σ3 / σ1 - σ3). The stress regime was obtained using the R values as classified by Delvaux et al. (1997): radial extensive (UF; vertical σ1, 0 <R <0.25); pure extensive (NF; σ1 vertical, 0.25 <R <0.75), transtensive (NS; σ1 vertical, 0.75 <R <1 or σ2 vertical, 1 <R <0.75); pure strike-slip (SS; σ2 vertical, 0.75 <R <0.25); transpressive (TS; σ2 vertical, 0.25 <R <0 or σ3 vertical, 0 <R <0.25); pure compressive (TF; σ3 vertical, 0.25 <R <0.75), and radial compressive (UF; σ3 vertical, 0.75 <R <1). Moment tensors are analogous to strain tensors and are represented by the P-T and B axes as the minimum, maximum, and intermediate moment tensor axes, respectively. This technique was developed to assess the distribution of earthquake focal mechanisms (Frohlich, 1992). We used the representation of moment tensors to gain insight into the kinematic behavior of the set of faults recorded in the area. Finally, the “Rotational Optimization” procedure employing the F5 function in the Win-Tensor program (Delvaux and Sperner, 2003) was used to compute paleostress fields from inverted fault data.

3.4.2 Geomorphic analysis

Erosional landscapes tend (or are trying) to achieve steady-state topographic forms if boundary conditions are held fix or vary gradually enough so that rock uplift is everywhere balanced by erosion (Hack, 1960; Montgomery, 2001). Temporal and spatial changes in boundary conditions may determine changes in relative baselevel, causing adjustments in channel form and an overall channel network response in the direction of the steady-state condition (Howard, 1994; Whipple and Tucker, 1999; Kirby and Whipple, 2012). Much of recent research builds on this framework to derive information about the tectonic history of landscapes from topographic data (e.g., Kirby and Whipple, 2012; Whittaker and Boulton, 2012; Duvall et al., 2020; Schwanghart and Scherler, 2020). Following such an approach, we explored spatial patterns in topographic metrics over the northern termination of the Mantiqueira Range and their relationships with potential controls, such as lithology, brittle structures, and precipitation patterns. The topographic data used was a seamless ALOS (Advanced Land Observation Satellite) digital elevation model (DEM) with a resolution of 30 m, downloaded from OpenTopography (https://opentopography.org/) and projected to UTM Zone 24S.

3.4.2.1 Channel profile analysis

Empirical studies in various geomorphic settings demonstrated that local channel slope (*S*) decreases as upstream drainage area (A) increases along a channel profile following the power-law relationship (Hack, 1957; Flint, 1974):

$$S = k_s A^{-\theta} , \qquad (1)$$

where the "channel steepness" (k_s) is a measure of channel slope normalized by catchment size according to a given concavity, and the "channel concavity" (θ) is a quantity that controls the scaling between S and A, defining how concave is a channel profile (Kirby and Whipple, 2012). Derived k_s values depend on the choice of θ, and thus most studies use a fixed "channel concavity" (θ_{ref}) to extract a "normalized channel steepness" (k_{sn}) from topographic data (Wobus et al., 2006; Kirby and Whipple, 2012). Numerous studies demonstrated that k_{sn} is positively related to river incision rates or catchment-averaged denudation rates (e.g., DiBiase et al., 2010; Scherler et al., 2014; Harel et al., 2016), implying that the spatial distribution of k_{sn} is expected to reflect the spatial distribution of erosion, with contrasts in k_{sn} resulting from differences in rock uplift, bedrock erodibility or climate conditions (Wobus et al., 2006; Kirby and Whipple, 2012). In contrast, θ is generally expected to be relatively insensitive to changes in rock uplift, bedrock erodibility, or climate conditions (Wobus et al., 2006; Kirby and Whipple, 2012).

We used the "integral method" of channel profile analysis (Perron and Royden, 2013) to compute the spatial distribution of k_{sn}. This method is based on the integration of Eq. (1) in the upstream direction from an arbitrarily baselevel at x_b, given that $S = dz/dx$ where z is channel elevation and x is the distance along the channel, resulting in:

$$z(x) = z(x_b) + \left(\frac{k_s}{{A_0}^{\theta}}\right)\int_{x_b}^{x}\left(\frac{A_0}{A(x)}\right)^{\theta} dx\,, \tag{2}$$

where A_0 is an arbitrary drainage area added to ensure that the area term is dimensionless (Perron and Royden, 2013). We then define a longitudinal coordinate (χ) with dimensions of length:

$$\chi = \int_{x_b}^{x}\left(\frac{A_0}{A(x)}\right)^{\theta} dx\,. \tag{3}$$

Eq. (2) informs that the slope of transformed channel profiles in χ-elevation space is k_{sn} if A_0 = 1 m^2 and the transformation is based on θ_{ref} (Perron and Royden, 2013). Transformed profiles of all rivers in equilibrium, meaning channels where rock uplift, bedrock erodibility, and climate conditions are invariant along-profile, and so are incision rates, show linear shapes in χ-elevation space, and all equilibrium channels in the network starting at x_b collapse in the same line in χ-elevation space (Perron and Royden, 2013). Spatial variations in incision rates resulting from differences in either rock uplift, bedrock erodibility, or climate conditions will be thus expressed as nonlinear shapes (i.e., inflections) in profiles in χ-elevation space (Perron and Royden, 2013).

We calculated k_{sn} for all rivers flowing in the northern termination of the Mantiqueira Range using routines implemented in the Topographic Analysis Kit (Forte and Whipple, 2019), which is based on functionalities of TopoToolbox (Schwanghart and Scherler, 2014). Following standard pre-processing using carving routines, the drainage network was extracted using a minimum supporting drainage area of 1 km^2 (e.g., Wobus et al., 2006). The k_{sn} extraction used a smoothing window of 1000 m, and we assumed a reference concavity of 0.45 to facilitate comparison between different catchments and other studies (e.g., Wobus et al., 2006; Kirby and Whipple, 2012). Profiles in χ-elevation space were produced using code implemented in TopoToolbox for every river in the studied stream network.

We explored whether spatial variations in k_{sn} are a function of variations in lithology using 1:400.000 geological maps as a base (Vieira and Menezes, 2015; Heilbron et al., 2016) and 1:100.000 and 1:1.000.000 complementary geological maps (Leite et al., 2004a, 2004b; Horn et al., 2007; Noce et al., 2007b; Novo et al., 2012, 2014). Rock units cropping out in the study area were classified into lithological classes based on age and composition (Fig. 3.2): Paleoproterozoic granulites; Neoproterozoic paragneiss; Neoproterozoic orthogranitoids, which includes pre and syn-collisional units; Cambrian granitoids; Neogene siliciclastic sediments, consisting of the Barreiras Fm.; and Quaternary covers, including alluvial-colluvial and coastal deposits.

3.4.2.2 Knickpoint extraction

Spatial or temporal changes in rock uplift, bedrock erodibility, catchment geometry, and climate conditions may determine transient adjustments in the river network and adjacent hillslopes so that the landscape attains equilibrium (Howard, 1994; Whipple and Tucker, 1999; Kirby and Whipple, 2012). River networks affected by spatially uniform changes in relative baselevel fall rates, resulting from, for example, variations in rock uplift (e.g., Whittaker and Boulton, 2012), denudational isostatic rebound (e.g., Bishop and Goldrick, 2010), eustatic sea-level changes (e.g., Bishop et al., 2005), and exposure of rocks with differential erodibility (e.g., Gallen, 2018), are expected to respond by increasing local channel slope in the vicinity of the baselevel, with the formation of knickpoints (Howard, 1994; Whipple and Tucker, 1999). The steepened channel reaches promote faster rates of local channel incision, determining that knickpoints migrate upstream. Tributary junctions are also lowered during the upstream migration of knickpoints, inducing the formation of knickpoints in every tributary, resulting in the transmission of the new baselevel through the entire drainage network (Kirby and Whipple, 2012). The celerity of this propagating wave of river incision depends on the characteristics of the forcing, bedrock channel incision rates, catchment geometry, and the spatial distribution of bedrock erodibility and runoff efficiency (Howard, 1994; Whipple and Tucker, 1999; Kirby and Whipple, 2012). Therefore, the presence, number, characteristics, and, particularly, the spatial distribution of knickpoints archive information on the geomorphic and tectonic history of landscapes (Kirby and Whipple, 2012; Gailleton et al., 2019).

We extracted knickpoints using the "knickpointfinder" code implemented in TopoToolbox (Schwanghart and Scherler, 2014). This automated procedure explores our understanding that elevation along a channel profile should decrease monotonically downstream by iteratively fitting strictly upward concave profiles to raw longitudinal profile data. This algorithm removes a curvature constraint where the offset in elevation between actual and modeled profiles is largest up to a point where this vertical offset is lower than a user-defined tolerance threshold. A higher tolerance threshold determines a lower number of knickpoints identified. We extracted knickpoints using a tolerance value to 70 m, which is a higher value than the uncertainty of our river profile data (69 m) estimated as the maximum difference between the downstream minima and upstream maxima of our data (Schwanghart and Scherler, 2017).

3.4.2.3 Extracting local relief and hillslope angle

Various empirical studies demonstrated that erosion processes are more effective when local relief and hillslope angle are higher, and these topographic metrics are often used to infer erosion rates (Ahnert, 1970; Montgomery and Brandon, 2002; Portenga and Bierman, 2011). Here we computed local relief as the elevation range in a neighborhood defined by a circular window using the "localtopography" code in TopoToolbox (Schwanghart and Scherler, 2014). The window size was defined based on a sensitivity analysis where local relief was calculated with window radius varying from 0.5 to 5.0 km (e.g., Peifer et al., 2021). We compared how mean values of local relief extracted using different window sizes correlate with mean values of k_{sn} for all catchments in the study area with stream-order higher than the second-order. Mean values of local relief extracted using a 1.5 km-radius circular window are more strongly correlated with mean values of k_{sn}, and hence we used this window size in this study. Hillslope angle measurements were taken for each cell in the DEM using the "gradient8" code in TopoToolbox (Schwanghart and Scherler, 2014).

3.4.2.4 Computing river network orientation

River networks are known to reorganize themselves dynamically in response to crustal deformation (e.g., Whipple and Tucker, 1999; Kirby and Whipple, 2012), and recent modeling studies indicate that river drainage patterns have the potential to archive information about the tectonic history of landscapes (e.g., Castelltort et al., 2012; Duvall et al., 2020). We explored spatial patterns of river network orientation in the study area using routines implemented in TopoToolbox (Schwanghart and Scherler, 2014), and we investigated how the orientation of river segments is distributed as a function of the orientation of morphostructural lineaments, lithology, ksn, and stream-order. To compute the river network orientation, we identified river segments and calculated segment geometry using the "orientation" routine in TopoToolbox, which computes the clockwise azimuthal values between the upstream and downstream coordinates for each defined channel segment. River segments were determined at every 1000 m of distance along a channel for the entire drainage network, which is large enough distance along the profile to avoid spurious large variability in geometry at short distances. Following recommendations in O' Leary et al. (1976), we used a combination of visualization methods in relief-shaded raster models produced using routines in TopoToolbox, with sun azimuth set at 0º, 45º, 90º, and 315º, to identify natural topographic lineaments (referring to linear, aligned landforms that may be related to underlying crustal structures such as faults, folds, and foliations). Mapped morphostructural lineaments were divided between lineaments > 5 km and < 5 km and plotted on rose diagrams in azimuthal values computed based on each feature's start and end point coordinates. We emphasize that some mapped morphostructural lineaments are structural features documented in the literature, such as the shear zones Guaçuí, Batatal, and Além Paraíba (Cunningham et al., 1998; Alkmim et al., 2006) and the fracture zones Alegre, Piúma and Colatina (Novais et al., 2003; Calegari et al., 2016; Lourenço et al., 2016).

3.5 Results

3.5.1 Field structural data

The studied outcrops (Fig. 3.S2) are distributed in two main lithological compartments: basement rocks (e.g., paragneisses, orthogneisses, migmatites, granites, amphibolites, granulites, and gabbros) and Neogene sediments from the Barreiras Fm. The basement outcrops occur as weathered rocks in different weathering stages, from fresh rocks to rocks in early weathering stages (with the most resistant minerals still preserved) and up to deeply weathered saprolitic rocks. The foliation data, collected in both weathered and fresh rocks, occur as gneissic banding and mylonitic foliation, composing two main NE-SW sets with SE medium to high dip angle (Fig. 3.3a). Joints occur mainly as continuous and regular discontinuities with a high dip angle distributed in three main sets in NNE-SSW, NW-SE, and WNW-ESE directions (Fig. 3.3b). Joints in fresh rocks (74% of our joint data) comprise two main groups distributed in the NE-SW and WNW-ESE directions (Fig. 3.3c), whereas joints in the weathered basement rocks (24% of our joint data) are oriented NW-SE (Fig. 3.3d) preferentially. Joints in the Barreiras Fm. (2% of our joint data) show less pronounced orientations, yet the NE-SW and NW-SE trends are apparent.

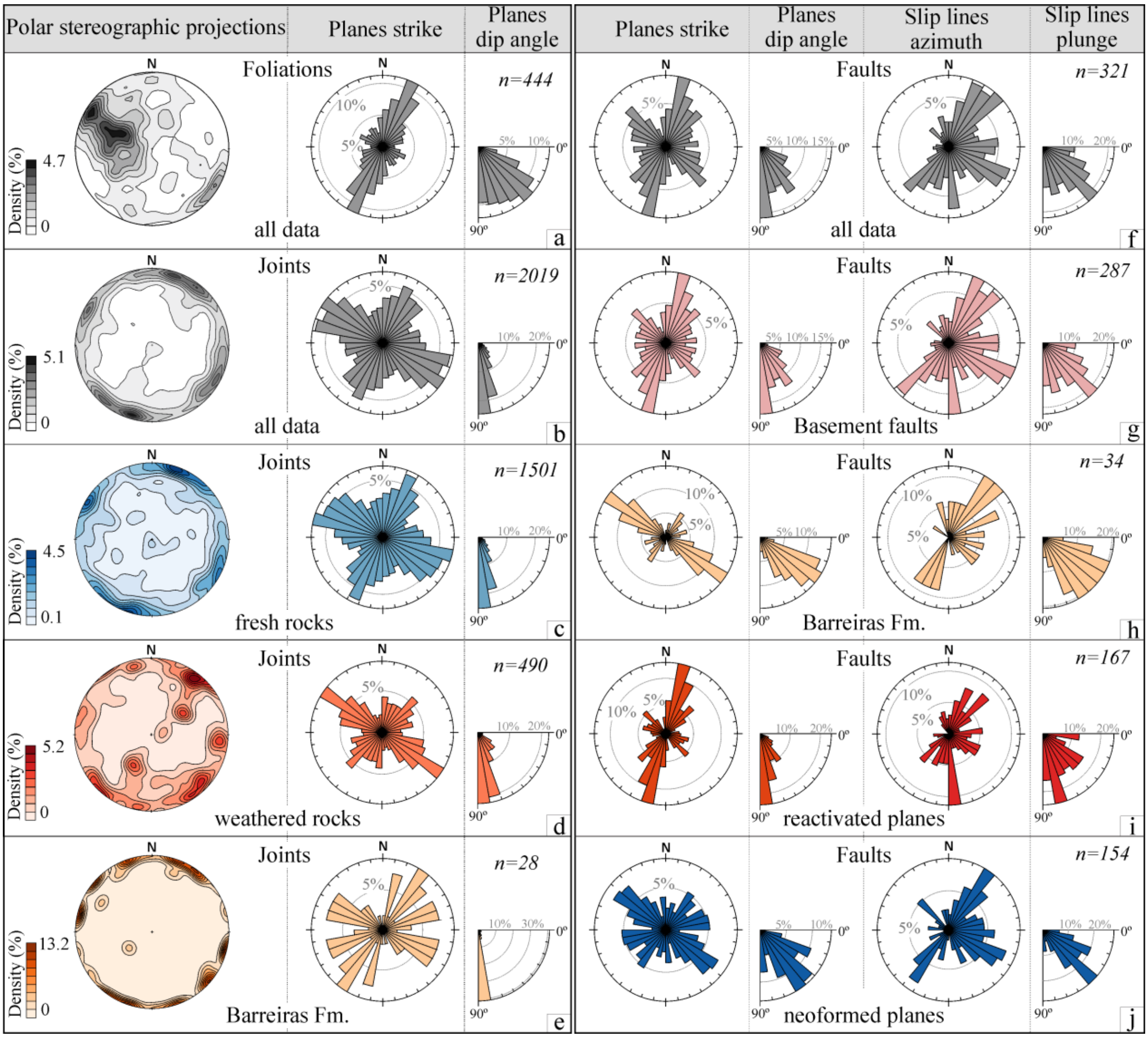

Fig 3.3: Polar stereographic projections and rose plots showing the structural data distribution measured in the field. (a) all foliation data; (b) all joint data; (c) fresh rock joints; (d) weathered rock joints; (e) Barreiras Fm. joints; (f) all fault data, (g) basement faults; (h) Barreiras Fm. faults; (i) reactivated fault planes and (j) neoformed fault planes. Polar stereographic projections employ a low hemisphere projection in a grid of equal area, and rose plots use equal-area distributions.

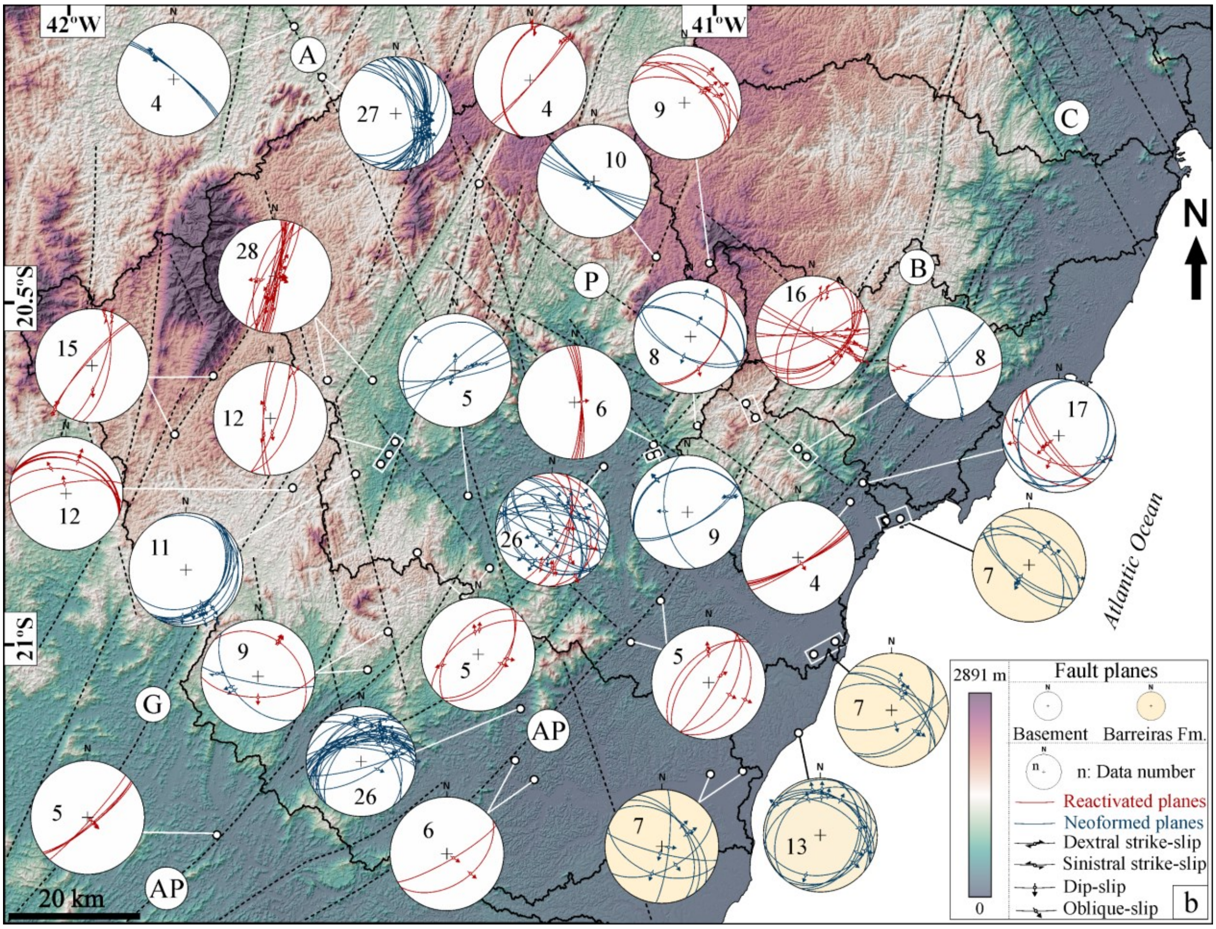

Fig 3.4: Spatial distribution of faults and slickensides draped over a 315° azimuth shaded relief. Dashed black lines show morphostructural lineaments, white points indicate outcrops with measured faults, and black lines delineate catchments' limits. The scientific color map of Thyng et al. (2016) was used to represent elevation data avoiding visual distortions. Polar stereographic projections employ a low hemisphere projection in a grid of equal area. Structural lineaments: A = Alegre; AP = Além Paraíba; B = Batatal; C = Colatina; G = Guaçuí.

We observe slickensides in thin layers of filling materials in faults in the weathered basement rocks (90% of our fault data) and Barreiras Fm. (10% of our fault data) (Fig. 3.4). These filling materials are composed of secondary minerals such as hydrobiotite, illite, kaolinite, hematite, goethite, and lithophorite (Calegari et al., 2020). Fault planes show two main directions, NNE-SSW with SE medium to high dip angle and NW-SE with sub-vertical dip (Figs. 3.3f, 3.4 and 3.S3). Fault planes in the Barreiras Fm. are neoformed, showing a marked NW-SE orientation trend (Figs. 3.4 and 3.5d), and their displacement components indicate transverse (oblique) movements along fault planes (Fig. 3.6). Fault planes in the weathered basement rocks are mainly reactivated from inherited structures, showing predominant NNE-SSW orientations and SE high dip angle (Figs. 3.3i, 3.4 and 3.S3), with primarily vertical and subordinately lateral displacement components (Fig. 3.6). Nonetheless, we also observe neoformed fault planes, showing an NW-SE orientation trend, in the weathered basement rocks, with displacement components indicating transverse (oblique) movements along fault planes (Fig. 3.6).

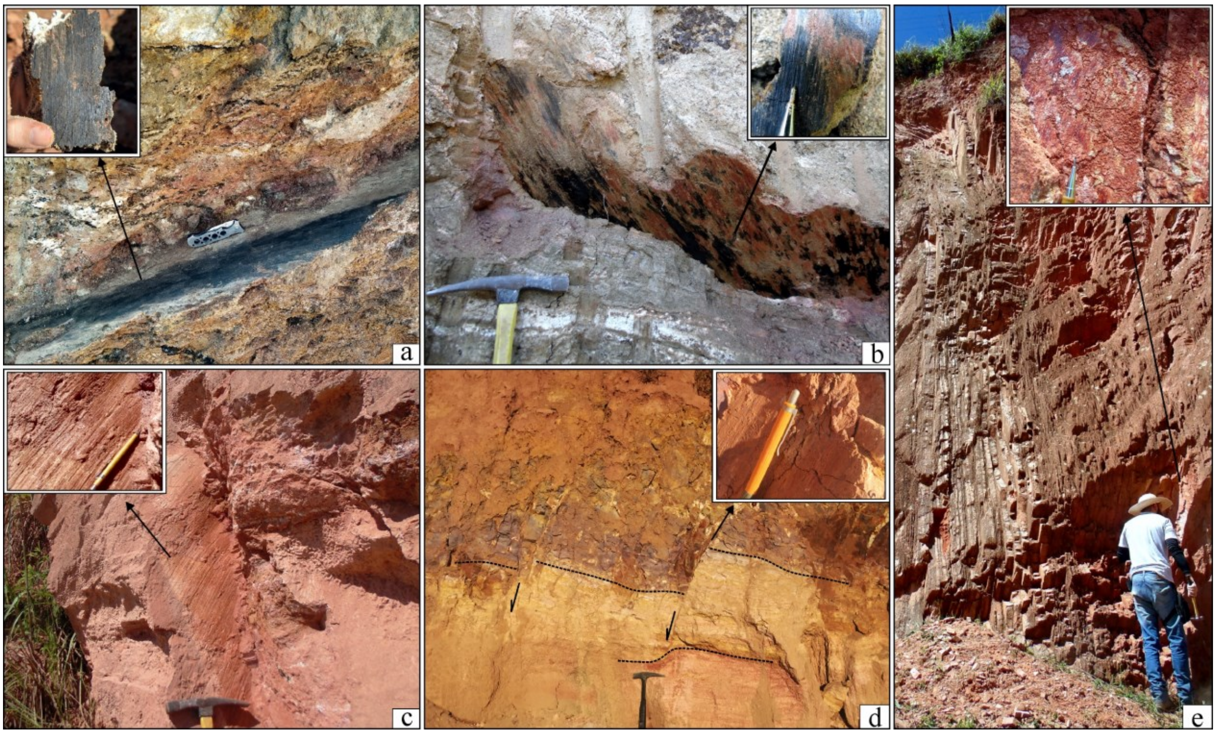

Fig 3.5: Fault planes with slickensides printed on filling materials. (a) Reactivated faults in gneiss foliation. (b-c) Neoformed structures affecting the weathered rocks. (d) Neoformed faults affecting the Barreiras Fm. (e) Reactivated faults with a high dip angle in the mylonitic foliation. Filling materials are mainly composed of manganese oxides, illite (a-b), and clay minerals (c-e).

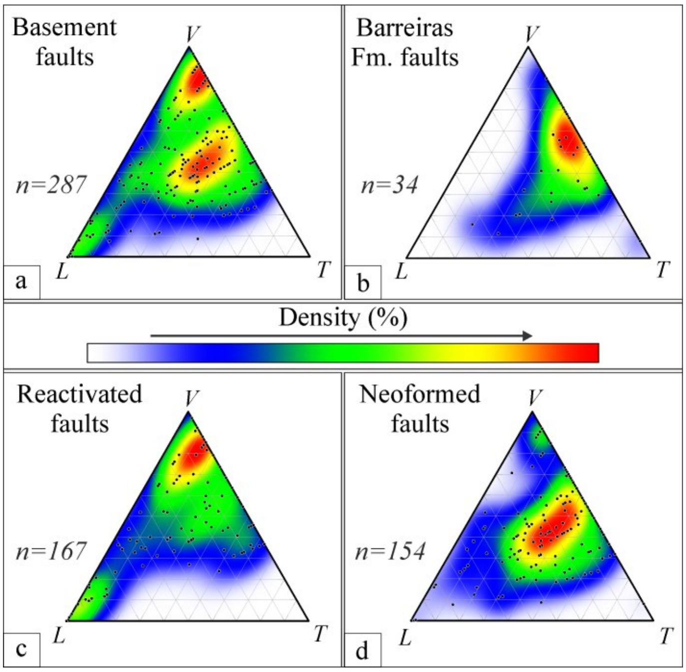

Fig 3.6: Fault-slip component diagram (FSC) showing the distribution of the lateral horizontal displacement (*L*), transversal horizontal displacement (*T*), and vertical displacement (*V*). (a) Basement faults; (b) Barreiras Fm. faults; (c) reactivated fault planes; and (d) neoformed fault planes. The contouring was performed using multivariate kernel density estimation.

3.5.2 Tectonic analysis

The FSC diagrams (Fig. 3.6) show rupture planes associated with normal, normal oblique, and strike-slip movements along fault planes, among which 50% are related to a pure extensive stress regime, 25% to a radial extensive stress regime, 13% to a transtensive stress regime, and 12% to a pure strike-slip stress regime. Displacement along fault planes in the weathered basement rocks occurs mainly through pure extensive and radial extensive stress regimes, whereas movements in the neoformed faults in Barreiras Fm. occur in a pure extensive regime (Fig. 3.7). Displacement components (fault plane and slickenside) in pre-existing planes reactivated predominantly in extensive radial regimes occur with a high dip angle, while neoformed faults originating from a pure extensive stress regime are marked by fault planes and slickensides with medium dip angles (Fig. 3.7).

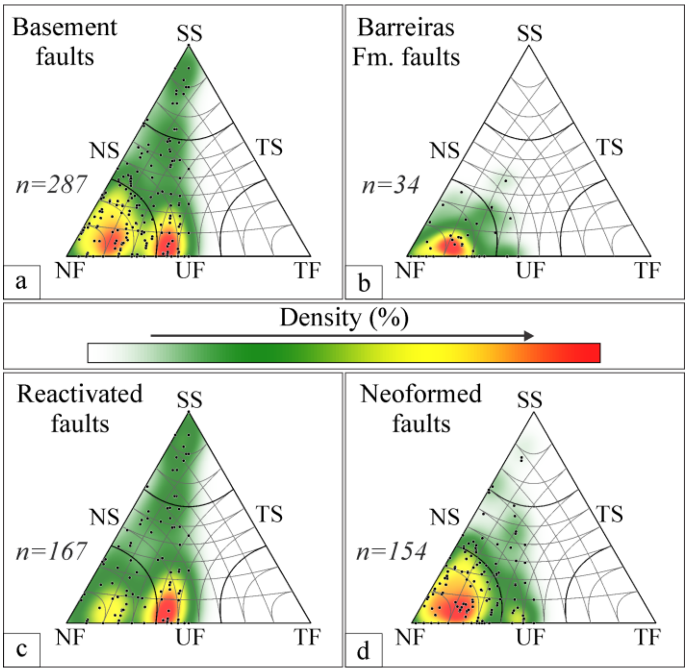

Fig 3.7: Moment tensor triangle plot obtained by the inversion of fault data. (a) Basement faults; (b) Barreiras Fm. faults; (c) reactivated fault planes; and (d) neoformed fault planes. Stress regime: UF = radial extensive and radial compressive; NF = pure extensive; NS = transtensive; SS = pure strike-slip; TS = transpressive; TF = pure compressive. The triangle plot contouring was performed using multivariate kernel density estimation.

We infer three paleostress fields from the inversion of fault data in the weathered basement rocks (n = 260 compatible faults): an E-W sinistral strike-slip stress regime (Fig. 3.8a), a WNW-ESE extension (Fig. 3.8b), and a NE-SW extension (Fig. 3.8c). In contrast, we infer only one paleostress field, a NNE-SSW extension, from the inversion of fault data in the Barreiras Fm. (n = 31 compatible faults). The E-W sinistral strike-slip regime in the weathered basement rocks (Fig. 3.8a) is linked to NNE-SSW dextral reactivated faults and NW-SE sinistral neoformed faults. The WNW-ESE extension regime in the weathered basement rocks (Fig. 3.8b) is associated with NE-SW reactivated faults with SE medium to high dip angle and NE-SW neoformed structures with NW and SE medium dip angles. Finally, inverted fault data imply NE-SW-trending extensional tectonic stress regimes in the weathered basement rocks and the Barreiras Fm. In the weathered basement rocks, a NE-SW extensional regime is associated with normal to oblique NW-SE faults (Fig. 3.8c). In the Barreiras Fm., a NNE-SSW extensional event is linked to neoformed faults (Fig. 3.8d).

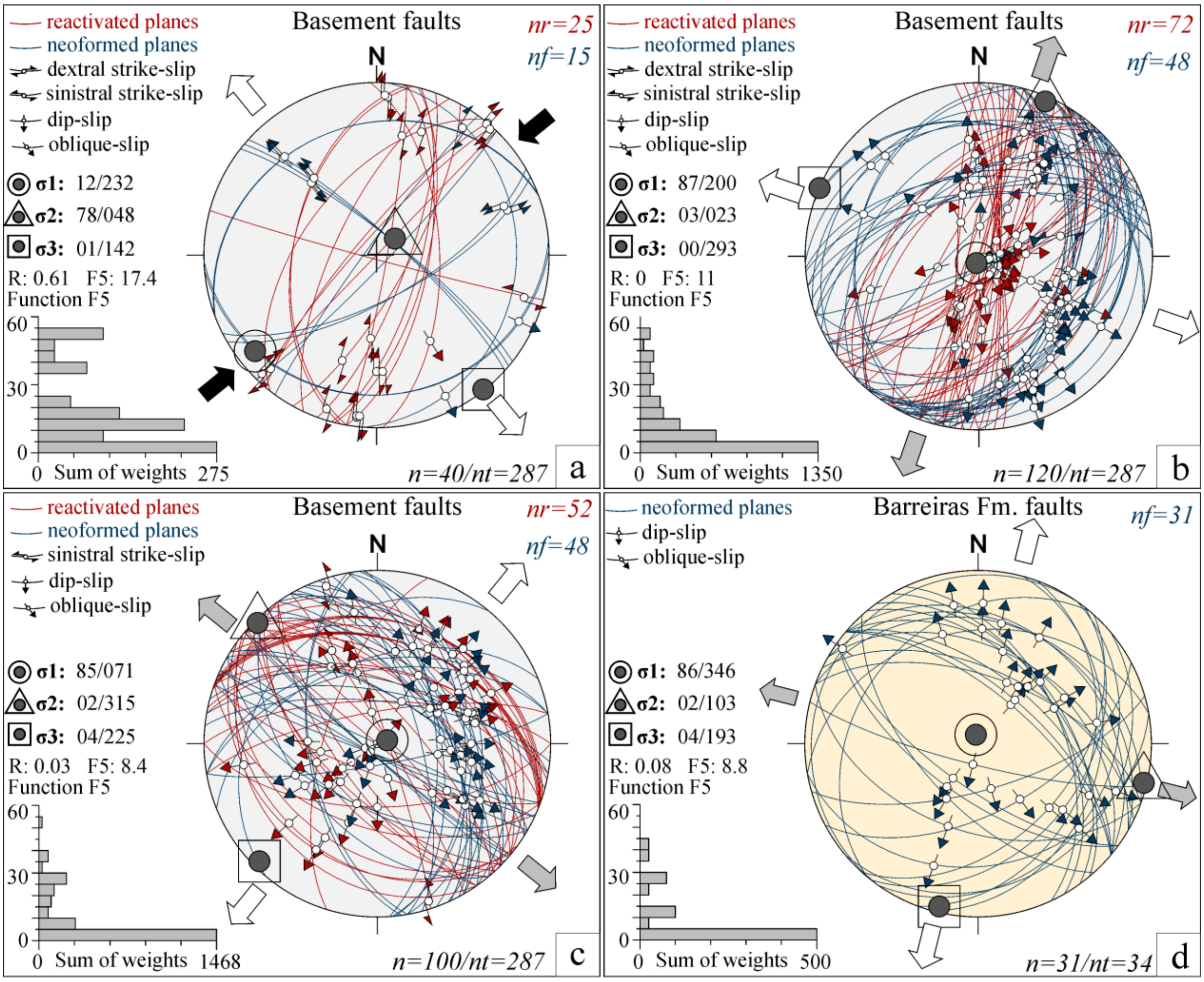

Fig 3.8: Paleostress regimes obtained by the inversion of fault data. (a) E-W sinistral strike-slip, (b) WNW-ESE extension, (c) NE-SW extension and (d) NNE-SSW extension. Stress axis: σ1 > σ2 > σ3; *n/nt* = number of compatible measures / total number of measures; *nr/nf* = number of reactivated / neoformed faults. Black, gray and white arrows represent the σ1, σ2 and σ3 axes, respectively.

3.5.3 Spatial distribution of topographic metrics

Topographic relief is spatially variable in the study area, with areas of subdued topographic expression, particularly in low elevation areas in the vicinity of the coast, and high topographic relief areas concentrated roughly in the middle portion of all seaward-dipping catchments (Figs. 3.9 and 3.10). Topographic metrics show a broad range of values, with histograms characterized by a right-skewed distribution with a long upper tail and central tendency offset toward lower values (Fig. 3.11).

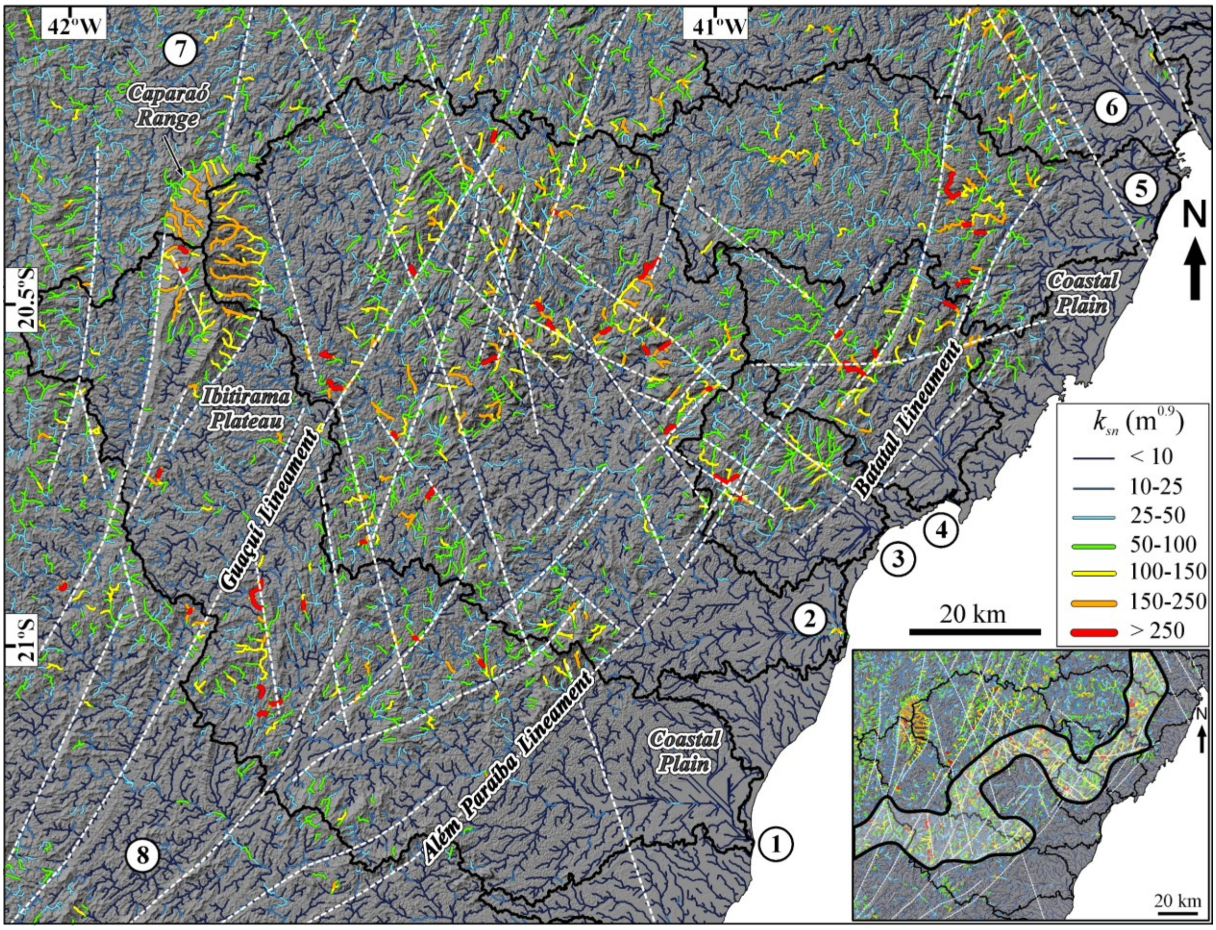

Fig 3.9: Normalized channel steepness (k_{sn}) draped over a 315° azimuth shaded relief. K_{sn} was calculated using the θ_{ref} = 0.45 and A_0 = 1 km^2. White dotted lines show morphostructural lineaments. The inset map highlights the interpreted regional zone of high channel steepness and local relief, delineated by thick black lines. Catchments: 1 = Itabapoana; 2 = Itapemirim; 3 = Iconha; 4 = Benevente; 5 = Jucu; 6 = Santa Maria; 7 = Manhuaçu; 8 = Muriaé.

We find that the normalized channel steepness (k_{sn}) varies from 0 to 1065 m$^{0.9}$, with a regional mean of 29 m$^{0.9}$ and a standard deviation of 44 m$^{0.9}$ (Fig. 3.9). Low values of k_{sn} (<50 m$^{0.9}$) are distributed primarily over the coastal region and the Ibitirama Plateau (Fig. 3.9). High values of k_{sn} (>100 m$^{0.9}$) are regionally distributed following an overall NE-SW orientation, and as seaward-dipping catchments in the study area are elongated in the NW-SE direction, trunk channels cross this regional "belt" of high k_{sn} perpendicularly (Fig. 3.9). Locally very steep channel reaches (with k_{sn} >250 m$^{0.9}$) are relatively common in the study area, and such high ksn values are comparable to the high-end of the distribution of k_{sn} extracted assuming a reference concavity of 0.45 in other post-orogenic settings (e.g., Gallen et al., 2013; Scharf et al., 2013) as well as tectonically active settings (e.g., Wobus et al., 2006; Kirby and Whipple, 2012). Furthermore, we observe that all rivers flowing away from the Caparaó Range and that rivers immediately upstream of the Guaçuí shear zone show high values of k_{sn} (Fig. 3.9).

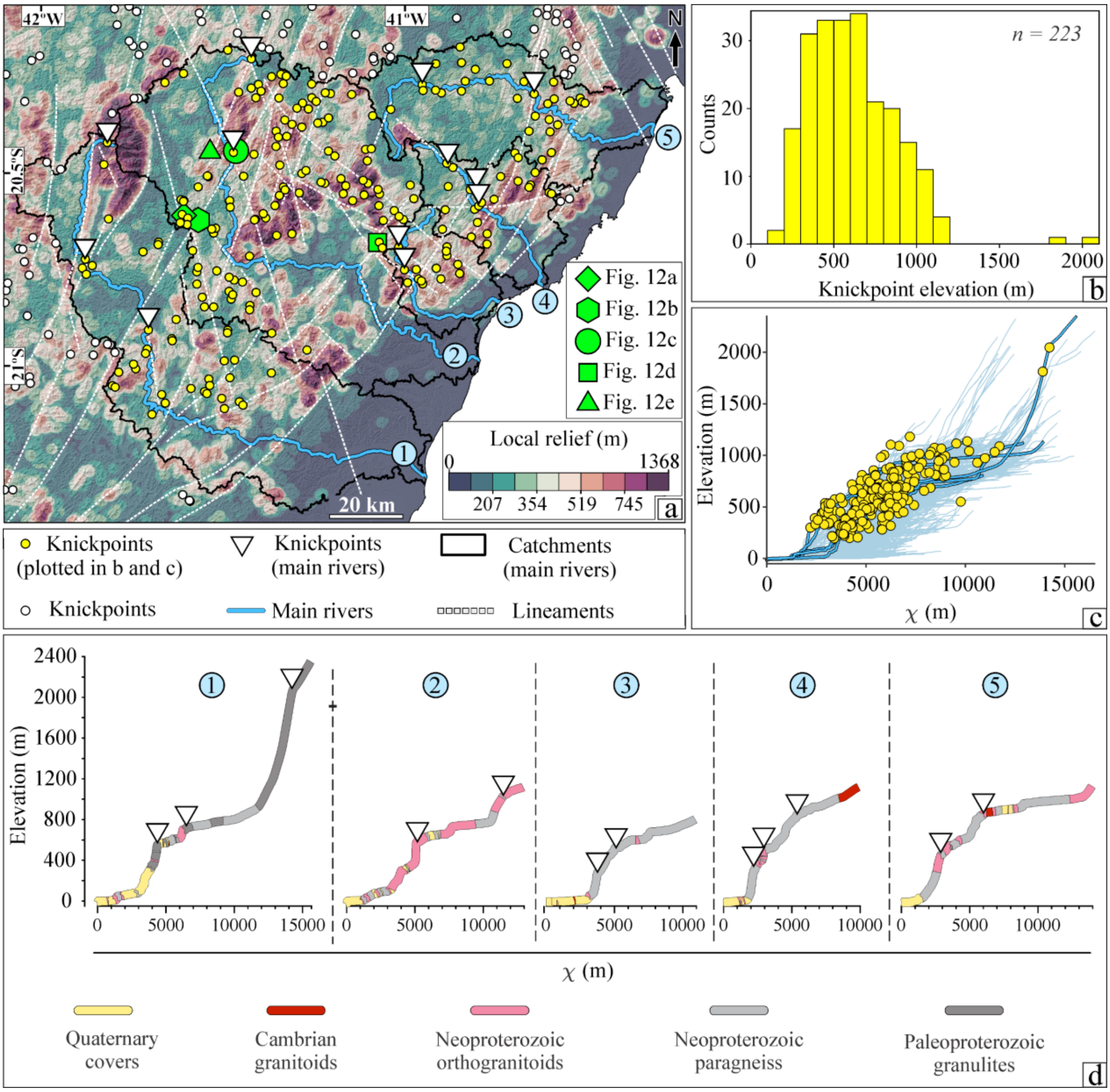

Fig 3.10: Knickpoints and transformed stream profiles in χ-elevation space. (a) Local relief (extracted using a 1.5 km radius window), knickpoints, main rivers, and lineaments in the study area. (b) Histogram of knickpoint elevation (in meters above sea level) for all the knickpoints extracted in catchments 1-5. (c) Knickpoints and profiles in χ-elevation space for all rivers flowing in catchments 1-5. (d) Transformed χ-elevation profiles for the main rivers flowing in the study area, with knickpoints and lithological variations highlighted. Local relief data is plotted using a scientific color ramp in Thyng et al. (2016) to avoid visual distortions. Catchments: 1 = Itabapoana; 2 = Itapemirim; 3 = Iconha; 4 = Benevente; 5 = Jucu.

We find that local relief ranges from 0 to 1347 m, with a regional mean of 335 m and a standard deviation of 192 m (Fig. 3.10). Local relief shows a similar spatial pattern to the observed for k_{sn}, with low values near the coastal region and the Ibitirama plateau and high values regionally distributed following a roughly NE-SW direction (Fig. 3.10). These spatial patterns in topography are likely not directly a function of variations in lithology. Comparison of topographic metrics per lithological class indicates similar mean and median values of local relief and k_{sn} for different lithologies (Fig. 3.11). However, we observe some degree of lithological control on the topography as areas underlain by crystalline rocks show substantially higher k_{sn} and local relief values than areas in quaternary sedimentary covers (Fig. 3.11). In particular, areas in Cambrian granitoids and Paleoproterozoic granulites exhibit the highest topographic metrics among crystalline rocks (Fig. 3.11). Nevertheless, lithological groups are distributed unevenly in the study area, with crystalline rocks composing 87% of the outcropping rock units, the majority consisting of Neoproterozoic paragneiss (43%) and orthogranitoids (28%). Quaternary covers only account for 8% of the study area, with 11% Paleoproterozoic granulites, 5% Cambrian granitoids, and 5% Neogene siliciclastic sediments (Barreiras Fm.).

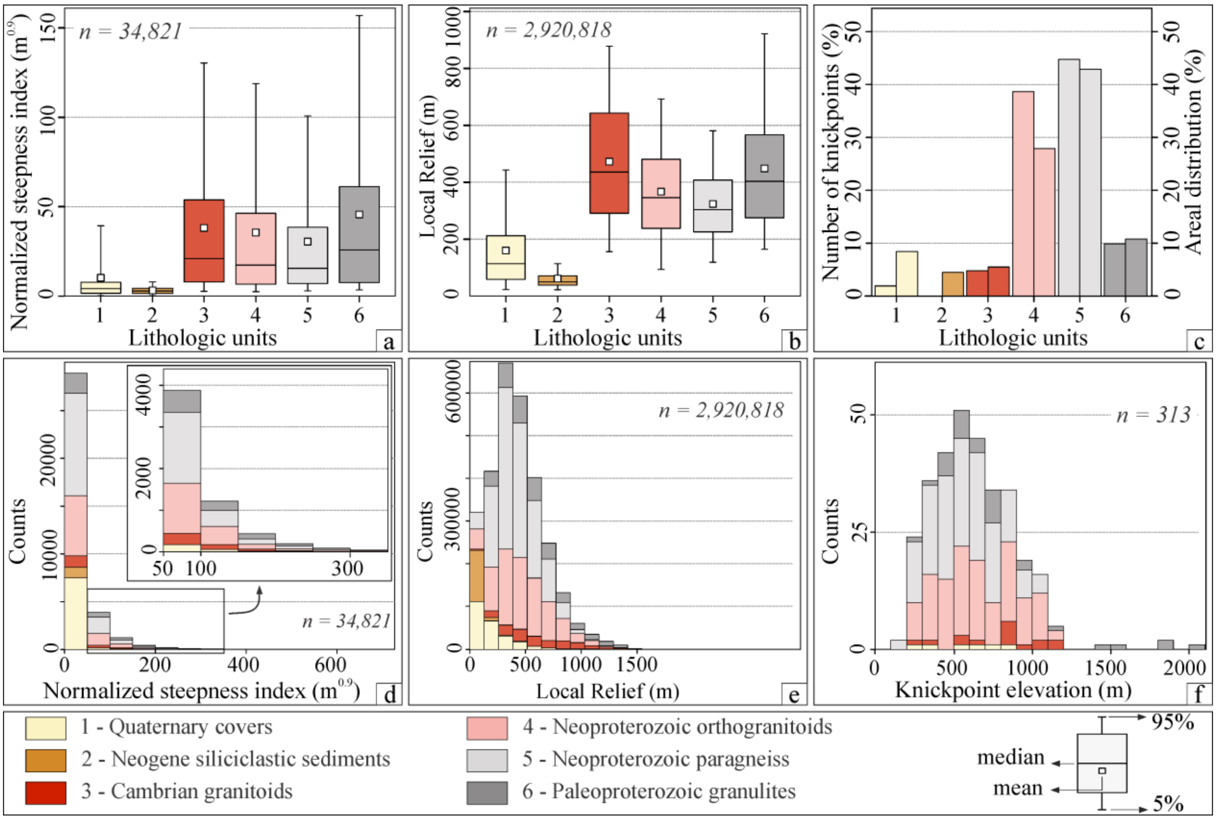

Fig 3.11: Distribution of geomorphic metrics per lithological units. Boxplots: (a) normalized channel steepness, and (b) local relief. Colored bars: (c) number of knickpoints and areal

distribution. Histograms: (d) normalized channel steepness, (e) local relief, and (f) knickpoint elevation. See Fig. 3.2 for the spatial distribution of lithological units.

3.5.4 Knickpoints and χ-elevation plots

We identify 313 knickpoints in the study area (Fig. 3.10). Knickpoint extraction was based on a tolerance value of 70 m, which is considerably higher than the tolerance threshold used in recent studies (tolerance of 20 m – Stolle et al. (2019); tolerance of 17 m - Alves et al. (2020); tolerance of 10 m – Cardoso Jr. et al. (2021)). Knickpoint height, which is the difference in elevation between the knickpoint and the strictly upward concave fitted profile and is thus a metric for knickpoint magnitude hereafter referred to as *dz*, ranges from 70 to 315 m. We observe thus a relatively large number of high-magnitude knickpoints in the study area that, in the field, are often expressed as waterfalls (Fig. 3.12). These knickpoints are not randomly distributed but are instead regionally concentrated following an overall NE-SW orientation that is roughly superposed with the distribution of high values of k_{sn} and local relief (Fig. 3.10). Rivers in the study area cross perpendicularly such NE-SW-trending zone of high topography at some point, and we observe knickpoints in these locations (Fig. 3.10); a single river often shows more than one knickpoint along their profile (Fig. 3.10d). Furthermore, a single river often shows more than one knickpoint along their profile (Fig. 3.10d).

We find that nonlinear shapes characterize χ-elevation profiles for most rivers flowing to the coast in the study area, and, in many cases, inflections in χ-elevation profiles correspond to knickpoints with $dz > 70$ m (Fig. 3.10c). Instead of being clustered at one or more horizontal positions, knickpoints are widely scattered in elevation and χ-elevation space (Fig. 3.10). Knickpoints occur between 194 and 2046 m of elevation, yet these are principally distributed in the 200 to 1100 m elevation range (Fig. 3.10b). We observe a few knickpoints in elevations higher than 1100 m, and all these high-elevation knickpoints are underlain by granulitic rocks (Fig. 3.11). Nevertheless, most knickpoints are not linked to specific geological contacts (Fig. 3.S4) and occur in various geological units (Fig. 3.11), indicating that lateral variations in lithology are likely not a dominant control on the formation of knickpoints. However, we identify knickpoints predominantly in crystalline rocks, particularly in Neoproterozoic paragneiss and orthogneisses, whereas knickpoints are nearly absent in sedimentary covers (Fig. 3.11).

Field observations suggest that knickpoints might be spatially associated with brittle structures such as NE-SW and NW-SE trending high-angle joints as well as NE-SW reactivated foliation planes (Fig. 3.12). We observe in the field that “minor” knickpoints extracted with a reduced tolerance threshold ($dz < 70$ m) may also be expressed as waterfalls spatially related to NW-SE brittle structures (Figs. 3.12b to e), indicating that knickpoints are widespread geomorphic features in the study area. In several cases, knickpoints and channel segments characterized by high values of k_{sn} lie upstream of morphostructural lineaments (Figs. 3.9, 3.10 and 3.S4) and, nevertheless, not every river crossing morphostructural lineaments show such a topographic pattern.

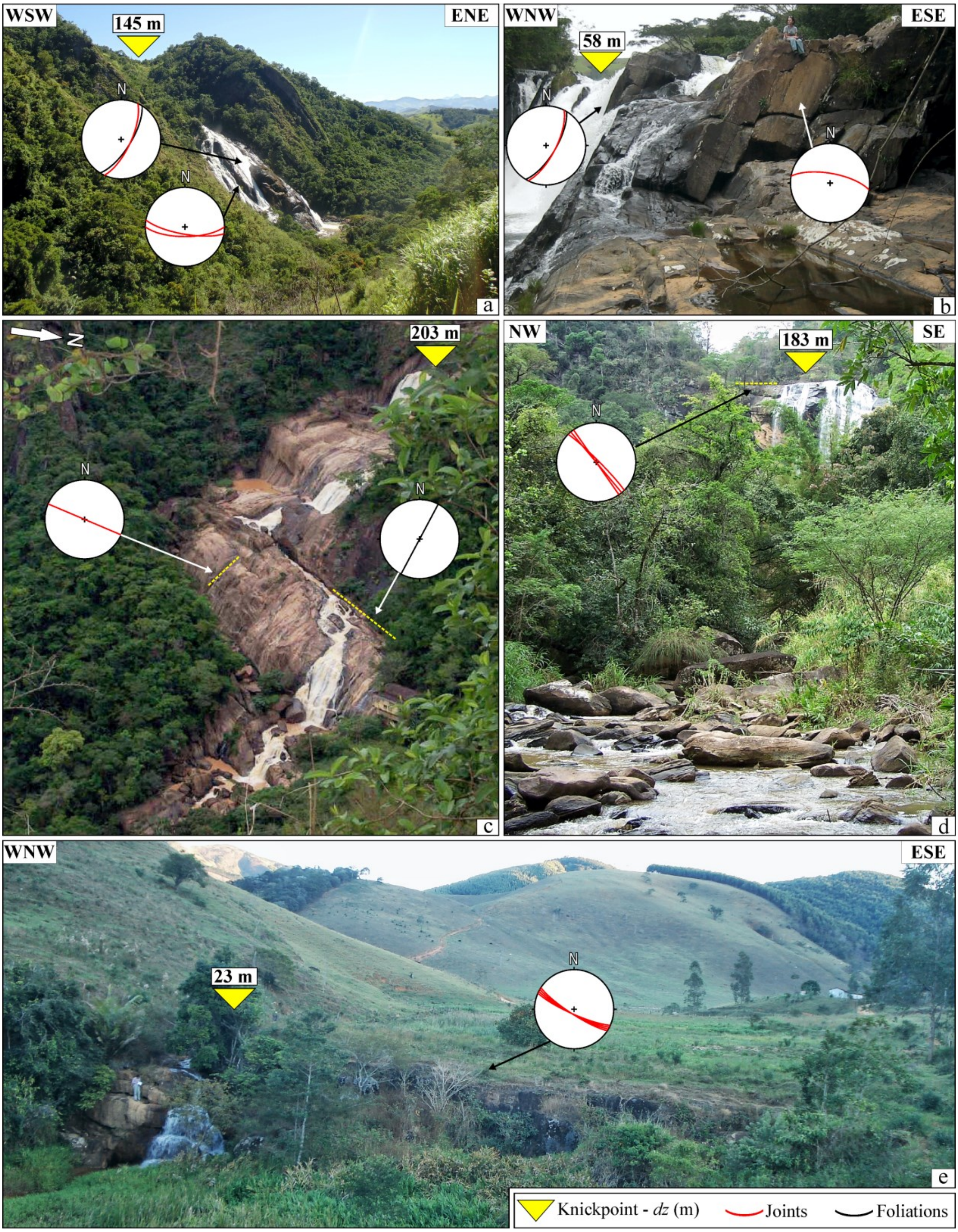

Fig 3.12: Examples of waterfalls corresponding to identified knickpoints and their relationship with geological structures measured in the field. Knickpoints with high *dz* values are linked to NE-SW reactivated brittle structures (a, c). However, in areas close to expressive NW-SE lineaments, high *dz* values occur associated with NW-SE brittle structures (d). Note that significant topographic gradient breaks also occur in channels with knickpoints with *dz* below

the 70 m tolerance used for knickpoint extraction (b, e). Polar stereographic projections employ a low hemisphere projection in a grid of equal area. See Fig. 3.10 for the location of waterfalls.

3.5.5 Drainage network orientation

The river network geometry shows a spatial pattern in which streams equal or less than third-order are scattered in a relatively similar manner in every direction, contrasting with streams of fourth or higher stream-order (representing trunk streams) that are distributed principally over the NE-SW and NW-SE directions (Figs. 3.13a to c). The orientation of morphostructural lineaments is comparable to the pattern observed for the trunk streams in the study area, with preferentially NE-SW, NW-SE, and NNW-SSE trends for lineaments of both greater and lesser persistence (> 5 km and <5 km) (Figs. 3.13d and e). Channel reaches characterized by low values of k_{sn} are distributed relatively indiscriminately in all directions (Fig. 3.13f). In contrast, channel reaches with high k_{sn} are preferentially oriented NW-SE and perpendicularly to the principal orientation of the morphostructural lineaments (i.e., NE-SW) (Fig. 3.13g). Rivers flowing in Neoproterozoic orthogranitoids and paragneiss (accounting for ~70% of the study area) and Quaternary deposits follow NE-SW and NW-SE directions (Figs. 3.13h, k and l). Differently, streams flowing in the Neogene deposits (Barreiras Fm.) show a robust NW-SE channel orientation (Fig. 3.13i). Channels flowing through Cambrian granitoids show a strong preferential NE-SW direction (Fig. 3.13j), and, finally, rivers flowing through granulitic Paleoproterozoic rocks do not show any preferential orientation (Fig. 3.13m).

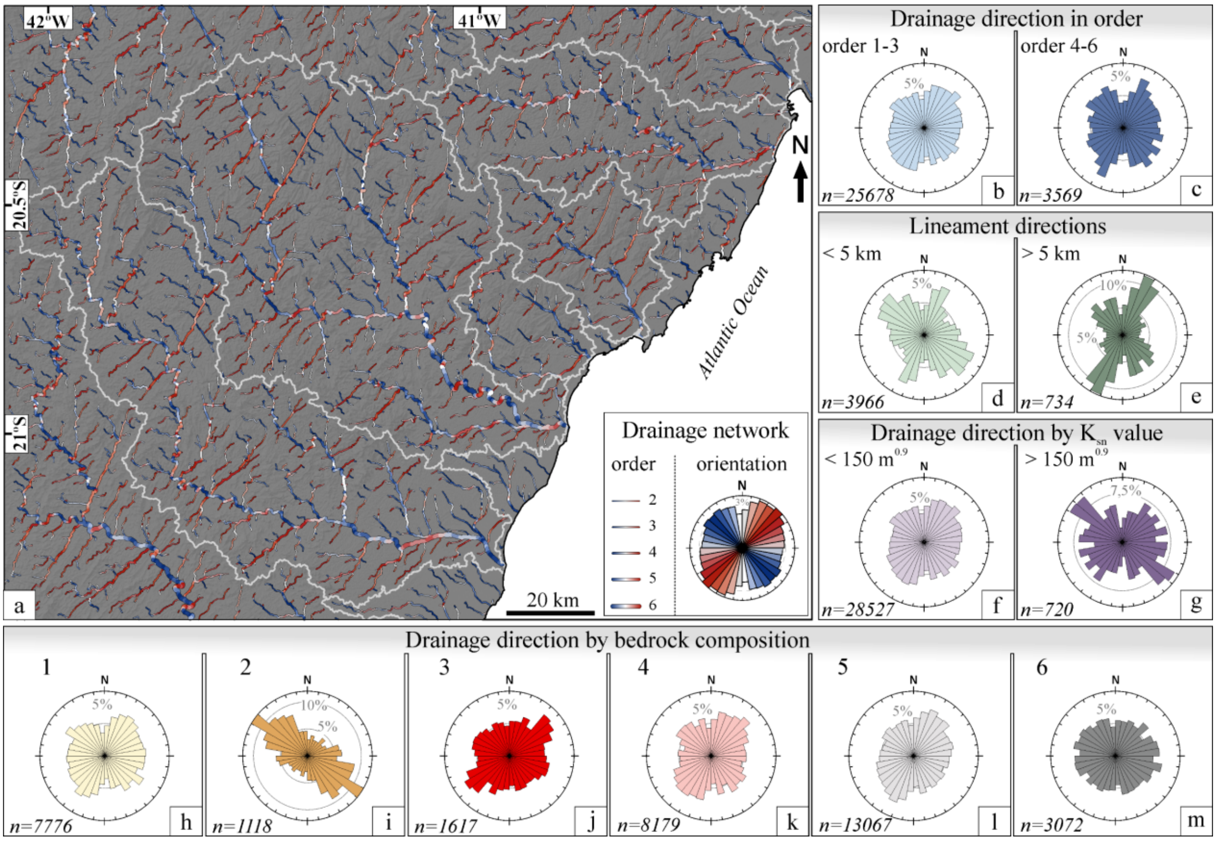

Fig 3.13: Planform orientation of the river network and morphostructural lineaments. (a) River network orientation calculated for each 1000-m segment. Rose diagrams showing the orientation of: (b-c) river channels as a function of stream-order; (d-e) morphostructural lineaments; (f-g) river channels as a function k_{sn} values and (h-m) river channels as a function of bedrock geology. Rose plots use equal-area distributions. Lithological units (h-m): 1 = Quaternary covers; 2 = Neogene siliciclastic sediments (Barreiras Fm.); 3 = Cambrian granitoids; 4 = Neoproterozoic orthogranitoids; 5 = Neoproterozoic paragneiss; 6 = Paleoproterozoic granulites.

3.6 Discussion

3.6.1 Influence of pre-existing structures on brittle reactivation

Our structural data indicate that the tectonic framework of the continental margin at the northern end of the Mantiqueira Range is strongly associated with the formation of NE-SW and NW-SE brittle structures, in agreement with the morphostructural lineaments' geometry (Figs. 3.3, 3.4 and 3.13). In southeastern Brazil, morphostructural lineaments following parallel to the coast reflect the orientation of Precambrian shear zones, which are reactivated weakness zones, while morphostructural lineaments extended in orthogonal and oblique directions are linked to fracture zones (e.g., Riccomini et al., 1989; Chang et al., 1992; Gontijo-Pascutti et al., 2010; Calegari et al., 2016; Lourenço et al., 2016). The relatively large number of joints and faults we observe oriented following these directions suggests that Precambrian basement discontinuities exert a dominant influence on the formation of younger structures. Such NE-SW and NW-SE brittle structures are likely originated from the local accumulation of regional stresses and the propagation of fractures in the same structural trend as the basement discontinuities in response to stresses generated at the plate boundaries (e.g., Dunbar and Sawyer, 1989; Sandiford et al., 2004; Gudmundsson et al., 2010).

The FSC diagrams imply that the association between brittle structures and basement anisotropies occur predominantly in NE-SW to NNE-SSW directions, with the brittle deformation accommodated in the Precambrian shear zones by vertical movements along the reactivated planes (Fig. 3.5e). The basement shear zones' geometry influences reactivated fault planes as observed in the moment tensor triangle plots, suggesting local stress variation. Furthermore, the radial extensive tectonic regime inferred from the reactivated faults indicates that the lower stress axis ($\sigma3$) may have suffered deflections, becoming parallel or perpendicular to the reactivated plane, which agrees with numerical stress field models (e.g., Simon et al., 1988; Kattenhorn et al., 2000). The deflection of the lower stress axis ($\sigma3$) due to reactivated structures was also observed in recent earthquakes in NE Brazil, where shear zones were reactivated as normal faults in a strike-slip regime (Ferreira et al., 2008).

3.6.2 Topographic rejuvenation due to the reactivation of pre-existing structures

The study area shows several topographic features similar to that expected for a transient landscape (Wobus et al., 2006; Kirby and Whipple, 2012). These include a large number of high-magnitude knickpoints not located at or near lithological contacts, widespread non-linear shapes characterizing channel profiles in χ-elevation space, and a regional zone of high values of k_{sn} and local relief extending continuously through the middle portion of all seaward-dipping catchments superposed with the presence of many knickpoints. If the landscape is responding to a regional transient signal, then the upstream limit of the regional zone of high topography should represent a mobile transition, characterized by a sharp break in topographic gradient, separating upstream areas that are yet to adjust to and downstream areas responding or in equilibrium with boundary conditions (Fig. 3.14; Kirby and Whipple, 2012). Similar patterns of regional transient landscape adjustment have been documented in erosive landscapes in various geomorphic scenarios, including EPCMs (e.g., Wobus et al., 2006; Berlin and Anderson, 2007; Gallen et al., 2013).

Different mechanisms can cause spatially uniform variations in relative baselevel fall rates, including eustatic sea-level changes (e.g., Bishop et al., 2005), exposure of rocks with differential erodibility (e.g., Gallen, 2018), and variations in tectonic uplift (e.g., Wobus et al., 2006; Whittaker and Boulton, 2012), yet abrupt or sustained baselevel lowering due to these mechanisms induces similar response patterns in the drainage network (cf., Kirby and Whipple, 2012). However, spatial and temporal changes in controls on channel incision processes (e.g., sediment flow, river erodibility, and drainage area) may result in deviations from such a transient response pattern (e.g., Whittaker et al., 2007; Attal et al., 2015; Shobe et al., 2016). Based on three observational constraints, we conjecture that our topographic data cannot be entirely explained by a transient signal (or signals) propagating upstream towards the drainage divides. First, we find that knickpoints in the study area are widely spread instead of being clustered in elevation and elevation-χ space, contrary to what is generally expected for mobile knickpoints resulting from synchronous, regional baselevel fall (Kirby and Whipple, 2012; Schwanghart and Scherler, 2020). Second, hillslope angles are not significantly different between areas upstream and downstream of the upper limit of the regional zone of high topography (Fig. 3.14a), which is at odds with the general expectation that a less pronounced topographic relief should characterize 'relict' uplands upstream of the mobile transient signal (e.g., Gallen et al., 2013). Third, knickpoints are underlain by different lithologies (Figs. 3.11 and 3.S4), with most of the knickpoints associated with Neoproterozoic paragneisses (45% of the knickpoints) and ortho-granitoids (39% of the knickpoints), which our data suggest to be more erodible than laterally adjacent lithologies such as Paleoproterozoic granulites or the Cambrian granitoids (Figs. 3.11 and 3.S4). Knickpoints in the study area are thus not concentrated in resistant lithologies, which is anticipated when a transient signal propagates upstream in a lithologically heterogeneous landscape (e.g., Bishop and Goldrick, 2010). Nonetheless, our topographic data imply some degree of lithological control in topographic forms, particularly topographic relief is steeper where Paleoproterozoic granulites, such as in the Caparaó Range, and massif post-collisional Cambrian granitoids are exposed, and gentler where quaternary sedimentary covers are exposed.

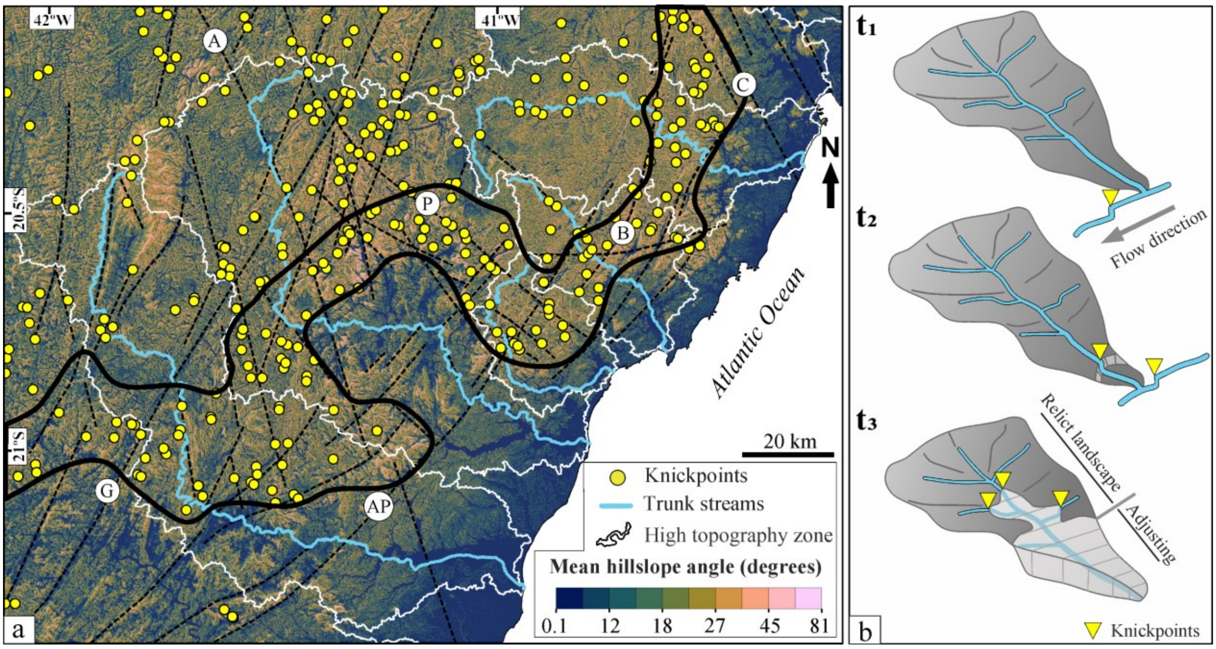

Fig 3.14: Spatial distribution of knickpoints and interpretations for their origin. (a) Knickpoints draped over a mean hillslope angle map in the study area. Morphostructural lineaments are represented as dashed black lines, and thick black lines delineate the interpreted regional zone of high topography. (b) A sketch representing the temporal evolution of a spatially uniform relative baselevel fall event modified from Gallen et al. (2013). An external perturbation triggers a transient channel response of incision and the formation of an upstream-migrating vertical slope-break knickpoint in the trunk stream. The migrating trunk stream knickpoint lowers the baselevel of its tributaries resulting in the formation of upstream-migrating knickpoints in these. Major structural lineaments: A = Alegre; AP = Além Paraíba; B = Batatal; C = Colatina; G = Guaçuí.

We hypothesize that the regional zone of high topography and the many knickpoints identified represent a regionally continuous knickzone anchored in space by reactivated structural boundaries. The observations supporting such conjecture include: (i) the geometry of the morphostructural lineaments is consistent with the structural arrangement of the NE-SW and NW-SE brittle structures measured in the field; (ii) the NE-SW and NW-SE brittle structural trends are reflected in the drainage network geometry, both in basement units and Cenozoic covers; (iii) channel reaches with low k_{sn} do not show any preferential orientation, whereas river segments with high k_{sn} are oriented perpendicularly to the principal directions of morphostructural lineaments; (iv) several knickpoints lie close or upstream of morphostructural lineaments; (v) field observations suggest that several of the knickpoints identified are likely genetically linked to brittle structures; (vi) trunk streams are roughly oriented following the direction of morphostructural lineaments, and the spatial distribution of the regional zone of high topography might be controlled by the geometry of the main morphostructural lineaments in the region; (vii) channel segments with high k_{sn} located higher up in the river network than the regional knickzone are positioned immediately upstream and follow orthogonally to the Guaçuí shear zone.

In this situation, we expect far-field stresses produced at plate margins to accumulate in the pre-existing weakness zones in the crust, especially in the Precambrian shear zones. The accumulation of local stresses in basement discontinuities might eventually lead to differential uplift, which is to some degree similar to common interpretations in the CRSB region (e.g., Hiruma et al., 2010; Cogné et al., 2012). Differential uplift of rocks in response to far-field stresses have been proposed in other post-orogenic settings (e.g., Hack, 1982; Quigley et al., 2007), and this conjecture is reasonably consistent with existing knowledge that zones of weakness promote the concentration of stresses driving intraplate seismicity (e.g., Zoback, 1992; Talwani, 2017). Although we infer that regional baselevel fall cannot explain the totality of the topographic pattern in the study area, this process may be superimposed to what we interpret as reactivation of structural boundaries. Furthermore, the numerous knickpoints we find in the study area record elevation drops of only a few hundred meters, suggesting that if the origin of these knickpoints is the reactivation of pre-existing structures, then such tectonic activity is of mild geomorphic expression. Furthermore, the numerous knickpoints we find record elevation drops of only a few hundred meters, suggesting that if the origin of these knickpoints is linked to the reactivation of pre-existing structures, then such tectonic activity is of mild expression. This interpretation is further supported by field observations of small fault displacement along fault planes (Fig. 3.5).

3.6.3 Post-rift tectonic scenario in the northern end of the Mantiqueira Range

Unraveling the timing of the post-rift brittle deformation in the study area is challenging, mainly due to the restricted occurrence of Cenozoic covers on the coast and the inexistence of stratigraphic markers in the basement rocks. We use stratigraphic bracketing and geochronological data in surrounding regions to infer relative ages for the paleostress regimes derived from the inversion of fault data. The semi-consolidated Neogene sediments from the Barreiras Fm. are generally accepted to have been deposited between the Miocene and Pliocene in the north and northeastern Brazilian Atlantic coast (Arai, 2006; Rossetti et al., 2013), whereas, in the southeastern coast, the deposition is accepted as having a Pliocene age (e.g., França et al., 2007). The brittle deformation we observe in the Barreiras Fm. necessarily postdates its deposition. However, the Barreiras Fm. is spatially limited to a few kilometers in the coastal plain (Fig. 3.2), and our structural data was primarily derived from basement rocks. In this case, the determination of relative ages is assisted by deformational structures in fresh and weathered rocks. Even if they originated from an older basement, weathered rocks are more recent since they result from the weathering of fresh rocks (e.g., Millot, 1970). This hierarchical relationship is more robust when slickensides occur in filling materials composed of clay minerals and Mn oxides (Calegari et al., 2020). In surrounding regions to the study area (Fig. 3.S5), $^{40}Ar/^{39}Ar$ ages of supergene Mn oxides in weathered rocks indicate that weathering profiles formed between the Miocene and the Present (Vasconcelos et al., 1994; Carmo and Vasconcelos, 2004, 2006; Vasconcelos and Carmo, 2018). Based on a putative association with such geochronological data, it is reasonable to assume that the brittle deformation we find in the weathered basement rocks, characterized by slickensides printed in filling materials (Fig. 3.5), record deformation that postdates the formation of such weathering profiles and is thus post-Miocene.

Assuming thus that brittle deformation in the northern end of the Mantiqueira Range occurred in an intraplate environment between the Miocene and Pleistocene, we propose relative temporal brackets for paleostress regimes derived from fault data. The E-W sinistral strike-slip and the WNW-ESE extension stress regimes inferred principally from reactivated faults measured in the weathered basement rocks, which are not recorded in the brittle faults measured in Barreiras Fm., are likely positioned between the Miocene and the beginning of the Pliocene, earlier than the deposition of the Barreiras Fm. Various authors identified a Miocene to Pliocene E-W sinistral strike-slip event in southeastern Brazil (e.g., Riccomini et al., 1989; Silva and Mello, 2011; Bricalli and Mello, 2013; West and Mello, 2020), yet our study is the first to infer the WNW-ESE extension event. However, the NE-SW to NNE-SSW normal faults generated by the WNW-ESE distensive regime may have developed through local stresses with the minimum stress axis ($\sigma 3$) positioned horizontally in the NW-SE direction, which is also consistent with an E-W sinistral strike-slip event, implying that the E-W sinistral strike-slip and the WNW-ESE extension events may be synchronous.

The NE-SW to NNE-SSW extensional stress regimes recorded in faults in the weathered basement rocks and the Barreiras Fm. are linked to reactivated and neoformed faults in the NW-SE direction. We interpret these paleostress regimes as contemporary principally because they exhibit minimum stress axis (σ3) oriented following the same NE-SW trend, with σ3 at 04/225º in the paleostress field derived for the weathered basement rocks and σ3 at 04/193º in the paleostress field derived for the Barreiras Fm. This NE-SW to NNE-SSW extensional event is the youngest registered in the study area, which is corroborated by the absence of NE-SW and NNE-SSW faults associated with previous events in the semi-consolidated sediments from the Barreiras Fm., the strong NW-SE alignment of rivers flowing in this unit, and the high frequency of NW-SE joints recorded in weathered rocks. The brittle structures generated by this event may have formed by the variation of local stresses with the minimum stress axis (σ3) in the NE-SW direction, which is consistent with a Pleistocene E-W dextral strike-slip event interpreted by various authors in southeastern Brazil (Riccomini et al., 1989, 2004; Silva and Mello, 2011; Bricalli and Mello, 2013; West and Mello, 2020). Based on the relative dates we assign for the brittle deformation in the study area, it is reasonable to assume that the topographic rejuvenation we infer is post-Miocene.

3.6.4 Topographic configuration of an EPCM not defined by a sharp escarpment

Our findings indicate topographic rejuvenation in the northern end of the Mantiqueira Range, which supports, to some extent, a view that the present-day morphology in EPCMs is young, subsequent to rifting and continental breakup (Japsen et al., 2012a; Green et al., 2013, 2018). However, this hypothesis implies that the entirety of the topography in an EPCM was developed long after the continental breakup. Indeed, the regional knickzone crossing roughly the middle portion of all seaward-dipping catchments we infer likely represents relatively young, post-rift geomorphic features associated with far-field-driven reactivation of pre-existing structural boundaries. Nonetheless, the onset of the perturbation (or perturbations) responsible for such topographic expression cannot explain all the topography in the northern end of the Mantiqueira Range. The high elevation and the topographic position of the regional drainage divide and adjacent areas located considerably upstream of the regional belt of high topography (ca. > 40 km upstream) and between 75 to 135 km away from the coast are not explained by such a topographic rejuvenation. The origin of the large-scale topography in the study area, meaning the arrangement of the regional drainage divide, following roughly parallel to the coast, and formation of the seaward-dipping catchments elongated in the NW-SE direction, must predate the onset of the topographic resurgence, implying the coexistence of younger and older topographic elements in the landscape. Topographic rejuvenation is often invoked to explain the origin and apparent longevity of high and steep escarpments in EPCMs (Japsen et al., 2012a; Green et al., 2013, 2018) and, nevertheless, we present data showing post-Miocene brittle deformation and topographic rejuvenation in an EPCM not characterized by a sharp escarpment, which postdates the origin of the large-scale morphology in the study area.

An outstanding issue to resolve in the Mantiqueira Range is why topographic relief differs strongly between its southern and northern parts, with a prominent escarpment and the presence of a continental Cenozoic rift system characterizing the southern end of the Mantiqueira Range (Fig. 3.1). This is a long-standing question that remains enigmatic in the study area and likely in other EPCMs that all show at least some degree of along-strike variations in topographic expression. We conjecture that the gravitational collapse (~58 to 20 Ma; Zalán and Oliveira, 2005) caused by the plate´s passage over the Trindade Plume (Thomaz Filho et al., 2005), resulting in the development of the Continental Rift of Southeastern Brazil (Riccomini et al., 1989, 2004; Zalán and Oliveira, 2005), did not affect the northern end of Mantiqueira Range to the same extent that affected its southern part. A sharp contrast in denudation magnitude during the Upper Cretaceous and Paleogene interpreted from low-temperature thermochronological data between the northern (~1.6-2.9 km; Jelinek et al., 2014; Van Ranst et al., 2020) and the southern end of the Mantiqueira Range (~ 2-4 km; Gallagher et al., 1994; Hiruma et al., 2010; Cogné et al., 2011; Engelmann de Oliveira et al., 2016; Gezatt et al., 2021) further supports this hypothesis.

3.7 Conclusions

Analysis of geometry and kinematics of brittle geological structures and spatial patterns in topographic relief, channel steepness, and river network orientation indicate post-Miocene brittle deformation and topographic rejuvenation in a passive margin not characterized by a sharp escarpment southeastern Brazil. The results of this study suggest a multiphase brittle evolution in the northern end of the Mantiqueira Range, with at least two main paleostress tectonic regimes between the Miocene and Pleistocene likely resulting from the local accumulation of far-field stresses in pre-existing basement structures. The older event is linked to the development of NE-SW brittle structures, consistent with a Miocene to Pliocene E-W sinistral strike-slip event interpreted by various authors in southeastern Brazil, but earlier than the deposition of the Barreiras Fm. The younger event is linked to the development of principally reactivated NW-SE brittle structures, which agrees with a Pleistocene E-W dextral strike-slip event commonly accepted in southeastern Brazil. Our topographic data show numerous high-magnitude knickpoints, overall non-linear shapes characterizing channel profiles in χ-elevation space, and brittle structural trends reflected in drainage network geometry, suggesting a regionally continuous, roughly NE-SW knickzone extending through the middle part of every seaward-dipping catchment. We interpret this regional knickzone as anchored in reactivated structural boundaries based principally on relationships between spatial patterns in topography and the distribution and orientation of pre-existing structures. Topographic rejuvenation in the study area is likely post-Miocene, as the relative dating of brittle structures suggests, which is considerably younger than rifting and continental breakup. However, the large-scale morphology of the landscape and, in particular, the origin of the regional drainage divide and adjacent areas must predate the brittle deformation and topographic resurgence we infer. This study shows that tectonic topographic rejuvenation and brittle deformation in a passive margin are not necessarily related to a prominent escarpment's persistence. Younger and older topographic elements likely coexist in EPCMs not characterized by a sharp escarpment.

3.8 Acknowledgments

We thank the National Council for Scientific and Technological Development (CNPq) for the scholarship granted to the first author (project no. 870103/2001-6, process no. 141700/2018-1), the Financier of Studies and Projects (FINEP) for research support (contract no 01.10.0808.00), and Sara Brinati Valentim for helping in the fieldwork. FAC is a Fellow of the Brazilian Research Council (CNPq) and acknowledges the support received. DP had support from the Coordenação de Aperfeiçoamento de Pessoal de Nível Superior (CAPES) under a CAPES-PrInt Postdoctoral fellowship (nº 88887.367976/2019-00). This study was financed in part by the Coordenação de Aperfeiçoamento de Pessoal de Nível Superior - Brasil (CAPES) - Finance Code 001. The scientific results of structural data were obtained using Win-Tensor, software developed by Dr. Damien Delvaux, Royal Museum for Central Africa, Tervuren, Belgium.

3.9 Supplementary Figures

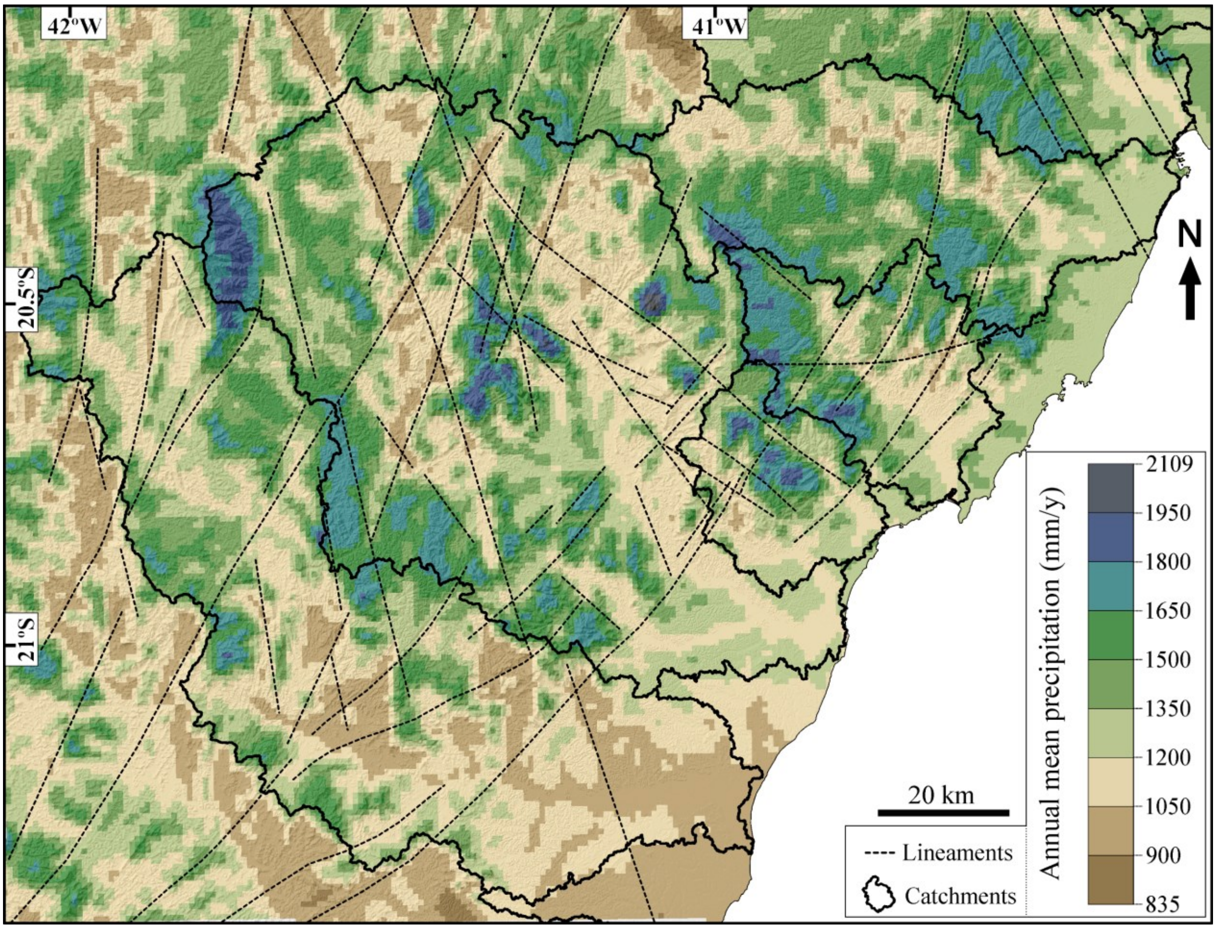

Fig 3.S1: Map of annual rainfall from CHELSA (Karger et al., 2017) in the study area. Mean annual precipitation varies from 835 to 2019 mm/yr in the study area.

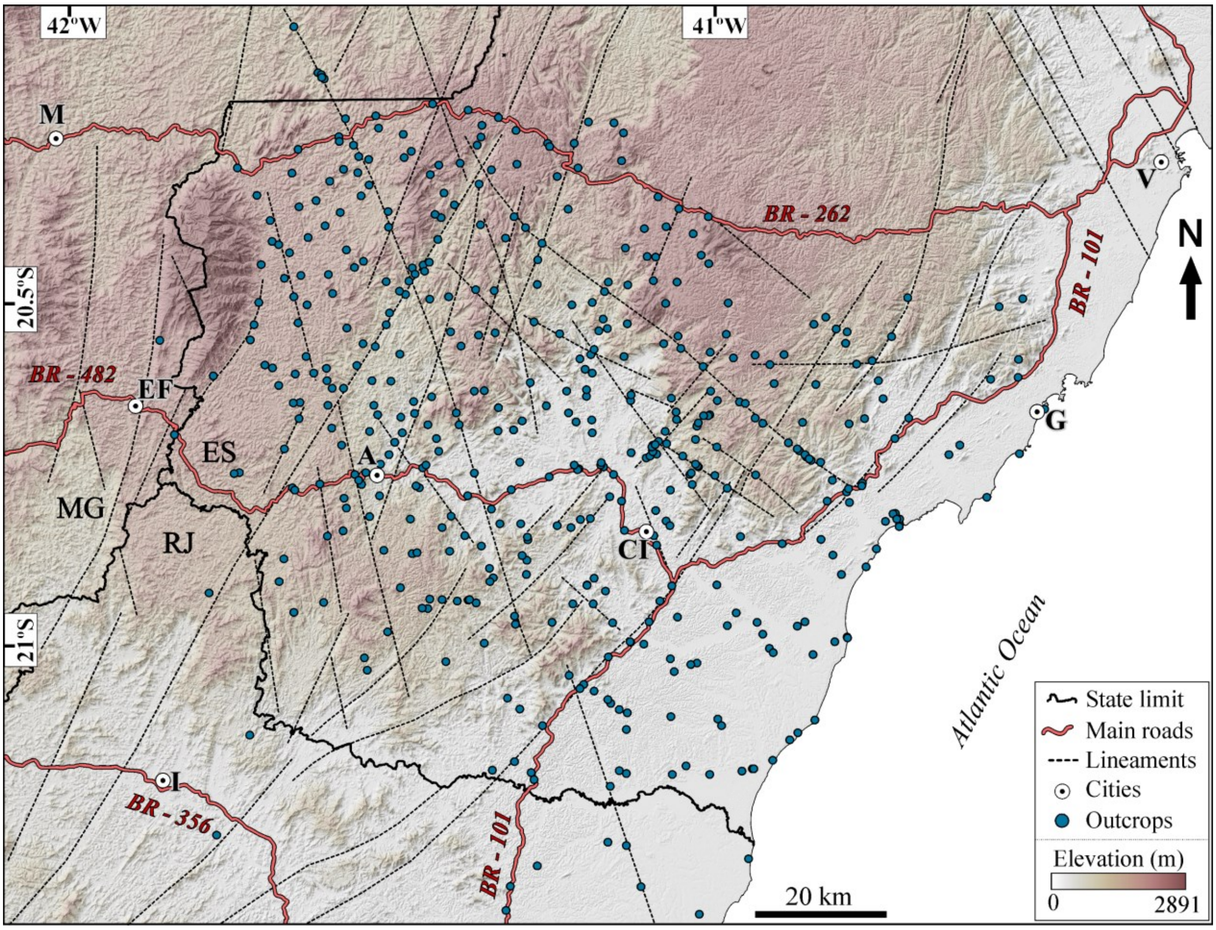

Fig 3.S2: Elevation map draped over a 315º azimuth shaded relief showing the location of the outcrops visited in the field. States: SP = São Paulo; MG = Minas Gerais; RJ = Rio de Janeiro; ES = Espírito Santo. Cities: A = Alegre; CI = Cachoeiro de Itapemirim; EF = Espera Feliz; G = Guarapari; I = Itaperuna; M = Manhuaçu; V = Vitória. States: ES = Espírito Santo, RJ = Rio de Janeiro, MG = Minas Gerais.

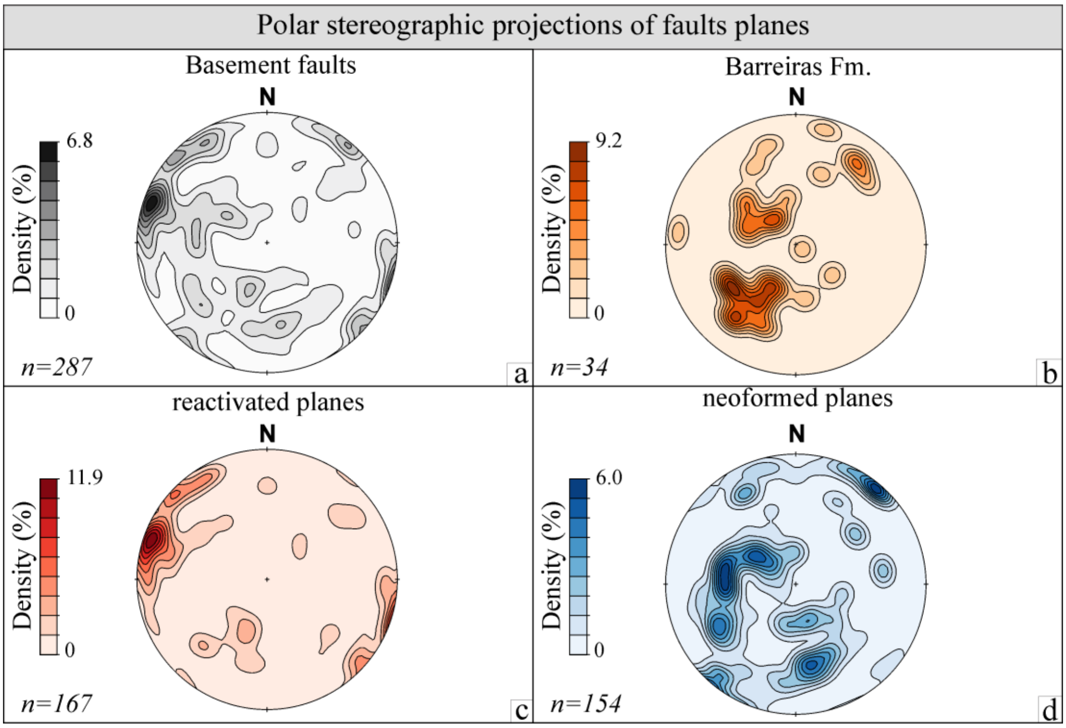

Fig 3.S3: Polar stereographic projections of fault planes. (a) basement faults; (b) Barreiras Fm. faults; (c) reactivated and (d) neoformed fault planes. Polar stereographic projections employ a low hemisphere projection in a grid of equal area, and rose plots use equal-area distributions.

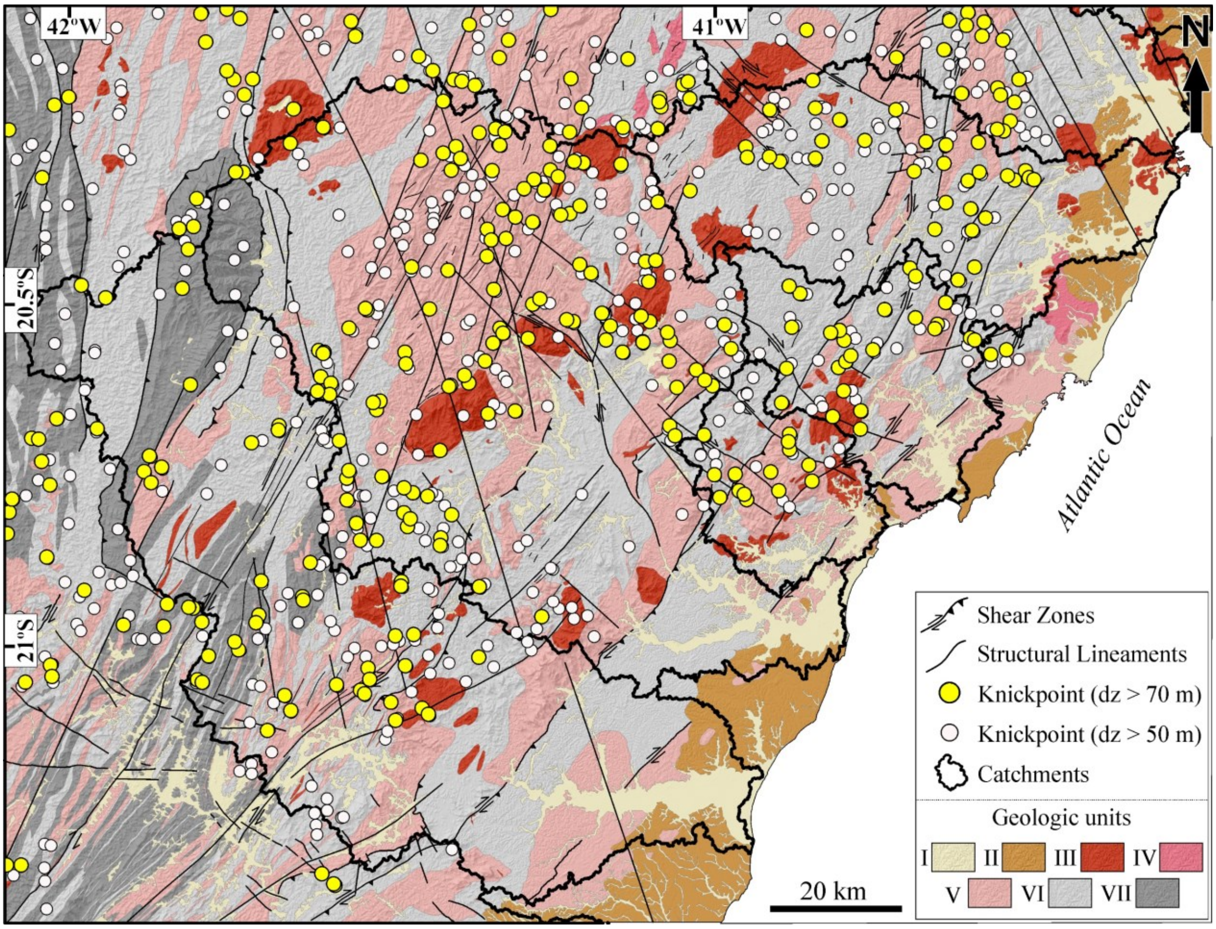

Fig 3.S4: Spatial distribution of knickpoints and bedrock geology in the study area. Knickpoints were extracted using a tolerance value of 70 m (yellow circles) and 50 m (white circles). Geologic units: I = Alluvial-colluvial/coastal deposits; II = Barreiras Formation; III = Post-collisional units; IV = Syn-collisional units; V = Pre-collisional units; VI = Neoproterozoic paragneiss complexes; VII = Paleoproterozoic basement.

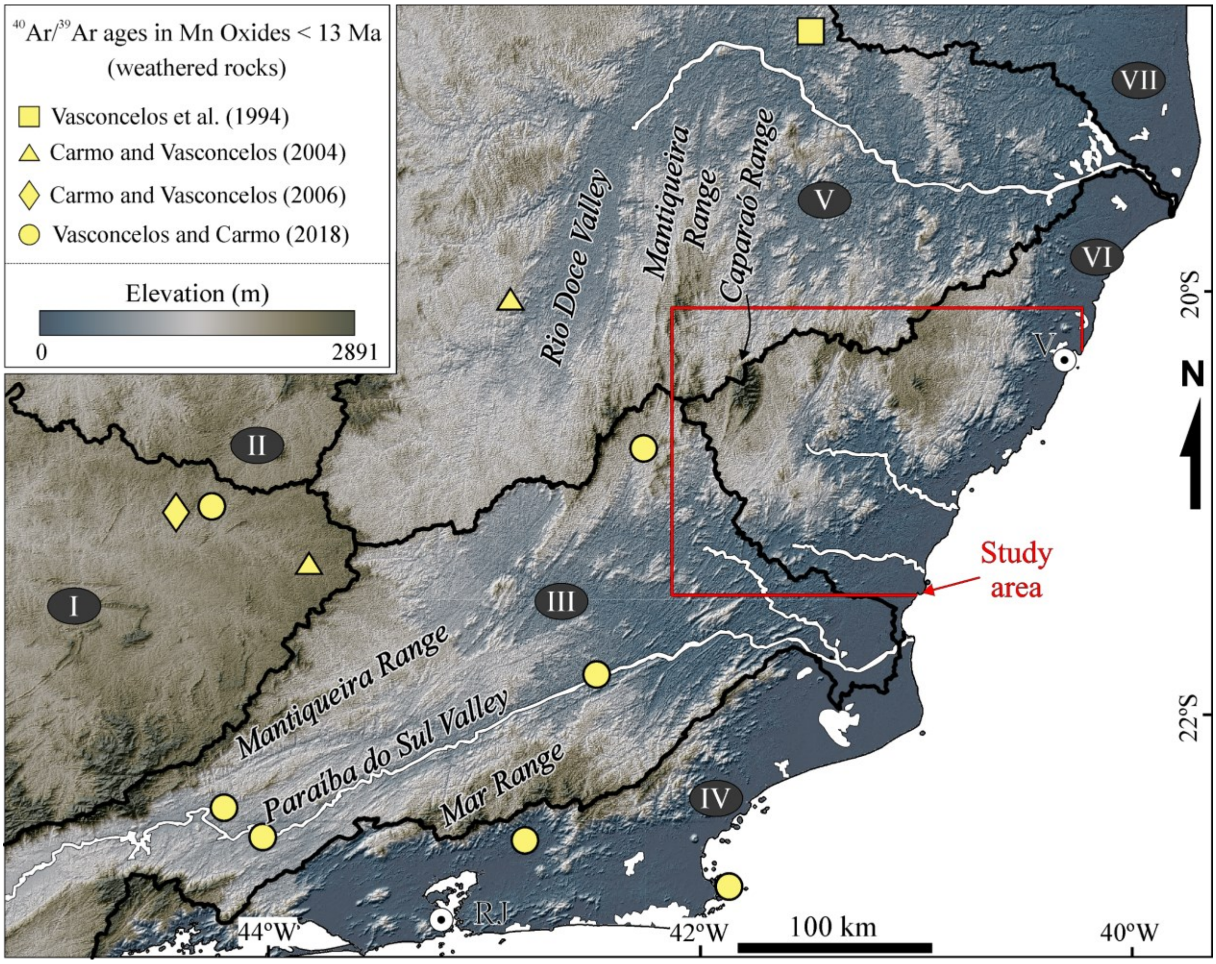

Fig 3.S5: Location of the sampling of existing ^{40}Ar/^{39}Ar ages in supergene Mn oxides in weathered rocks southeastern Brazil. In surrounding regions to the study area, ^{40}Ar/^{39}Ar ages indicate that weathering profiles formed between the Miocene and the Present. Geocrhonological data: Vasconcelos et al., (1994); Carmo and Vasconcelos (2004, 2006); Vasconcelos and Carmo (2018). Main river catchments: I = Paraná; II = São Francisco; III = Paraíba do Sul; IV = Rio de Janeiro seaward-dipping catchments; V = Doce; VI = Espírito Santo seaward-dipping catchments; VII = São Mateus and Itanhém

Capítulo IV

Considerações Finais

4.1 Conclusões gerais

A combinação entre dados geológicos de campo, mineralogia de materiais de preenchimento em estruturas rúpteis e a extração de métricas da topografia, permitiu avançar no entendimento sobre a evolução geológica pós-rifte e o papel das estruturas rúpteis na evolução topográfica da terminação norte da Serra da Mantiqueira. As contribuições mais importantes exibidas nessa Tese são resumidas abaixo:

(i) A margem continental sudeste do Brasil na porção Sul do Espírito Santo apresenta forte estruturação nas direções NE-SW e NW-SE associadas a deformações rúpteis com movimentações predominantemente normais e subordinadamente normais oblíquas e transcorrentes;

(ii) Os materiais de preenchimento em estruturas rúpteis são formados por minerais primários, oriundos de rocha fresca, e por minerais secundários, entre eles hidrobiotita, caulinita, hematita, goethita, litioforita, birnessita e illita. A associação mineralógica encontrada nos materiais de preenchimento denota a ação de fluidos com a precipitação mineral nas descontinuidades rúpteis durante os processos de alteração intempérica. Illita pode ter sido formada também por processos de intemperismo físico, causado pela cominuição da parede da falha em função do atrito durante o desenvolvimento da falha;

(iii) A relação entre a composição dos minerais de preenchimento e a formação de perfis de alteração na região Sudeste do Brasil indica que as falhas, cujas estrias são marcadas nos materiais de preenchimento, originaram-se após a precipitação mineral (no caso dos óxidos de manganês) ou durante (no caso da illita), com idade máxima de deformação na época do Mioceno;

(iv) Três eventos tectônicos pós-miocênicos são inferidos a partir das relações hierárquicas entre as rochas do embasamento alterado e os sedimentos da Fm. Barreiras: (a) uma transcorrência sinistral E-W e (b) uma distensão WNW-ESE, ambos atuantes entre o

Mioceno e o início do Plioceno; e (c) um evento distensivo NE-SW a NNE-SSW, posicionado no Pleistoceno;

(v) As estruturas rúpteis orientadas a NE-SW e NW-SE são formadas pela concentração de tensões locais desenvolvidas nas descontinuidades do embasamento Pré-Cambriano, provavelmente em resposta a esforços regionais gerados nos limites da placa;

(vi) A distribuição de *knickpoints* de alta magnitude, perfis de canais com formas não lineares no espaço elevação-χ e os padrões de orientação das estruturas rúpteis indicam a presença de uma knickzona regionalmente contínua orientada a NE-SW e ancorada em limites estruturais reativados.

(vii) Os padrões de topografia, drenagem e estruturas rúpteis mostram que o rejuvenescimento topográfico na terminação norte da Serra da Mantiqueira ocorreu provavelmente após o Mioceno. Entretanto, a morfologia em grande escala da paisagem e, em particular, a origem dos divisores de drenagem regionais deve ser anterior à deformação rúptil e ao rejuvenescimento topográfico pós-miocênico. Elementos topográficos mais jovens e mais velhos provavelmente coexistem em MCPEs não caracterizadas por uma escarpa íngreme.

4.2 Perspectivas futuras e lacunas no conhecimento

Ainda existem muitas lacunas no conhecimento da evolução geológica pós-rifte da margem sudeste do Brasil, bem como quanto ao papel das heterogeneidades preexistentes no embasamento sobre o desenvolvimento da topografia em porções elevadas da Serra da Mantiqueira. Dessa forma, uma perspectiva para futuros estudos na região é sugerida abaixo:

(i) Para uma melhor restrição da movimentação tectônica cenozoica em terrenos antigos da região Sudeste do Brasil, os materiais de preenchimento presente em estruturas rúpteis precisam ser analisados em detalhe:

   a. A presença da caulinita em superfícies falhadas tem sido associada a alterações intempéricas do *gouge* de falha ou da parede da falha, posteriores à atividade tectônica. Contudo, pequenas lentes de caulinita e montmorilonita podem se precipitar pela ação de fluidos meteóricos entre dois ou mais eventos de deformação. Essa concentração de argilominerais em descontinuidades presentes em terrenos geológicos antigos pode agir no aumento das taxas de deslizamento, favorecendo assim a movimentação neotectônica e consequentemente mudanças na dinâmica crustal rasa;

  b. A presença de minerais de illita em superfícies falhadas pode indicar origem diretamente relacionada com a movimentação tectônica rúptil. Maiores frações de illita autigênica (formadas pela movimentação rúptil) e em relação a illita detrítica (originadas por processo de fragmentação da parede da falha) resultam em idades mais recentes de deformação, temperaturas mais baixas e profundidades crustais rasas. Essa relação pode ser estabelecida pela diminuição do tamanho da fração granulométrica dos minerais autigênicos em relação aos minerais detríticos. A identificação dessas fases minerais pode ser realizada a partir de análises de difratometria de raios-x e datação por métodos de K/Ar e ^{40}Ar/^{39}Ar das diferentes frações granulométricas, tanto da parede das falhas quanto dos *gouges* de falhas.

(ii) A configuração topográfica de porções elevadas alinhadas à costa sudeste do Brasil não está totalmente definida.

  a. A posição geográfica dos divisores de drenagem regionais com distâncias que chegam a mais de 150 km da costa na terminação norte da Serra da Mantiqueira, em comparação com bacias localizadas mais ao norte, cujos divisores estão mais próximos da costa, pode indicar que houve reorganização de rede drenagem na região. Nesse sentido, é necessária a implementação de modelos numéricos de celeridade de *knickpoints* e estudos sobre a distribuição do padrão espacial de variáveis topográficas, como a distribuição dos valores de chi (χ) em escala regional. Essas análises podem ajudar a identificar a agressividade dos divisores de drenagem, bem como idades mais precisas de diferentes ondas de migração das *knickpoints* a montante;

  b. Adicionalmente, faz-se necessária a utilização de dados de nuclídeos cosmogênicos para a obtenção de taxas de erosão em diferentes porções da paisagem na região. A obtenção de taxas de erosão milenares nas bacias costeiras do Espírito Santo e em bacias vizinhas, como a Bacia do Rio Doce, em comparação com diferentes métricas topográficas, poderá indicar locais de ajuste da paisagem;

  c. Embora alguns trabalhos sobre a evolução da paisagem em longo termo tenham sido realizados nos entornos da região, a porção Sul do Espírito Santo ainda não foi estudada. Enquanto são reportados ao menos três tensores tectônicos pós-miocênicos na região, idades de exumação e denudação indicam diferentes mecanismos para as idades de soerguimento no Neógeno, como mudanças climáticas bruscas ou reorganização da rede drenagem. Estudos sobre as taxas de denudação e exumação podem ser obtidas a partir de dados de termocronologia de baixa temperatura, como traços de fissão e datação (U-Th)/He em apatitas nessa porção da margem costeira, que é pobremente estudada.

Referências Bibliográficas

Ahnert, F., 1970. Functional relationships between denudation, relief, and uplift in large, mid-latitude drainage basins. Am. J. Sci. 268, 243–263. https://doi.org/10.2475/ajs.268.3.24

Alkmim, F.F., Marshak, S., Pedrosa-Soares, A.C., Peres, G.G., Cruz, S.C.P., Whittington, A., 2006. Kinematic evolution of the Araçuaí-West Congo orogen in Brazil and Africa: Nutcracker tectonics during the Neoproterozoic assembly of Gondwana. Precambrian Res. 149, 43–64. https://doi.org/10.1016/j.precamres.2006.06.007

Allaby, M., 2008. Dictionary of Earth Sciences, 3rd ed. Ed. Oxford, Oxford University Press.

Almeida, F.F.M., Hasui, Y., de Brito Neves, B.B., Fuck, R.A., 1981. Brazilian structural provinces: An introduction. Earth-Science Rev. 17, 1–29. https://doi.org/10.1016/0012-8252(81)90003-9

Almeida, J., Dios, F., Mohriak, W.U., Valeriano, C.D.M., Heilbron, M., Eirado, L.G., Tomazzoli, E., 2013. Pre-rift tectonic scenario of the eo-cretaceous Gondwana break-up along SE Brazil-SW Africa: Insights from tholeiitic mafic dyke swarms. Geol. Soc. Spec. Publ. 369, 11–40. https://doi.org/10.1144/SP369.24

Alvares, C.A., Stape, J.L., Sentelhas, P.C., Moraes Gonçalves, J.L., Sparovek, G., 2013. Köppen's climate classification map for Brazil. Meteorol. Zeitschrift 22, 711–728. https://doi.org/10.1127/0941-2948/2013/0507

Alves, F.C., Rossetti, D.F., Valeriano, M.M., 2020. Detecting neotectonics in the lowlands of Amazonia through the analysis of river long profiles. J. South Am. Earth Sci. 100, 102553. https://doi.org/10.1016/j.jsames.2020.102553

Alves, F.C., Rossetti, D.F., Valeriano, M.M., Andrades Filho, C.O., 2019. Neotectonics in the South American passive margin: Evidence of Late Quaternary uplifting in the northern Paraiba Basin (NE Brazil). Geomorphology 325, 1–16. https://doi.org/10.1016/j.geomorph.2018.09.028

Anand, R.R., Paine, M., 2002. Regolith geology of the Yilgarn Craton, Western Australia: implications for exploration. Aust. J. Earth Sci. 49, 3–162.

Angelier, J., Mechler, P., 1977. Sur une methode graphique de recherche des contraintes principales egalement utilisables en tectonique et en seismologie: la methode des diedres droits. Bull. Soc. Géologique Fr. 7, 1309–1318. https://doi.org/10.2113/gssgfbull.s7-xix.6.1309

Anthony, J.W., Bideaux, R.A., Bladh, K.W., Nichols, M.C., 2001. Handbook of Mineralogy. Mineralogical Society of America, Chantilly, VA, USA.

Arai, M., 2006. A grande elevação eustática do Mioceno e sua influência na origem do Grupo Barreiras. Geol. USP. Série Científica 6, 1–6. https://doi.org/10.5327/S1519-874X2006000300002

Attal, M., Mudd, S.M., Hurst, M.D., Weinman, B., Yoo, K., Naylor, M., 2015. Impact of change in erosion rate and landscape steepness on hillslope and fluvial sediments grain size in the Feather River basin (Sierra Nevada, California). Earth Surf. Dyn. 3, 201–222. https://doi.org/10.5194/esurf-3-201-2015

Audet, P., Bürgmann, R., 2011. Dominant role of tectonic inheritance in supercontinent cycles. Nat. Geosci. 4, 184–187. https://doi.org/10.1038/ngeo1080

Augustin, C.R., Lopes, M.R.S., Silva, S.M., 2013. Lateritas: Um Conceito Ainda Em Construção. Rev. Bras. Geomorfol. 14, 241–257. https://doi.org/10.20502/rbg.v14i3.202

Balsamo, F., Bezerra, F.H.R., Vieira, M.M., Storti, F., 2013. Structural control on the formation of iron-oxide concretions and Liesegang bands in faulted, poorly lithified Cenozoic sandstones of the Paraiba Basin, Brazil. Geol. Soc. Am. Bull. 125, 913–931. https://doi.org/10.1130/B30686.1

Berlin, M.M., Anderson, R.S., 2007. Modeling of knickpoint retreat on the Roan Plateau, western Colorado. J. Geophys. Res. Earth Surf. 112, 1–16. https://doi.org/10.1029/2006JF000553

Bezerra, F.H.R., Rossetti, D.F., Oliveira, R.G., Medeiros, W.E., Neves, B.B.B., Balsamo, F., Nogueira, F.C.C., Dantas, E.L., Andrades Filho, C., Góes, A.M., 2014. Neotectonic reactivation of shear zones and implications for faulting style and geometry in the continental margin of NE Brazil. Tectonophysics 614, 78–90. https://doi.org/10.1016/j.tecto.2013.12.021

Bezerra, F.H.R., Vita-Finzi, C., 2000. How active is a passive margin? Palaeoseismicity in Northeastern Brazil. Geology 28, 591–594. https://doi.org/10.1130/0091-7613(2000)28<591:HAIAPM>2.0.CO;2

Bierman, P.R., Caffee, M., 2001. Slow Rates of Rock Surface Erosion and Sediment Production across the Namib Desert and Escarpment, Southern Africa. Am. J. Sci. 301, 326–358. https://doi.org/10.2475/ajs.301.4-5.326

Bishop, P., Goldrick, G., 2010. Lithology and the evolution of bedrock rivers in post-orogenic settings: Constraints from the high-elevation passive continental margin of SE Australia. Geol.

Soc. Spec. Publ. 346, 267–287. https://doi.org/10.1144/SP346.14

Bishop, P., Hoey, T.B., Jansen, J.D., Artza, I.L., 2005. Knickpoint recession rate and catchment area: the case of uplifted rivers in Eastern Scotland. Earth Surf. Process. Landforms 30, 767–778. https://doi.org/10.1002/esp.1191

Bradley, D.C., 2008. Passive margins through earth history. Earth-Science Rev. 91, 1–26. https://doi.org/10.1016/j.earscirev.2008.08.001

Braun, J., 2018. A review of numerical modeling studies of passive margin escarpments leading to a new analytical expression for the rate of escarpment migration velocity. Gondwana Res. 53, 209–224. https://doi.org/10.1016/j.gr.2017.04.012

Braun, J., Beaumont, C., 1989. A physical explanation of the relation between flank uplifts and the breakup unconformity at rifted continental margins. Geology 17, 760. https://doi.org/10.1130/0091-7613(1989)017<0760:APEOTR>2.3.CO;2

Braun, J., van der Beek, P., 2004. Evolution of passive margin escarpments: What can we learn from low-temperature thermochronology? J. Geophys. Res. 109, F04009. https://doi.org/10.1029/2004JF000147

Bricalli, L.L., Mello, C.L., 2013. Padrões de lineamentos relacionados a litoestrutura e fraturamento neotectônico (Estado do Espírito Santo-SE do Brasil). Rev. Bras. Geomorfol. 14, 301–311. https://doi.org/10.20502/rbg.v14i3.405

Brideau, M.-A., Yan, M., Stead, D., 2009. The role of tectonic damage and brittle rock fracture in the development of large rock slope failures. Geomorphology 103, 30–49. https://doi.org/10.1016/j.geomorph.2008.04.010

Brindley, G.W., Brown, G., 1980. Crystal Structures of Clay Minerals and their X-Ray Identification, Crystal Structures of Clay Minerals and their X-Ray Identification. London, Mineralogical Society. https://doi.org/10.1180/mono-5

Brito Neves, B.B., Neto, M.C.C., Fuck, R.A., 1999. From Rodinia to Western Gondwana: An approach to the Brasiliano-Pan African Cycle and orogenic collage. Episodes 22, 155–166. https://doi.org/10.18814/epiiugs/1999/v22i3/002

Brown, R.W., Gallagher, K., Gleadow, A.J.W., Summerfield, M. A., 2000. Morphotectonic evolution of the South Atlantic margins of Africa and South America, in: Summerfield, Michael A. (Ed.), Geomorphology and Global Tectonics. John Wiley & Sons, pp. 255–281.

Brown, R.W., Summerfield, M.A., Gleadow, A.J.W., 2002. Denudational history along a transect across the Drakensberg Escarpment of southern Africa derived from apatite fission track thermochronology. J. Geophys. Res. Solid Earth 107, ETG 10-1-ETG 10-18. https://doi.org/10.1029/2001JB000745

Caine, J.S., Evans, J.P., Forster, C.B., 1996. Fault zone architecture and permeability structure. Geology 24, 1025–1028. https://doi.org/10.1130/0091-7613(1996)024<1025:FZAAPS>2.3.CO;2

Calegari, S.S., Aiolfi, T.R., Neves, M.A., Soares, C.C.V., Marques, R.D.A., Caxito, F.D.A., 2020. Filling Materials in Brittle Structures as Indicator of Cenozoic Tectonic Events in Southeastern Brazil. Anuário do Inst. Geociências - UFRJ 43, 237–254. https://doi.org/10.11137/2020_2_237_254

Calegari, S.S., Neves, M.A., Guadagnin, F., França, G.S., Vincentelli, M.G.C., 2016. The Alegre Lineament and its role over the tectonic evolution of the Campos Basin and adjacent continental margin, Southeastern Brazil. J. South Am. Earth Sci. 69, 226–242. https://doi.org/10.1016/j.jsames.2016.04.005

Cardoso Jr., M., Silveira, A.S. da, Vargas, M.R. de, de Oliveira, J.M.M.T., Barbosa, D.V.E., de Oliveira, L.F.B., Fredere, A.C., Lôndero, V., 2021. Geomorphic expression of shear zones in Southern Brazilian and Uruguayan Shields. Geomorphology 382, 107678. https://doi.org/10.1016/j.geomorph.2021.107678

Carmo, I. O., Vasconcelos, P.M., 2006. ^{40}Ar/^{39}Ar geochronology constraints on late miocene weathering rates in Minas Gerais, Brazil. Earth Planet. Sci. Lett. 241, 80–94. https://doi.org/10.1016/j.epsl.2005.09.056

Carmo, I.O., Vasconcelos, P., 2004. Geochronological evidence for pervasive Miocene weathering, Minas Gerais, Brazil. Earth Surf. Process. Landforms 29, 1303–1320. https://doi.org/10.1002/esp.1090

Castelltort, S., Goren, L., Willett, S.D., Champagnac, J.D., Herman, F., Braun, J., 2012. River drainage patterns in the New Zealand Alps primarily controlled by plate tectonic strain. Nat. Geosci. 5, 744–748. https://doi.org/10.1038/ngeo1582

Chang, H.K., Kowsmann, R.O., Figueiredo, A.M.F., Bender, A., 1992. Tectonics and stratigraphy of the East Brazil Rift system: an overview. Tectonophysics 213, 97–138. https://doi.org/10.1016/0040-1951(92)90253-3

Churchman, G.J., Lowe, D.J., 2012. Alteration, formation, and occurrence of minerals in soils, in: Huang, P.M., Li, Y., Sumner, M.. (Eds.), Handbook of Soil Sciences. Properties and Processes. CRC Press, Florida, pp. 20.1-20.72.

Clarke, B.A., Burbank, D.W., 2010. Bedrock fracturing, threshold hillslopes, and limits to the magnitude of bedrock landslides. Earth Planet. Sci. Lett. 297, 577–586. https://doi.org/10.1016/j.epsl.2010.07.011

Cobbold, P.R., Meisling, K.E., Mount, V.S., 2001. Reactivation of an obliquely rifted margin, Campos and Santos basins, southeastern Brazil. Am. Assoc. Pet. Geol. Bull. 85, 1925–1944. https://doi.org/10.1306/8626D0B3-173B-11D7-8645000102C1865D

Cobbold, P.R., Rossello, E.A., Roperch, P., Arriagada, C., Gómez, L.A., Lima, C., 2007. Distribution, timing, and causes of Andean deformation across South America. Geol. Soc. London, Spec. Publ. 272, 321–343. https://doi.org/10.1144/GSL.SP.2007.272.01.17

Cockburn, H.A.P., Brown, R.W., Summerfield, M.A., Seidl, M.A., 2000. Quantifying passive margin denudation and landscape development using a combined fission-track thermochronology and cosmogenic isotope analysis approach. Earth Planet. Sci. Lett. 179, 429–435. https://doi.org/10.1016/S0012-821X(00)00144-8

Cogné, N., Cobbold, P.R., Riccomini, C., Gallagher, K., 2013. Tectonic setting of the Taubaté Basin (Southeastern Brazil): Insights from regional seismic profiles and outcrop data. J. South Am. Earth Sci. 42, 194–204. https://doi.org/10.1016/j.jsames.2012.09.011

Cogné, N., Gallagher, K., Cobbold, P.R., 2011. Post-rift reactivation of the onshore margin of southeast Brazil: Evidence from apatite (U-Th)/He and fission-track data. Earth Planet. Sci. Lett. 309, 118–130. https://doi.org/10.1016/j.epsl.2011.06.025

Cogné, N., Gallagher, K., Cobbold, P.R., Riccomini, C., Gautheron, C., 2012. Post-breakup tectonics in southeast Brazil from thermochronological data and combined inverse-forward thermal history modeling. J. Geophys. Res. Solid Earth 117, n/a-n/a. https://doi.org/10.1029/2012JB009340

Collettini, C., Niemeijer, A., Viti, C., Marone, C., 2009. Fault zone fabric and fault weakness. Nature 462, 907–910. https://doi.org/10.1038/nature08585

Contreras, J., Zühlke, R., Bowman, S., Bechstädt, T., 2010. Seismic stratigraphy and subsidence analysis of the southern Brazilian margin (Campos, Santos and Pelotas basins). Mar. Pet. Geol. 27, 1952–1980. https://doi.org/10.1016/j.marpetgeo.2010.06.007

Costa, C.H., Cesco, J.C., Morán, R.J., 1997. A simple graphical method for estimating the components of the fault-slip vector. J. Struct. Geol. 19, 1245–1247. https://doi.org/10.1016/S0191-8141(97)00046-1

Costa, M.L., 1991. Aspectos Geológicos dos Lateritos da Amazônia. Rev. Bras. Geociências

21, 146–160. https://doi.org/10.25249/0375-7536.1991146160

Crider, J.G., Peacock, D.C.P., 2004. Initiation of brittle faults in the upper crust: A review of field observations. J. Struct. Geol. 26, 691–707. https://doi.org/10.1016/j.jsg.2003.07.007

Cunningham, D., Alkmim, F.F., Marshak, S., 1998. A structural transect across the coastal mobile belt in the Brazilian Highlands (latitude 20°S): the roots of a Precambrian transpressional orogen. Precambrian Res. 92, 251–275. https://doi.org/10.1016/S0301-9268(98)00077-1

De Campos, C.P., Mendes, J.C., Ludka, I.P., de Medeiros, S.R., de Moura, J.C., Wallfass, C., 2004. A review of the Brasiliano magmatism in southern Espírito Santo, Brazil, with emphasis on post-collisional magmatism. J. Virtual Explor. 17, 1–35. https://doi.org/10.3809/jvirtex.2004.00106

De Putter, T., Ruffet, G., Yans, J., Mees, F., 2015. The age of supergene manganese deposits in Katanga and its implications for the Neogene evolution of the African Great Lakes Region. Ore Geol. Rev. 71, 350–362. https://doi.org/10.1016/j.oregeorev.2015.06.015

Delvaux, D., Moeys, R., Stapel, G., Petit, C., Levi, K., Miroshnichenko, A., Ruzhich, V., San'kov, V., 1997. Paleostress reconstructions and geodynamics of the Baikal region, Central Asia, Part 2. Cenozoic rifting. Tectonophysics 282, 1–38. https://doi.org/10.1016/S0040-1951(97)00210-2

Delvaux, D., Sperner, B., 2003. New aspects of tectonic stress inversion with reference to the TENSOR program. Geol. Soc. Spec. Publ. 212, 75–100. https://doi.org/10.1144/GSL.SP.2003.212.01.06

Deng, X., Li, J., 2013. ^{40}Ar/^{39}Ar dating of cryptomelane from the Baye manganese deposit, SW Yunnan, China: Implications for growth rate of supergene Mn-oxide veins. Sci. China Earth Sci. 56, 1654–1663. https://doi.org/10.1007/s11430-013-4591-8

DiBiase, R.A., Whipple, K.X., Heimsath, A.M., Ouimet, W.B., 2010. Landscape form and millennial erosion rates in the San Gabriel Mountains, CA. Earth Planet. Sci. Lett. 289, 134–144. https://doi.org/10.1016/j.epsl.2009.10.036

Dixon, T.H., Stern, R.J., Hussein, I.M., 1987. Control of Red Sea rift geometry by Precambrian structures. Tectonics 6, 551–571. https://doi.org/10.1029/TC006i005p00551

Dunbar, J.A., Sawyer, D.S., 1989. How preexisting weaknesses control the style of continental breakup. J. Geophys. Res. 94, 7278. https://doi.org/10.1029/JB094iB06p07278

Dunn, P.J., Leavens, P.B., Norberg, J.A., Ramik, R.A., 1981. Bannisterite: new chemical data and empirical formulae. Am. Mineral. 66, 1063–1067.

Duvall, A.R., Harbert, S.A., Upton, P., Tucker, G.E., Flowers, R.M., Collett, C., 2020. River patterns reveal two stages of landscape evolution at an oblique convergent margin, Marlborough Fault System, New Zealand. Earth Surf. Dyn. 8, 177–194. https://doi.org/10.5194/esurf-8-177-2020

Engelmann de Oliveira, C.H., Jelinek, A.R., Chemale, F., Cupertino, J.A., 2016. Thermotectonic history of the southeastern Brazilian margin: Evidence from apatite fission track data of the offshore Santos Basin and continental basement. Tectonophysics 685, 21–34. https://doi.org/10.1016/j.tecto.2016.07.012

ERSDAC. 2013. Earth Remote Sensing Data Analysis Center (ASTER GDEM). Available in: http://gdem.ersdac.jspacesystems.or.jp. Accessed 10 set 2013.

Faulkner, D.R., Jackson, C.A.L., Lunn, R.J., Schlische, R.W., Shipton, Z.K., Wibberley, C.A.J., Withjack, M.O., 2010. A review of recent developments concerning the structure, mechanics and fluid flow properties of fault zones. J. Struct. Geol. 32, 1557–1575. https://doi.org/10.1016/j.jsg.2010.06.009

Féboli, W., 1983. Programa Levantamentos Geológicos Básicos: Folha Piúma (SF. 24-V-A-VI), Estado do Espírito Santo, escala 1:100.000. Brasília: DNPM/CPRM.

Ferrari, A.L., 2001. Evolução Tectônica do Graben da Guanabara. Univ. São Paulo. Universidade de São Paulo, São Paulo, 421p. https://doi.org/10.11606/T.44.2001.tde-29082013-152530

Ferreira, J.M., Bezerra, F.H.R., Sousa, M.O.L., Nascimento, A.F., Sá, J.M., França, G.S., 2008. The role of Precambrian mylonitic belts and present-day stress field in the coseismic reactivation of the Pernambuco lineament, Brazil. Tectonophysics 456, 111–126. https://doi.org/10.1016/j.tecto.2008.01.009

Fetter, M., 2009. The role of basement tectonic reactivation on the structural evolution of Campos Basin, offshore Brazil: Evidence from 3D seismic analysis and section restoration. Mar. Pet. Geol. 26, 873–886. https://doi.org/10.1016/j.marpetgeo.2008.06.005

Flint, J.J., 1974. Stream gradient as a function of order, magnitude, and discharge. Water Resour. Res. 10, 969–973. https://doi.org/10.1029/WR010i005p00969

Fonseca, A.C.L., Novo, T.A., Nachtergaele, S., Fonte-Boa, T.M.R., Van Ranst, G., De Grave, J., 2021. Differential Phanerozoic evolution of cratonic and non-cratonic lithosphere from a thermochronological perspective: São Francisco Craton and marginal orogens (Brazil). Gondwana Res. 93, 106–126. https://doi.org/10.1016/j.gr.2021.01.006

Forte, A.M., Whipple, K.X., 2019. Short communication: The Topographic Analysis Kit (TAK) for TopoToolbox. Earth Surf. Dyn. 7, 87–95. https://doi.org/10.5194/esurf-7-87-2019

França, R.L., Del Rey, A.C., Tagliari, C.V., Brandão, J.R., De Rossi Fontanelli, P., 2007. Bacia do Espírito Santo. Bol. Geociencias da Petrobras 15, 501–509.

Franco-Magalhaes, A.O.B., Cuglieri, M.A.A., Hackspacher, P.C., Saad, A.R., 2014. Long-term landscape evolution and post-rift reactivation in the southeastern Brazilian passive continental margin: Taubaté basin. Int. J. Earth Sci. 103, 441–453. https://doi.org/10.1007/s00531-013-0967-4

Frohlich, C., 1992. Triangle diagrams: ternary graphs to display similarity and diversity of earthquake focal mechanisms. Phys. Earth Planet. Inter. 75, 193–198. https://doi.org/10.1016/0031-9201(92)90130-N

Fuck, R.A., Brito Neves, B.B., Schobbenhaus, C., 2008. Rodinia descendants in South America. Precambrian Res. https://doi.org/10.1016/j.precamres.2007.04.018

Gailleton, B., Mudd, S.M., Clubb, F.J., Peifer, D., Hurst, M.D., 2019. A segmentation approach for the reproducible extraction and quantification of knickpoints from river long profiles. Earth Surf. Dyn. 7, 211–230. https://doi.org/10.5194/esurf-7-211-2019

Gallagher, K., Brown, R., Johnson, C., 1998. Fission track analysis and its applications to geological problems. Annu. Rev. Earth Planet. Sci. 26, 519–572. https://doi.org/10.1146/annurev.earth.26.1.519

Gallagher, K., Hawkesworth, C.J., Mantovani, M.S.M., 1994. The denudation history of the onshore continental margin of SE Brazil inferred from apatite fission track data. J. Geophys. Res. 99, 18117–18145. https://doi.org/10.1029/94jb00661

Gallen, S.F., 2018. Lithologic controls on landscape dynamics and aquatic species evolution in post-orogenic mountains. Earth Planet. Sci. Lett. 493, 150–160. https://doi.org/10.1016/j.epsl.2018.04.029

Gallen, S.F., Wegmann, K.W., Bohnenstiehl, D.W.R., 2013. Miocene rejuvenation of topographic relief in the southern Appalachians. GSA Today 23, 4–10. https://doi.org/10.1130/GSATG163A.1

Gatto, L.C.S., Ramos, V.L.S., Nunes, B.T.A., Mamede, L., Góes, M.H.B., Mauro, C.A., Alvarenga, S.M., Franco, E.M.S., Quirico, A.F., Neves, L.B., 1983. Geomorfologia, in: Moreira, H.F. (Ed.), Projeto RADAMBRASIL - Levantamento de Recursos Naturais: Folhas SF-23/24, Rio de Janeiro/Vitória. 32. pp. 305–384.

GEBCO Compilation Group, 2020. The GEBCO_2020 Grid - a continuous terrain model of the global oceans and land. https://doi.org/https://doi.org/10.5285/a29c5465-b138-234d-e053-6c86abc040b9

GEOBASES. 2002. Sistema Integrado de Bases Geoespaciais do Estado do Espírito Santo. INCAPER. Available in: http://www.geobases.es.gov.br/. Accessed 28 ago 2016.

Gezatt, J.N., Macdonald, D.I.M., Stephenson, R., Jelinek, A.R., Carter, A., 2021. South Atlantic passive margin evolution: A thermochronology case study from the Rio de Janeiro-Três Rios section, SE Brazil. J. South Am. Earth Sci. 106, 103051. https://doi.org/10.1016/j.jsames.2020.103051

Gilchrist, A.R., Summerfield, M.A., 1990. Differential denudation and flexural isostasy in formation of rifted-margin upwarps. Nature 346, 739–742. https://doi.org/10.1038/346739a0

Gontijo-Pascutti, A., Bezerra, F.H.R., Terra, E. La, Almeida, J.C.H., 2010. Brittle reactivation of mylonitic fabric and the origin of the Cenozoic Rio Santana Graben, southeastern Brazil. J. South Am. Earth Sci. 29, 522–536. https://doi.org/10.1016/j.jsames.2009.06.007

Green, P.F., Japsen, P., Chalmers, J.A., Bonow, J.M., Duddy, I.R., 2018. Post-breakup burial and exhumation of passive continental margins: Seven propositions to inform geodynamic models. Gondwana Res. 53, 58–81. https://doi.org/10.1016/j.gr.2017.03.007

Green, P.F., Lidmar-Bergström, K., Japsen, P., Bonow, J.M., Chalmers, J.A., 2013. Stratigraphic landscape analysis, thermochronology and the episodic development of elevated, passive continental margins. Geol. Surv. Denmark Greenl. Bull. 30, 1–150. https://doi.org/10.34194/geusb.v30.4673

Grohmann, C.H.., Campanha, G.A.C.., Soares Junior, A.V., 2011. OpenStereo: um programa Livre e multiplataforma para análise de dados estruturais 26–28.

Grohmann, C.H., Campanha, G.A., 2010. OpenStereo: Open Source, Cross-Platform Software for Structural Geology Analysis. 2010 Fall Meet. AGU, San Fr. Calif., 13-17 Dec. 1–35.

Guardado, L.R., Gamboa, L.A.P., Lucchesi, C.F., 1989. Petroleum geology of the Campos Basin, Brazil, a model for a producing Atlantic type basin. Divergent/passive margin basins 3–79.

Gudmundsson, A., Simmenes, T.H., Larsen, B., Philipp, S.L., 2010. Effects of internal structure and local stresses on fracture propagation, deflection, and arrest in fault zones. J. Struct. Geol. 32, 1643–1655. https://doi.org/10.1016/j.jsg.2009.08.013

Gunnell, Y., Fleitout, L., 1998. Shoulder uplift of the Western Ghats passive margin, India: a denudational model. Earth Surf. Process. Landforms 23, 391–404. https://doi.org/10.1002/(SICI)1096-9837(199805)23:5<391::AID-ESP853>3.0.CO;2-5

Gunnell, Y., Harbor, D.J., 2010. Butte detachment: how pre-rift geological structure and drainage integration drive escarpment evolution at rifted continental margins. Earth Surf. Process. Landforms 35, 1373–1385. https://doi.org/10.1002/esp.1973

Hack, J.T., 1957. Studies of longitudinal stream profiles in Virginia and Maryland, Professional Paper. https://doi.org/10.3133/pp294B

Hack, J.T., 1960. Interpretation of erosional topography in humid temperate regions. Bobbs-Merrill.

Hack, J.T., 1982. Physiographic divisions and differential uplift in the Piedmont and Blue Ridge. Geol Surv Prof Pap US 1–49.

Hackspacher, P.C., Ribeiro, L.F.B., Ribeiro, M.C.S., Fetter, A.H., Neto, J.C.H., Tello, C.E.S., Dantas, E.L., 2004. Consolidation and Break-up of the South American Platform in Southeastern Brazil: Tectonothermal and Denudation Histories. Gondwana Res. 7, 91–101. https://doi.org/10.1016/S1342-937X(05)70308-7

Harel, M.A., Mudd, S.M., Attal, M., 2016. Global analysis of the stream power law parameters based on worldwide 10Be denudation rates. Geomorphology 268, 184–196. https://doi.org/10.1016/j.geomorph.2016.05.035

Harman, R., Gallagher, K., Brown, R., Raza, A., Bizzi, L., 1998. Accelerated denudation and tectonic/geomorphic reactivation of the cratons of northeastern Brazil during the Late Cretaceous. J. Geophys. Res. Solid Earth 103, 27091–27105. https://doi.org/10.1029/98jb02524

Heilbron, M.., Eirado, L.G., Almeida, J., 2016. Mapa Geológico e de Recursos Minerais do Estado do Rio de Janeiro. Escala 1:400.000. Programa Geologia do Brasil (PGB), Mapas Geológicos Estaduais. CPRM-Serviço Geológico do Brasil.

Heilbron, M., Pedrosa-Soares, A.C., Neto, M. da C.C., Silva, L.C. da, Trouw, R.A.J., Janasi, V. A., 2004. Província Mantiqueira, in: Geologia Do Continente Sul-Americano: Evolução Da Obra de Fernando Flávio Marques de Almeida. pp. 180–212.

Hiruma, S.T., Riccomini, C., Modenesi-Gauttieri, M.C., Hackspacher, P.C., Neto, J.C.H.H., Franco-Magalhães, A.O.B., 2010. Denudation history of the Bocaina Plateau, Serra do Mar, southeastern Brazil: Relationships to Gondwana breakup and passive margin development. Gondwana Res. 18, 674–687. https://doi.org/10.1016/j.gr.2010.03.001

Horn, A.H., Faria, B., Gardini, G.M., Vasconcellos, L., Mara Regina de Oliveira, 2007. Mapa Geológico Folha Espera Feliz – SE24-V-A-IV. Companhia de Pesquisa de Recursos Minerais-CPRM/Serviço Geológico do Brasil.

Howard, A.D., 1994. A detachment-limited model of drainage basin evolution. Water Resour. Res. 30, 2261–2285. https://doi.org/10.1029/94WR00757

Japsen, P., Bonow, J.M., Green, P.F., Chalmers, J.A., Lidmar-Bergström, K., 2006. Elevated, passive continental margins: Long-term highs or Neogene uplifts? New evidence from West Greenland. Earth Planet. Sci. Lett. 248, 330–339. https://doi.org/10.1016/j.epsl.2006.05.036

Japsen, P., Bonow, J.M., Green, P.F., Chalmers, J.A., Lidmar-Bergström, K., 2009. Formation, uplift and dissection of planation surfaces at passive continental margins - a new approach. Earth Surf. Process. Landforms 34, 683–699. https://doi.org/10.1002/esp.1766

Japsen, P., Chalmers, J.A., Green, P.F., Bonow, J.M., 2012a. Elevated, passive continental margins: Not rift shoulders, but expressions of episodic, post-rift burial and exhumation. Glob. Planet. Change 90–91, 73–86. https://doi.org/10.1016/j.gloplacha.2011.05.004

Japsen, P., Bonow, J.M., Green, P.F., Cobbold, P.R., Chiossi, D., Lilletveit, R., Magnavita, L.P., Pedreira, A., 2012b. Episodic burial and exhumation in NE Brazil after opening of the South Atlantic. Bull. Geol. Soc. Am. 124, 800–816. https://doi.org/10.1130/B30515.1

Jelinek, A.R., Chemale, F., van der Beek, P.A., Guadagnin, F., Cupertino, J.A., Viana, A., 2014. Denudation history and landscape evolution of the northern East-Brazilian continental margin from apatite fission-track thermochronology. J. South Am. Earth Sci. 54, 158–181. https://doi.org/10.1016/j.jsames.2014.06.001

Jones, S.M., White, N., Clarke, B.J., Rowley, E., Gallagher, K., 2002. Present and past influence of the Iceland Plume on sedimentation. Geol. Soc. London, Spec. Publ. 196, 13–25. https://doi.org/10.1144/GSL.SP.2002.196.01.02

Karger, D.N., Conrad, O., Böhner, J., Kawohl, T., Kreft, H., Soria-Auza, R.W., Zimmermann, N.E., Linder, H.P., Kessler, M., 2017. Climatologies at high resolution for the earth's land surface areas. Sci. Data 4, 170122. https://doi.org/10.1038/sdata.2017.122

Karl, M., Glasmacher, U.A., Kollenz, S., Franco-Magalhaes, A.O.B., Stockli, D.F., Hackspacher, P.C., 2013. Evolution of the South Atlantic passive continental margin in southern Brazil derived from zircon and apatite (U–Th–Sm)/He and fission-track data. Tectonophysics 604, 224–244. https://doi.org/10.1016/j.tecto.2013.06.017

Kattenhorn, S.A., Aydin, A., Pollard, D.D., 2000. Joints at high angles to normal fault strike: an explanation using 3-D numerical models of fault-perturbed stress fields. J. Struct. Geol. 22, 1–23. https://doi.org/10.1016/S0191-8141(99)00130-3

Kirby, E., Whipple, K.X., 2012. Expression of active tectonics in erosional landscapes. J. Struct. Geol. 44, 54–75. https://doi.org/10.1016/j.jsg.2012.07.009

Kurz, W., Imber, J., Wibberley, C.A.J., Holdsworth, R.E., Collettini, C., 2008. The internal structure of fault zones: Fluid flow and mechanical properties. Geol. Soc. Spec. Publ. 299, 1–3. https://doi.org/10.1144/SP299.1

Leite, C.A.S., Souza, J.D., Silva, S.L., Kosin, M., Silva, L.C., Bento, R. V., Vieira, V.., Camozzato, E., Paes, V.J.C., Netto, C., Junqueira, P., 2004a. Folha SE-24-Rio Doce. Escala 1:1.000.000, in: Schobbenhaus, C., Gonçalves, J.H., Santos, J.O.S., Abram, M.B., Leão Neto, R., Matos, G.M.M. (Eds.), Carta Geológica Do Brasil Ao Milionésimo.

Leite, C.A.S., Perrotta, M.M., Silva, L.C., Silva, M.A., Heineck, C.A., Salvador, E.D., Vieira, V.S., Lopes, R.C., Silva, M.G.M., Drumond, J.B.V., Malouf, R.F., Lacerda Filho, J.V., 2004b. Folha SF-23-Rio de Janeiro. Escala 1:1.000.000, in: Schobbenhaus, C., Gonçalves, J.H., Santos, J.O.S., Abram, M.B., Leão Neto, R., Matos, G.M.M. (Eds.), Carta Geológica Do Brasil Ao Milionésimo.

Lima, C.C.U., Bezerra, F.H.R., Nogueira, F.C.C., Maia, R.P., Sousa, M.O.L., 2014. Quaternary fault control on the coastal sedimentation and morphology of the São Francisco coastal plain, Brazil. Tectonophysics 633, 98–114. https://doi.org/10.1016/j.tecto.2014.06.026

Lima, J.C.F., Bezerra, F.H.R., Rossetti, D.F., Barbosa, J.A., Medeiros, W.E., de Castro, D.L., Vasconcelos, D.L., 2017. Neogene–Quaternary fault reactivation influences coastal basin sedimentation and landform in the continental margin of NE Brazil. Quat. Int. 438, 92–107. https://doi.org/10.1016/j.quaint.2016.03.026

Lourenço, F.S., Alkmim, F.F. de, Araújo, M.N.C. de, Romeiro, M.A.T., Matos, G.C. de, Crósta, A.P., 2016. The Piúma lineament, southern Espirito Santo: structural expression and tectonic significance. Brazilian J. Geol. 46, 531–546. https://doi.org/10.1590/2317-4889201620150038

Maciel, I.B., Mello, C.L., Silva, A.T., 2017. Caracterização da deformação rúptil em afloramento da Formação Resende, Bacia de Volta Redonda, Estado do Rio de Janeiro. Geol. USP - Ser. Cient. 17, 113–124. https://doi.org/10.11606/issn.2316-9095.v17-391

Michon, L., Sokoutis, D., 2005. Interaction between structural inheritance and extension direction during graben and depocentre formation: An experimental approach. Tectonophysics 409, 125–146. https://doi.org/10.1016/j.tecto.2005.08.020

Millot, G., 1970. Geology of Clays, Geoforum. Springer Berlin Heidelberg, Berlin, Heidelberg. https://doi.org/10.1007/978-3-662-41609-9

Modenesi-Gauttieri, M.C., Toledo, M.C.M., Hiruma, S.T., Taioli, F., Shimada, H., 2011. Deep weathering and landscape evolution in a tropical plateau. CATENA 85, 221–230. https://doi.org/10.1016/j.catena.2011.01.006

Molnar, P., Anderson, R.S., Anderson, S.P., 2007. Tectonics, fracturing of rock, and erosion. J. Geophys. Res. 112, F03014. https://doi.org/10.1029/2005JF000433

Monteiro, H.S., Vasconcelos, P.M., Farley, K.A., Spier, C.A., Mello, C.L., 2014. (U-Th)/He geochronology of goethite and the origin and evolution of cangas. Geochim. Cosmochim. Acta 131, 267–289. https://doi.org/10.1016/j.gca.2014.01.036

Montgomery, D.R., 2001. Slope Distributions, Threshold Hillslopes, and Steady-state Topography. Am. J. Sci. 301, 432–454. https://doi.org/10.2475/ajs.301.4-5.432

Montgomery, D.R., Brandon, M.T., 2002. Topographic controls on erosion rates in tectonically active mountain ranges. Earth Planet. Sci. Lett. 201, 481–489. https://doi.org/10.1016/S0012-821X(02)00725-2

Morais, R.M.O., Mello, C.L., Costa, F.O., Santos, P.F., 2006. Fácies sedimentares e ambientes deposicionais associados aos depósitos da Formação Barreiras no estado do Rio de Janeiro. Geol. USP. Série Científica 6, 19–30. https://doi.org/10.5327/s1519-874x2006000300004

Morais Neto, J.M., Hegarty, K.A., Karner, G.D., Alkmim, F.F., 2009. Timing and mechanisms for the generation and modification of the anomalous topography of the Borborema Province, northeastern Brazil. Mar. Pet. Geol. 26, 1070–1086. https://doi.org/10.1016/j.marpetgeo.2008.07.002

Noce, C.M., Pedrosa-Soares, A.C., Silva, L.C., Alkmim, F.F., 2007a. O Embasamento Arqueano e Paleoproterozóico do Orógeno Araçuaí. Geonomos 15, 17–21. https://doi.org/10.18285/geonomos.v15i1.104

Noce, C.M., Costa, A.G., Piuzana, D., Vieira, V.S., Carvalho, C., 2007b. Mapa Geológico Folha Manhuaçu - SF.23-X-B-III. Companhia de Pesquisa de Recursos Minerais-CPRM/Serviço Geológico do Brasil.

Novais, L.C.C., Teixeira, L.B., Neves, M.T., Rodarte, J.B.M., Almeida, J.C., Valeriano, C.M., 2003. Novas ocorrências de diwues de diabásio na faixa Colatina - ES: Estruturas rúpteis associadas e implicações tectônicas para as bacias de Campos e do Espírito Santo. Bol. Geociencias da Petrobras 12, 191–194.

Novo, T., Noce, C.M., Figueiredo, C., Pedrosa-Soares, A.C., 2012. Mapa Geológico Folha Carangola SF.23-X-B-VI. Companhia de Pesquisa de Recursos Minerais-CPRM/Serviço Geológico do Brasil.

Novo, T.A., Noce, C.M., Batista, G.A.P., Quéméneur, J.J.G., Martins, B. de S., Santos, S.W.M., Carneiro, G.A., Horn, A.H., 2014. Mapa Geológico Folha Manhumirim SF.24-V-A-I. Companhia de Pesquisa de Recursos Minerais-CPRM/Serviço Geológico do Brasil.

O' Leary, D.W., Friedman, J.D., Pohn, H.A., 1976. Lineament, linear, lineation: Some proposed new standards for old terms. Geol. Soc. Am. Bull. 87, 1463–1469. https://doi.org/10.1130/0016-7606(1976)87<1463:LLLSPN>2.0.CO;2

Oberlin, A., Couty, R., 1970. Conditions of kaolinite formation during alteration of some silicates by water at 200 °C. Clays Clay Miner. https://doi.org/10.1346/ccmn.1970.0180607

Ojeda, H.A.O., 1982. Structural Framework, Stratigraphy, and Evolution of Brazilian Marginal Basins. Am. Assoc. Pet. Geol. Bull. 66, 732–749. https://doi.org/10.1306/03B5A309-16D1-11D7-8645000102C1865D

Pedrosa-Soares, A.C., Alkmim, F.F., Tack, L., Noce, C.M., Babinski, M., Silva, L.C., Martins-Neto, M.A., 2008. Similarities and differences between the Brazilian and African counterparts of the Neoproterozoic Araçuaí-West Congo orogen, in: Geological Society Special Publication. pp. 153–172. https://doi.org/10.1144/SP294.9

Pedrosa-Soares, A.C., De Campos, C.P., Noce, C., Silva, L.C., Novo, T., Roncato, J., Medeiros, S., Castañeda, C., Queiroga, G., Dantas, E., Dussin, I., Alkmim, F., 2011. Late Neoproterozoic-Cambrian granitic magmatism in the Araçuaí orogen (Brazil), the Eastern Brazilian Pegmatite Province and related mineral resources. Geol. Soc. Spec. Publ. 350, 25–51. https://doi.org/10.1144/SP350.3

Pedrosa-Soares, A.C., Noce, C.M., Alkmim, F.F., Silva, L.C., Babinski, M., Cordani, U., Castañeda, C., 2007. Orógeno Araçuaí: síntese do conhecimento 30 anos após Almeida 1977. Geonomos 15, 1–16. https://doi.org/10.18285/geonomos.v15i1.103

Pedrosa-Soares, A.C., Noce, C.M., Wiedemann, C.M., Pinto, C.P., 2001. The Araçuaí-West-Congo Orogen in Brazil: An overview of a confined orogen formed during Gondwanaland assembly. Precambrian Res. 110, 307–323. https://doi.org/10.1016/S0301-9268(01)00174-7

Pedrosa-Soares, A.C., Wiedemann-Leonardos, C.M., 2000. Evolution of Araçuaí Belt and its connection to the Ribeira Belt, eastern Brazil, in: Tectonic Evolution of South America. https://doi.org/10.13140/2.1.3802.5928

Peifer, D., Persano, C., Hurst, M.D., Bishop, P., Fabel, D., 2021. Growing topography due to contrasting rock types in a tectonically dead landscape. Earth Surf. Dyn. 9, 167–181. https://doi.org/10.5194/esurf-9-167-2021

Perron, J.T., Royden, L., 2013. An integral approach to bedrock river profile analysis. Earth Surf. Process. Landforms 38, 570–576. https://doi.org/10.1002/esp.3302

Petersen, K.D., Schiffer, C., 2016. Wilson cycle passive margins: Control of orogenic inheritance on continental breakup. Gondwana Res. 39, 131–144. https://doi.org/10.1016/j.gr.2016.06.012

Portenga, E.W., Bierman, P.R., 2011. Understanding Earth's eroding surface with 10Be. GSA Today 21, 4–10. https://doi.org/10.1130/G111A.1

Quigley, M.C., Sandiford, M., Cupper, M.L., 2007. Distinguishing tectonic from climatic controls on range-front sedimentation. Basin Res. 19, 491–505. https://doi.org/10.1111/j.1365-2117.2007.00336.x

Riccomini, C., Peloggia, A.U.G., Saloni, J.C.L., Kohnke, M.W., Figueira, R.M., 1989. Neotectonic activity in the Serra do Mar rift system (southeastern Brazil). J. South Am. Earth Sci. 2, 191–197. https://doi.org/10.1016/0895-9811(89)90046-1

Riccomini, C., Sant'Anna, L.G., Ferrari, A.L., 2004. Evolução geológica do rift continental do sudeste do Brasil, in: Mantesso-Neto, V., Bartorelli, A., Carneiro, C.D.R., Brito Neves, B.. (Eds.), Geologia Do Continente Sul-Americano: Evolução Da Obra de Fernando Flávio Marques de Almeida. Editora Beca São Paulo, pp. 383–405.

Righi, D., Meunier, A., 1995. Origin of Clays by Rock Weathering and Soil Formation, in: Origin and Mineralogy of Clays. Springer Berlin Heidelberg, Berlin, Heidelberg, pp. 43–161. https://doi.org/10.1007/978-3-662-12648-6_3

Romano, A.W., Castañeda, C., 2006. A tectônica distensiva pós-mesozóica no condicionamento dos depósitos de bauxita da zona da mata mineira. Geonomos 14, 1–5.

Ross, J.L.S., 2011. Relevo Brasileiro: Uma Proposta de Classificação. Rev. Do Dep. Geogr. 4, 25–39. https://doi.org/10.7154/RDG.1985.0004.0004

Rossetti, D.F., Bezerra, F.H.R., Dominguez, J.M.L., 2013. Late Oligocene–Miocene transgressions along the equatorial and eastern margins of Brazil. Earth-Science Rev. 123, 87–112. https://doi.org/10.1016/j.earscirev.2013.04.005

Roy, S.G., Koons, P.O., Upton, P., Tucker, G.E., 2015. The influence of crustal strength fields on the patterns and rates of fluvial incision. J. Geophys. Res. Earth Surf. 120, 275–299. https://doi.org/10.1002/2014JF003281

Royden, L., Keen, C.E., 1980. Rifting process and thermal evolution of the continental margin of Eastern Canada determined from subsidence curves. Earth Planet. Sci. Lett. 51, 343–361. https://doi.org/10.1016/0012-821X(80)90216-2

Sacek, V., Braun, J., van der Beek, P., 2012. The influence of rifting on escarpment migration on high elevation passive continental margins. J. Geophys. Res. Solid Earth 117, 1–8. https://doi.org/10.1029/2011JB008547

Salazar-Mora, C.A., Huismans, R.S., Fossen, H., Egydio-Silva, M., Salazar-Mora, C.A., Huismans, R.S., Fossen, H., Egydio-Silva, M., 2018. The Wilson Cycle and Effects of Tectonic Structural Inheritance on Rifted Passive Margin Formation. Tectonics 37, 3085–3101. https://doi.org/10.1029/2018TC004962

Salomon, E., Koehn, D., Passchier, C., Hackspacher, P.C., Glasmacher, U.A., 2015. Contrasting stress fields on correlating margins of the South Atlantic. Gondwana Res. 28, 1152–1167. https://doi.org/10.1016/j.gr.2014.09.006

Salvador, E.D., Riccomini, C., 1995. Neotectônica da região do Alto Estrutural de Queluz (SP-RJ, Brasil). Rev. Bras. Geociências 25, 151–164. https://doi.org/10.25249/0375-7536.1995151164

Sandiford, M., Wallace, M., Coblentz, D., 2004. Origin of the in situ stress field in south-eastern Australia. Basin Res. 16, 325–338. https://doi.org/10.1111/j.1365-2117.2004.00235.x

Santiago, R., Caxito, F.A., Pedrosa-Soares, A., Neves, M.A., Dantas, E.L., 2020a. Tonian island arc remnants in the northern Ribeira orogen of Western Gondwana: The Caxixe batholith (Espírito Santo, SE Brazil). Precambrian Res. 351, 105944. https://doi.org/10.1016/j.precamres.2020.105944

Santiago, R., Caxito, F.A., Neves, M.A., Dantas, E.L., Medeiros Júnior, E.B., Queiroga, G.N., 2020b. Two generations of mafic dyke swarms in the Southeastern Brazilian coast: reactivation of structural lineaments during the gravitational collapse of the Araçuaí-Ribeira Orogen (500 Ma) and West Gondwana breakup (140 Ma). Precambrian Res. 340, 105344. https://doi.org/10.1016/j.precamres.2019.105344

Santos, M., Ladeira, F.S.B., 2006. Tectonismo em perfis de alteração da serra de Itaqueri (SP): Análise através de indicadores cinemáticos de falhas. Geociencias 25, 135–149.

Scharf, T.E., Codilean, A.T., de Wit, M., Jansen, J.D., Kubik, P.W., 2013. Strong rocks sustain ancient postorogenic topography in southern Africa. Geology 41, 331–334. https://doi.org/10.1130/G33806.1

Scheinost, A.C., 2004. Metal Oxides, in: Encyclopedia of Soils in the Environment. pp. 428–438. https://doi.org/10.1016/B0-12-348530-4/00194-6

Scherler, D., Bookhagen, B., Strecker, M.R., 2014. Tectonic control on 10Be-derived erosion rates in the Garhwal Himalaya, India. J. Geophys. Res. Earth Surf. 119, 83–105. https://doi.org/10.1002/2013JF002955

Schwanghart, W., Scherler, D., 2014. Short Communication: TopoToolbox 2 – MATLAB-based software for topographic analysis and modeling in Earth surface sciences. Earth Surf. Dyn. 2, 1–7. https://doi.org/10.5194/esurf-2-1-2014

Schwanghart, W., Scherler, D., 2017. Bumps in river profiles: uncertainty assessment and smoothing using quantile regression techniques. Earth Surf. Dyn. 5, 821–839. https://doi.org/10.5194/esurf-5-821-2017

Schwanghart, W., Scherler, D., 2020. Divide mobility controls knickpoint migration on the Roan Plateau (Colorado, USA). Geology 48, 698–702. https://doi.org/10.1130/G47054.1

Shobe, C.M., Tucker, G.E., Anderson, R.S., 2016. Hillslope-derived blocks retard river incision. Geophys. Res. Lett. 43, 5070–5078. https://doi.org/10.1002/2016GL069262

Shuster, D.L., Farley, K.A., Vasconcelos, P.M., Balco, G., Monteiro, H.S., Waltenberg, K., Stone, J.O., 2012. Cosmogenic 3He in hematite and goethite from Brazilian "canga" duricrust demonstrates the extreme stability of these surfaces. Earth Planet. Sci. Lett. 329–330, 41–50. https://doi.org/10.1016/j.epsl.2012.02.017

Sibson, R.H., 1977. Fault rocks and fault mechanisms. J. Geol. Soc. London. 133, 191–213. https://doi.org/10.1144/gsjgs.133.3.0191

Silva, L.C., McNaughton, N.J., Armstrong, R., Hartmann, L.A., Fletcher, I.R., 2005. The neoproterozoic Mantiqueira Province and its African connections: A zircon-based U-Pb geochronologic subdivision for the Brasiliano/Pan-African systems of orogens. Precambrian Res. 136, 203–240. https://doi.org/10.1016/j.precamres.2004.10.004

Silva, M.A., Camozzato, E., Paes, V.J.C., Junqueira, P.A., Ramgrab, G.E., 2004. Folha SF.24-

Vitoria. Escala 1:1.000.000, in: Schobbenhaus, C., Gonçalves, J.H., Santos, J.O.S., Abram, M.B., Leão Neto, R., Matos, G.M.M. (Eds.), Carta Geológica do Brasil ao Milionésimo.

Silva, T.P., Mello, C.L., 2011. Reativações neotectônicas na Zona de Cisalhamento do Rio Paraíba do Sul (sudeste do Brasil). Geol. USP. Série Científica 11, 95–111. https://doi.org/10.5327/Z1519-874X2011000100006

Simon, J.L., Seron, F.J., Casas, A.M., 1988. Sress deflection and fracture development in a multidirectional extension regime. Mathematical and experimental approach with field examples. Ann. Tectonicae II, 21–32.

Sosa Gonzalez, V., Bierman, P.R., Fernandes, N.F., Rood, D.H., 2016. Long-term background denudation rates of southern and southeastern Brazilian watersheds estimated with cosmogenic 10Be. Geomorphology 268, 54–63. https://doi.org/10.1016/j.geomorph.2016.05.024

Souza, D.H., Hackspacher, P.C., Silva, B. V., Siqueira-Ribeiro, M.C., Hiruma, S.T., 2020. Temporal and spatial denudation trends in the continental margin of southeastern Brazil. J. South Am. Earth Sci. 102931. https://doi.org/10.1016/j.jsames.2020.102931

Souza, P.C.M., Schmitt, R. S., Stanton, N., 2017. Meso-Cenozoic tectonic evolution of the SE Brazilian continental margin: Petrographic, kinematic and dynamic analysis of the onshore Araruama Lagoon Fault System. J. Struct. Geol. 102, 37–57. https://doi.org/10.1016/j.jsg.2017.07.003

Sperner, B., Zweigel, P., 2010. A plea for more caution in fault–slip analysis. Tectonophysics 482, 29–41. https://doi.org/10.1016/j.tecto.2009.07.019

Spier, C.A., Vasconcelos, P.M., Oliviera, S.M.B., 2006. ^{40}Ar/^{39}Ar geochronological constraints on the evolution of lateritic iron deposits in the Quadrilátero Ferrífero, Minas Gerais, Brazil. Chem. Geol. 234, 79–104. https://doi.org/10.1016/j.chemgeo.2006.04.006

Stanton, N., Schmitt, R., Galdeano, A., Maia, M., Mane, M., 2010. Crustal structure of the southeastern Brazilian margin, Campos Basin, from aeromagnetic data: New kinematic constraints. Tectonophysics 490, 15–27. https://doi.org/10.1016/j.tecto.2010.04.008

Stolle, A., Schwanghart, W., Andermann, C., Bernhardt, A., Fort, M., Jansen, J.D., Wittmann, H., Merchel, S., Rugel, G., Adhikari, B.R., Korup, O., 2019. Protracted river response to medieval earthquakes. Earth Surf. Process. Landforms 44, 331–341. https://doi.org/10.1002/esp.4517

Sugden, D., Denton, G., 2004. Cenozoic landscape evolution of the Convoy Range to Mackay Glacier area, Transantarctic Mountains: Onshore to offshore synthesis. Geol. Soc. Am. Bull.

116, 840–857. https://doi.org/10.1130/B25356.1

Summerfield, M.A., 2014. Global Geomorphology, Global Geomorphology. Routledge. https://doi.org/10.4324/9781315841182

Takaku, J., Tadono, T., Tsutsui, K., 2014. Generation of High Resolution Global DSM from ALOS PRISM. ISPRS - Int. Arch. Photogramm. Remote Sens. Spat. Inf. Sci. XL–4, 243–248. https://doi.org/10.5194/isprsarchives-XL-4-243-2014

Talwani, P., 2017. On the nature of intraplate earthquakes. J. Seismol. 21, 47–68. https://doi.org/10.1007/s10950-016-9582-8

Tedeschi, M., Novo, T., Pedrosa-Soares, A., Dussin, I., Tassinari, C., Silva, L.C., Gonçalves, L., Alkmim, F., Lana, C., Figueiredo, C., Dantas, E., Medeiros, S., De Campos, C., Corrales, F., Heilbron, M., 2016. The Ediacaran Rio Doce magmatic arc revisited (Araçuaí-Ribeira orogenic system, SE Brazil). J. South Am. Earth Sci. 68, 167–186. https://doi.org/10.1016/j.jsames.2015.11.011

Tello Saenz, C.A., Hackspacher, P.C., Hadler Neto, J.C., Iunes, P.J., Guedes, S., Ribeiro, L.F.B., Paulo, S.R., 2003. Recognition of Cretaceous, Paleocene, and Neogene tectonic reactivation through apatite fission-track analysis in Precambrian areas of southeast Brazil: Association with the opening of the south Atlantic Ocean. J. South Am. Earth Sci. 15, 765–774. https://doi.org/10.1016/S0895-9811(02)00131-1

Tello Saenz, C.A., Hadler Neto, J.C., Iunes, P.J., Guedes, S., Hackspacher, P.C., Ribeiro, L.F.B., Paulo, S.R., Osorio A, A.M., 2005. Thermochronology of the South American platform in the state of São Paulo, Brazil, through apatite fission tracks. Radiat. Meas. 39, 635–640. https://doi.org/10.1016/j.radmeas.2004.08.005

Thomaz Filho, A., Cesero, P. De, Mizusaki, A.M., Leão, J.G., 2005. Hot spot volcanic tracks and their implications for south American plate motion, Campos basin (Rio de Janeiro state), Brazil. J. South Am. Earth Sci. 18, 383–389. https://doi.org/10.1016/j.jsames.2004.11.006

Thompson, R.N., Gibson, S.A., Mitchell, J.G., Dickin, A.P., Leonardos, O.H., Brod, J.A., Greenwood, J.C., 1998. Migrating Cretaceous-Eocene Magmatismin the Serra do Mar Alkaline Province, SE Brazil: Melts from the Deflected Trindade Mantle Plume? J. Petrol. 39, 1493–1526. https://doi.org/10.1093/petroj/39.8.1493

Thyng, K.M., Greene, C.A., Hetland, R.D., Zimmerle, H.M., DiMarco, S.F., 2016. True Colors of Oceanography: Guidelines for Effective and Accurate Colormap Selection. Oceanography 29, 9–13. https://doi.org/10.5670/oceanog.2016.66

van der Beek, P., Summerfield, M.A., Braun, J., Brown, R.W., Fleming, A., 2002. Modeling postbreakup landscape development and denudational history across the southeast African (Drakensberg Escarpment) margin. J. Geophys. Res. Solid Earth 107, ETG 11-1-ETG 11-18. https://doi.org/10.1029/2001JB000744

Van Ranst, G., Pedrosa-Soares, A.C., Novo, T., Vermeesch, P., De Grave, J., 2020. New insights from low-temperature thermochronology into the tectonic and geomorphologic evolution of the south-eastern Brazilian highlands and passive margin. Geosci. Front. 11, 303–324. https://doi.org/10.1016/j.gsf.2019.05.011

Vasconcelos, P.M., Becker, T.A., Renne, P.R., Brimhall, G.H., 1992. Age and duration of weathering by ^{40}K-^{40}Ar and ^{40}Ar/^{39}Ar analysis of potassium-manganese oxides. Science. 258, 451–455. https://doi.org/10.1126/science.258.5081.451

Vasconcelos, P.M., Carmo, I.O., 2018. Calibrating denudation chronology through ^{40}Ar/^{39}Ar weathering geochronology. Earth-Science Rev. 179, 411–435. https://doi.org/10.1016/j.earscirev.2018.01.003

Vasconcelos, P.M., Renne, P.R., Brimhall, G.H., Becker, T.A., 1994. Direct dating of weathering phenomena by ^{40}Ar/^{39}Ar and K-Ar analysis of supergene K-Mn oxides. Geochim. Cosmochim. Acta 58, 1635–1665. https://doi.org/10.1016/0016-7037(94)90565-7

Velde, B., Meunier, A., 2008. The origin of clay minerals in soils and weathered rocks, The Origin of Clay Minerals in Soils and Weathered Rocks. https://doi.org/10.1007/978-3-540-75634-7

Vieira, V.S., Menezes, R.G. de, 2015. Geologia e Recursos Minerais do Estado do Espírito Santo: texto explicativo do mapa geológico e de recursos minerais. Escala 1:400.000. Série Programa de Geologia do Brasil – PGB, Coleção Mapas Geológicos Estaduais, Serviço Geológico do Brasil - CPRM.

Vodyanitskii, Y.N., Vasil ev, A.A., Lesovaya, S.N., Sataev, E.F., Sivtsov, A. V, 2004. Formation of manganese oxides in soils. Eurasian Soil Sci. c/c Pochvovedenie 37, 572–584.

Vollmer, F.W., 2015. Orient 3: A new integrated software program for orientation data analysis, kinematic analysis, spherical projections, and Schmidt plots. Abstr. with Programs - Geol. Soc. Am. 47, 49.

Weissel, J.K., Karner, G.D., 1989. Flexural uplift of rift flanks due to mechanical unloading of the lithosphere during extension. J. Geophys. Res. Solid Earth 94, 13919–13950. https://doi.org/10.1029/JB094iB10p13919

Weissel, J.K., Seidl, M.A., 1997. Influence of rock strength properties on escarpment retreat across passive continental margins. Geology 25, 631. https://doi.org/10.1130/0091-7613(1997)025<0631:IORSPO>2.3.CO;2

West, D.C., Mello, C.L., 2020. Distribuição da Formação Barreiras na Região Sul do Espírito santo e sua relação com a deformação neotectônica. Rev. Bras. Geomorfol. 21, 155–170. https://doi.org/http://dx.doi.org/10.20502/rbg.v21i1.1667

Whipple, K.X., Tucker, G.E., 1999. Dynamics of the stream-power river incision model: Implications for height limits of mountain ranges, landscape response timescales, and research needs. J. Geophys. Res. Solid Earth 104, 17661–17674. https://doi.org/10.1029/1999jb900120

Whittaker, A.C., Boulton, S.J., 2012. Tectonic and climatic controls on knickpoint retreat rates and landscape response times. J. Geophys. Res. Earth Surf. 117, 1–19. https://doi.org/10.1029/2011JF002157

Whittaker, A.C., Cowie, P.A., Attal, M., Tucker, G.E., Roberts, G.P., 2007. Bedrock channel adjustment to tectonic forcing: Implications for predicting river incision rates. Geology 35, 103–106. https://doi.org/10.1130/G23106A.1

Wiedemann, C.M., Medeiros, S.R., Ludka, I.P., Mendes, J.C., Costa-de-Moura, J., 2002. Architecture of Late Orogenic Plutons in the Araçuaí-Ribeira Fold Belt, Southeast Brazil. Gondwana Res. 5, 381–399. https://doi.org/10.1016/S1342-937X(05)70730-9

Wildman, M., Cogné, N., Beucher, R., 2019. Fission-Track Thermochronology Applied to the Evolution of Passive Continental Margins, in: Malusà, M.G., Fitzgerald, P.G. (Eds.), Fission-Track Thermochronology and Its Application to Geology. pp. 351–371. https://doi.org/10.1007/978-3-319-89421-8_20

Wobus, C., Whipple, K.X., Kirby, E., Snyder, N., Johnson, J., Spyropolou, K., Crosby, B., Sheehan, D., 2006. Tectonics from topography: Procedures, promise, and pitfalls, in: Willett, S.., Hovius, N., Brandon, M.T., Fisher, D.M. (Eds.), Special Paper of the Geological Society of America. Geological Society of America, pp. 55–74. https://doi.org/10.1130/2006.2398(04)

Zalán, P.V., Oliveira, J.A.B., 2005. Origem e evolução estrutural do Sistema de Rittes Cenozóicos do Sudeste do Brasil. Bol. Geociencias da Petrobras 13, 269–300.

Zhang, Y., Schaubs, P.M., Zhao, C., Ord, A., Hobbs, B.E., Barnicoat, A.C., 2008. Fault-related dilation, permeability enhancement, fluid flow and mineral precipitation patterns: numerical models. Geol. Soc. London, Spec. Publ. 299, 239–255. https://doi.org/10.1144/SP299.15

Zoback, M. Lou, 1992. First- and second-order patterns of stress in the lithosphere: The World

Stress Map Project. J. Geophys. Res. 97, 11703. https://doi.org/10.1029/92JB00132